NTNU
Norwegian University of
Science and Technology

Fatigue Strength of Glued-Laminated Timber Loaded in Shear Along Grain and Withdrawal of Threaded Rods.

Arild Farestveit Kvittingen

Department of Structural Engineering

Faculty of Engineering Science and Technology
NTNU- Norwegian University of Science and Technology

MASTER THESIS 2017

SUBJECT AREA:	DATE:	NO. OF PAGES:
Timber Structures	11.06.2017	94

TITLE:

Fatigue Strength of Glued-Laminated Timber Loaded in Shear Along Grain and Withdrawal of Threaded Rods.

Utmattingsegenskaper i fiberretning for skjærbelastet limtre og limtre med aksielt belastede gjengestenger

BY:

Arild F. Kvittingen

SUMMARY:

This thesis involves the investigation of both static and fatigue performance of two different longitudinal shear situations. The first being axially loaded threaded rods with small rod to grain angles. The second situation is longitudinal radial and longitudinal tangential shear properties for GL30c glulam. This thesis is therefore divided in three parts. The first part consists of introduction and general literature. The second part is the investigation of threaded rods. The third part is the investigation of longitudinal shear properties of GL30c.

For the second part, a total of 10 static and 11 fatigue specimens were tested, this results in 20 static connections and 22 fatigue connections. The fatigue strength was better than anticipated with the slope of the SN-curve being 0,0374 for withdrawal in grain direction and 0,0398 for withdrawal at 5-degrees to grain direction.

For the third part, a total of 51 static tests and 48 fatigue tests were conducted for two different designs which both had longitudinal radial and longitudinal tangential orientation. The specimen was modeled numerically, and strains were measured on the surface using video extensometer.

Approximately 77 % of specimen failed by fracture propagation of a single plane. While the remaining 23% formed two planes. This is a considerable improvement compared to previous optimization.

The characteristic shear strength $f_{v,g,k}$ ranged between 3.51 MPa and 4.26 MPa depending on specimen design and orientation. The mean G-modulus was found to be 619 MPa for longitudinal radial orientation and 1145 for longitudinal tangential. The slope of the SN curve was between 0,0527 and 0,0815 depending on design and orientation. These values correspond well with literature.

RESPONSIBLE TEACHER: Kjell A. Malo

SUPERVISOR(S)Kjell A. Malo, Haris Stamatopoulos

CARRIED OUT AT: Department of Structural Engineering

Institutt for konstruksjonsteknikk

FAKULTET FOR INGENIØRVITENSKAP OG TEKNOLOGI
NTNU – Norges teknisk-naturvitenskapelige universitet

MASTEROPPGAVE 2017

for

Arild F. Kvittingen

Fatigue Strength of Glued-Laminated Timber Loaded in Shear Along Grain and Withdrawal of Threaded Rods.

Utmattingsegenskaper i fiberretning for skjærbelastet limtre og limtre med aksielt belastede gjengestenger.

The aim of this thesis is to experimentally investigate the fatigue properties of Glue laminated timber in grain direction with regards to two cases. The first case is glued laminated timber with inserted rods with small rod to grain angles. And the other case is glued-laminated timber loaded in shear along grain*.* The background for this work is to increase the usability of timber and timber connectors in general, but especially connections with threaded rods. Important attributes of threaded rods are stiffer connections, energy dissipation and productional aspects. Typical applications for threaded rods are connections in timber arch bridges, beam to column connections and column base connections, and more. These applications may impose fatigue damage, a situation which has undergone little research in the past. Thus, the goal of this thesis becomes:

Goal:

1. Experimental investigation of connections with axially loaded rods in small rod-to-grain angles. Followed by evaluation of both static and fatigue results.
2. Experimental investigation of glued-laminated timber loaded in longitudinal shear. Followed by evaluation of both static and fatigue results.

Veileder(e):   Kjell A. Malo og Haris Stamatopoulos

Besvarelsen skal leveres til Institutt for konstruksjonsteknikk innen 11. juni 2017.

Preface

This Master thesis has been submitted to the Norwegian University of Science and Technology (NTNU) as a fulfilling part of the 2 year masters course Civil and Environmental Engineering. The work has been carried out at the department of Structural Engineering, NTNU. The supervisors for this thesis has been Kjell Arne Malo and Haris Stamatopoulos.

Trondheim, 10.06.2017

_____
    Arild F. Kvittingen

Acknowledgements

I would like to thank my supervisors Kjell Arne Malo and Haris Stamatopoulos for their helpful advice and guidance during the work on this thesis but also for their encouragement and motivational disciplinary enthusiasm.

I am especially grateful to Katarzyna Ostapska- Luczkowska for her enthusiasm and strong disciplinary support. I have learned a lot from her though enthusiastic and often lengthy discussions. Her understanding and clues have been a key component in the work on this thesis.

A large part of this thesis has been experimental testing and throughout this work I have received motivation, help and guidance from the laboratory staff, especially Terje Petersen and Christian Frugone have been exceptionally helpful.

Grateful is an underestimated word when it comes to my family. My brothers and parents have been motivating, and has shown understanding and support throughout my studies. Mom and dad, I'll soon start to pay my own phone bill, I promise. I am especially grateful for my twin brother whom have studied the same subjects as me, and with whom I have built up motivation and encouragement for the difficult parts of the road, I'm especially going to miss our gingerbread breaks.

Least but Mostly, I must thank my beautiful wife, whom has followed me throughout my studies in different parts of Norway, whom has patiently waited for me to complete my studies, and whom have lovingly cared for our daughter while I was away. I look forward to a future with you!

Abstract

This thesis involves the investigation of both static and fatigue performance of two different longitudinal shear situations. The first being axially loaded threaded rods with small rod to grain angles. The second situation is longitudinal radial and longitudinal tangential shear properties for GL30c glulam. This thesis is therefore divided in three parts. The first part consists of introduction and general literature. The second part is the investigation of threaded rods. The third part is the investigation of longitudinal shear properties of GL30c.

For the second part, a total of 10 static and 11 fatigue specimens were tested, this results in 20 static connections and 22 fatigue connections. For fatigue testing, a stress ratio of 0.1 were used. The normalized maximum stress was 75%, and the frequency were 5 hertz.

The static capacity found from static testing were lower than anticipated. While the fatigue strength was better than anticipated with the slope of the SN-curve being 0,0374 for withdrawal in grain direction and 0,0398 for withdrawal at 5-degrees to grain direction.

For the third part, a total of 51 static tests and 48 fatigue tests were conducted for two different designs which both had longitudinal radial and longitudinal tangential orientation. This part also included an optimization of the shear test which was used. This optimization was done as part of a collaboration. The specimen was modeled numerically, and strains were measured on the surface using video extensometer.

Approximately 77 % of specimen failed by fracture propagation of a single plane. While the remaining 23% formed two planes. This is a considerable improvement compared to previous optimization.

The characteristic shear strength $f_{v,g,k}$ ranged between 3.51 MPa and 4.26 MPa depending on specimen design and orientation. The mean G-modulus was found to be 619 for longitudinal radial orientation and 1145 for longitudinal tangential. The longitudinal tangential value is somewhat high as it comprised of contributions from both planes and needs to be transformed. These values correspond overall well with literature.

The slope of the SN curve was between 0,0527 and 0,0815 depending on design and orientation. These values correspond well with literature.

Sammendrag

Denne oppgaven tar for seg undersøkelse av å bade statisk og utmattingskapasitet for to ulike skjærsituasjoner. Den første situasjonen er aksielt belastede gjengestenger nær fiberretning. Den andre situasjonen er langsgående skjæregenskaper i Gl30c Limtre. Denne oppgaven er derfor inndelt i tre deler. Del 1 omhandler introduksjon og generell utmattingsteori i tre. Del 2 omhandler undersøkelse av aksielt belastede gjengestenger. Del 3 Omhandler skjæregenskaper i tre.

I del 2 er det utført 10 statiske og 11 dynamiske forsøk som gir 20 statiske forbindelser og 22 dynamiske forbindelser. For utmattingstestingen er de viktigeste last parameterne som følger. Stress forholdet R er 0.1, den normaliserte maksimale laster er 75% og frekvensen er 5 hertz.

Den statiske kapasiteten fra del 2 var lavere enn forventet. Derimot var utmattingskapasiteten bedre enn forventet. Helningen på SN-kurven var 0,0374 for uttrekk i fiberretningen og 0.0398 for uttrekk 5 grader på fiberretningen

I del 3 ble det utført 51 statiske forsøk og 48 utmattingsforsøk, dette inkluderer to ulike design av skjærtesten hvor hver av disse er testet i både tangentiell og radiell retning. Denne delen innebær også en optimalisering av skjærtesten som ble gjennomført i et samarbeid. Skjærtesten ble modellert numerisk og tøyninger ble registrert på overflaten med bruk optisk måling.

Om lag 77% av forsøkene dannet en enkel bruddflate mens de resterende 23 % dannet to bruddflater. Dette er en betraktelig forbedring fra tidligere optimalisering.

Den karakteristiske skjærkapasiteten $f_{v,g,k}$ ble estimert mellom 3.51 MPa og 4.26 MPa avhengig av design og orientering. Dette stemmer godt overens med verdier fra litteraturen. Den gjennomsnittlige G-modulen ble estimert til 619 MPa for radiell retning og 1145 MPa for tangentiell retning. Den tangentielle verdien er noe høy sammenlignet med litteraturen. Dette forekommer som et resultat av manglende transponering. Den oppgitte verden består av bidrag fra både radiell og tangentiell retning.

Helningen til SN-kurven ble estimert til mellom 0.0527 og 0.0815, avhengig av orientering og test type.

Table of contents

Part I - Introduction, overview and general literature review.

Part II – Static and fatigue testing of axially loaded threaded rod in small rod to grain angles

Part III – Static and fatigue testing of longitudinal shear

List of figures

List of tables

Abbreviations

NTNU	Norwegian University of Science and Technology
LCF	Low cycle fatigue
HCF	High cycle fatigue
EW	Earlywood
LW	Latewood
DIC	Digital image correlation
TL	Tangential Longitudinal
RL	Radial Longitudinal
MC	Moisture content
DOL	Duration of Load
RH	Relative humidity
COV	Coefficient of variation
FEA	Finite Element Analysis
Glulam	Glued-laminated timber
EC5	Eurocode 5

Symbol list Part 2

H	Heigth of specimen [mm]
w	Width of specimen [mm]
d	Depth of specimen [mm]
$f_{ax,\alpha}$	Characteristic withdrawal capacity
F_{est}	Estimated maximum static failure load
f_k	The relevant characteristic strength
l_{eff}	Embedment depth
N	Number of cycles
NOC	Number of cycles
$\Delta\sigma$	stress range
Δf	Normalized load range
ρ_{12}	Density at 12% moisture content
σ_a	Amplitude
σ_m	Mean stress level
σ_{min}	Minimum stress level
σ_{max}	Maximum stress level

Symbol list Part 3

H	Total height of specimen [mm]
d	Depth of specimen [mm]
w	Width of specimen [mm]
h	Height of shear zone in [mm]
t_1	Thickness of cut 1
t_2	Thickness of cut 2
b_1	Distrance from egde 1 to shear plane
b_2	Distrance from egde 2 to shear plane
V_{12}	Volume of specimen with 12% moisture content [kg/m^3]
ρ_{12}	Density of specimen with 12% moisture content
A_{shear}	Shear area
F	Force, load applied
E	Modulus of elasticity [N/mm^2]
G	Shear modulus [N/mm^2]
σ	stress
τ	Shear stress
s	Standard deviation
y	Mean
N	Number of cycles
NOC	Number of cycles
N90	Notched-90 design
N45	Notched-45 design
R	stress ratio

Part I - Introduction, overview and general literature review.

1 Introduction

1.1 Background and problem statement, threaded rod

Due to its unique structural properties, environmental low impact and esthetic qualities, timber structures are becoming more and more attractive. However, timber structure's competitiveness is largely dominated by its connections.[1] New connections therefore holds great potential in a wide scope of structures, both new and renovated. Such a new connection is the threaded rod, see figure below for possible applications. The threaded rod is very promising in terms of manufacture, performance, aesthetics and cost, other desirable attributes are [2]:

- Stiffer connections for beam-to-column connections, giving lower deformation and favorable moment distributions with regards to load carrying capacity.
- Stiffer connections give stiffer structural systems with increased load carrying capacity for horizontal forces, and reduced deformation.
- Better vibration performance.
- Better energy dissipation giving more robust structures and better performance under seismic load.
- Reduced assembly time and easier production of connection compared to dowel type connections.
- Better control of production compared to glued in rods.
- Reinforcement towards splitting cracks when mounted with an angle to the grain.

Several of these attributes are especially important in structures which experience dynamic loading such as factory building floors with vehicle loads, timber roofs with wind load and bridges with traffic load. However little research has gone into investigating the fatigue properties of axially loaded threaded rods. Stamatopoulos [2] concluded for future work that the effect of dynamic loading was of major importance to such structures.

As there exists little research on this topic, this thesis will focus on experimental results and investigation, as this will contribute the most to the future development and application of threaded rods.

A similar study of threaded rods was conducted in 2016 by Løkken [3]. Løkken wrote her master thesis on fatigue of threaded rods perpendicular to grain. However, due to large penetration depths, the steel rods failed first, giving few results on the fatigue of timber. There were also some issues related to her setup for testing in fatigue.
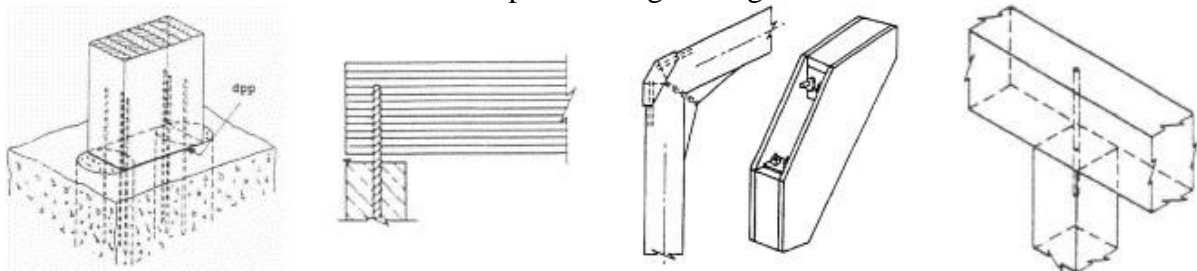
Figure 1 – Some possible applications for threaded rods in glulam [1]

1.2 Background and problem statement, shear testing.

Fatigue life of glued laminated timber is dependent on the stress situation due to timbers orthotropy. For connections like withdrawal of rods in grain direction. Longitudinal shear is imposed on the timber along the timber-rod interface. Fatigue testing of the longitudinal shear properties are therefore important not only to threaded rods but also to other connectors. Several setups for longitudinal shear testing of timber exists, but the majority of these produce a stress situation comprising of normal and shear stresses, which underestimates the capacity or makes it difficult to interpret. The theory for a new shear test was developed by Professor Kjell Arne Malo[1]. This test will be experimentally investigated with regards to both static and fatigue properties in longitudinal tangential (hereafter LT) and longitudinal radial direction (hereafter LR). The experimental investigation is conducted parallel to optimization of the specimen in a collaboration with PhD-student Katarzyna Ostapska- Luczkowska[2]. Therefore two different designs are tested.

1.3 Objective and structure of thesis

Based on section 1.1 and 1.2 the objective of this thesis is to give a more comprehensive knowledge on the fatigue properties of axially loaded threaded rods, as well as the fatigue properties of glue laminated timber in longitudinal shear. The focus will be on production of results as this is assumed to contribute the most to the development of timber structures in fatigue applications. Similarities between the longitudinal shear and the threaded rods with regards to properties, is not part of the scope for this thesis and will only be mentioned in brief, hence this thesis is divided in three parts each with its own objective. This is done in order to make this thesis easier to read and at the same time, underline the disconnection of parts.
:

Part 1 – Introduction, overview and general literature review.	The objective of this part is description of objectives and limitations as well as a general literature review on fatigue in timber.
Part 2 – Static and fatigue testing of axially loaded threaded rod in small rod to grain angles.	The objective for this part is to experimentally investigate the fatigue properties of threaded rods with small grain to rod angles.
Part 3 – Static and fatigue testing of longitudinal shear	The objective for this part is to experimentally investigate the fatigue properties of longitudinal shear in glued laminated timber, using a new shear specimen.

1.4 Limitations

Fatigue testing is time consuming and the following limitations will therefore apply for the fatigue testing of axially loaded rods, originally the aim was a wider scope of parameters, but due to a high number of cycles, the parameters are limited to the following:
- Only one penetration depth is considered t=180 mm.
- The load parameters are limited to R=0.10, f_{max}=0.75 and a frequency of 3,5 Hz.
- Climate class 1 implying 65% relative humidity and 20°C.

---

[1] Professor, Dept. of Structural Engineering, Norwegian University of Science and Technology NTNU
[2] Ph.D-student, Dept. of Structural Engineering, Norwegian University of Science and Technology NTNU

- The testing is limited to 0 and 5 degrees. Specimens were produced for 15 degrees as well, but never tested.
- The effect of duration of load (DOL) is not investigated as we assume that testing will be conducted for shorter periods of time.
- The microstructure of the fracture is not investigated.
- The withdrawal stiffness is not considered due to time limitations, the withdrawal stiffness was also thoroughly investigated by Stamatopoulos [2]
- Hysteresis loops are not considered.

For the shear testing the following limitations apply:
- The load parameters are limited to R=0.10, f_{max}=0.75 and a frequency of 5 Hz.
- Climate class 1 implying 65% relative humidity and 20°C.
- The effect of duration of load (DOL) is not investigated as we assume that testing will be conducted for shorter periods of time.
- The microstructure of the fracture is not investigated.
- A size effect is not investigated in this thesis, see Spera et al [4] for more information on size effect in laminated Douglas fir/epoxy composite material.
- Hysteresis loops are not considered.

2 Fatigue, state of the art

From section 1.1 and 1.2, it is seen that timber connections are desirable in structures that experience dynamic loading like factory building floors with vehicle loads, timber roofs with wind load and bridges with traffic load. To evaluate threaded rods and glue laminated timber, and their usability in such applications, the fatigue life (or fatigue strength), must be determined. The following chapters contains a review of the most important theory concerning the fatigue life of timber.

2.1 Introduction

Fatigue damage is the accumulation of microstructural damage due to dynamic loads, which eventually lead to fatigue failure at a lower load level than the static short-term capacity. The fatigue life is defined as the number of cycles N, at which a structure can withstand at a specified stress level or range. More on the fatigue load parameters in chapter 2.3-Fatigue load parameters.

It is important to be aware that structural timber is not free of fatigue damage prior to service life, because wood contains inherent damage, accumulated throughout the lifetime of the tree prior to service. This damage can be developed prior to service life, during harvesting, during cutting, or during service. Biological agents might also impose fatigue damage, see [5] for more information. A large portion of variability in mechanical properties and fatigue life expectancy is due to this inherent damage. [5]

Since this thesis involves timber connectors with steel components, a familiarity with fatigue in steel is advised. Good literature for this can be found in [6]. For this thesis, it is presumed adequately to mention that steels fatigue damage and accumulation is different to timber and is highly dependent on the surface quality, finish and stress distribution. Welding will introduce stress gradients and cracks which severely shortens the fatigue life of steel. The materials behave quite different under stress. Wood for example, is less sensitive to tension stresses than steel, as the microstructural damage is distributed among the microfibrils in the cross-sectional surface, more on this in chapter 2.2-Microstructure . [5]

The microstructure of the cell wall, the fatigue loading parameters and the moisture content are the predominate sources to woods response and damage to static and fatigue loading. [7] Therefore these topics will be reviewed in the following chapters.

2.2 Microstructure

To understand the mechanical aspect of fracture and fatigue in timber, it is necessary to take a brief look at the microstructure of wood. The most characteristic appearance of timber is the centric arrangements of annular rings. These rings are composed of light earlywood (EW) and dark latewood (LW). EW is produced early in the growth season and has less density to allow for more moisture transportation than the denser LW which play an important part in the loadbearing of the three. The boarders between LW and EW are important crack stopping interfaces when the timber is subjected to fatigue and static loads. [7] The weakest link however is the radial cells (medullar rays) which propagate from the pith to the bark, see figure 2. Wood easily cracks along these rays forming radial-longitudinal cracks which the fracture in fatigue often propagate onto. This tendency is clearly visible in the static and fatigue testing of shear specimens, see figure 2 and later chapters.

Figure 2 - radial cracks in both lamellas in a radial Longditudional test specimen D1-12.

Another important aspect of fatigue can be seen when examining the cellular walls in the microstructure of wood. In softwoods 3-5 mm long tracheids make up approximately 90-95% of the volume and is the key component in determining the mechanical properties of softwood. [5] Because of this, In the cross-sectional plane, wood is a strong anisotropic material. The tracheids are from the outside to the inside comprised as described in Table 2.1. Table 2.2 shows black lines which describe the orientation of the microfibrils which has a thickness of approximately 15 μm. The microfibrils are bundles of crystalline cellulose molecules, which are entwined in a matrix of amorphous lignin and hemicellulose, which also can be regarded as amorphous. This structure of microfibrils is the main loadbearing component in timber, and the change in static and fatigue load capacity is mainly due to change in this structure.[5, 7]

From outside to inside	Parts	Relative thickness	Composition
Outside: Middle lamella		5%	Rich on Lignin and holds the thracheids togheter
Primary wall		Together with middle lamella	Extremely thin wall that is usually associated with the middle lamella, has loosely packed microfibrillis.
Secondary wall	S1- Outer	10%	Cross-laminated microfibrillis.
	S2 – Middle	75%	Thickest layer, comprising aprox. 85% of the thickness of the cell wall. The microfibrillis in this layer has a right hand orientation by aprox 10-30 degrees.
	S3 – Inner	10%	Cross-laminated microfibrillis.
Innside: Void or lumen			Hollow core which transports water in the living part (Sapwood) and stores sap in the dead part (Heartwood). Each cell void is interconnected via openings in the cell walls.

Table 2.1 - Microstructure of cell walls, based on [5, 7]
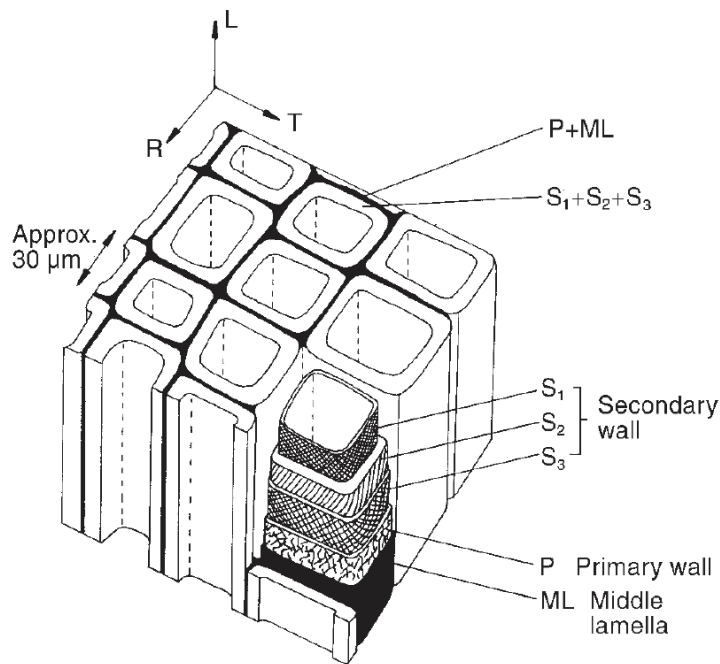
Table 2.2 – Microstructure of wood cell wall

2.3 Fatigue load parameters and load configuration, and their effect on fatigue life

When reviewing the fatigue load, several parameters and aspects should be considered. In the following these parameters and their effect on the fatigue life are reviewed.

2.3.1 High cycle fatigue (HCF) and low cycle fatigue (LCF)

When considering the fatigue process, it can be separated between low cycle fatigue (LCF) and high cycle fatigue (HCF). This separation is due to the fact that accumulation of damage in the two scenarios behave quite different. It can be separated between the two based on number of cycles (N) before failure occurs. For metals, it is usual to differentiate between HCF and LCF for 10000 cycles [6]. This boundary limit has been suggested reasonable for wood as well [5].

LCF is characterized by higher load levels relative to ultimate static capacity which gives plastic deformation. This is typical for rarer higher loads with fewer cycles before failure, such as earthquakes.

HCF is characterized by lower load levels relative to ultimate static capacity resulting in three phases of crack propagation; damage initiation, steady damage propagation, and increased rate of energy dissipation up to failure, see [8] for more information. HCF failure is typical for normal load situations like traffic load on a bridge where many cycles can be expected, with a frequent load before failure occurs.

This thesis focus mainly on HCF as this is the common fatigue process when considering fatigue due to normal structural loads. However, due to variation in ultimate capacity both cases are registered in the results.

2.3.2 Harmonized waves and stress ratios

For practical and economic reasons, harmonized waves are used to measure the fatigue life when conduction fatigue experiments. These harmonized waves are solely described by the

6

parameters σ_{max}, σ_{max} and the frequency. The following formulas are used to describe the stress variation.

$$\sigma_m = \frac{\sigma_{max} - \sigma_{min}}{2} \tag{1}$$

$$\sigma_a = \frac{\sigma_{max} - \sigma_{min}}{2} \tag{2}$$

$$\Delta\sigma = \sigma_{max} - \sigma_{min} \tag{3}$$

$$R = \frac{\sigma_{min}}{\sigma_{max}} \tag{4}$$

Where:

σ_{max}	Maximum stress level for the cycle
σ_{min}	Minimum stress level for the cycle
σ_m	Mean stress level
σ_a	Stress amplitude
$\Delta\sigma$	Stress range
R	Stress ratio
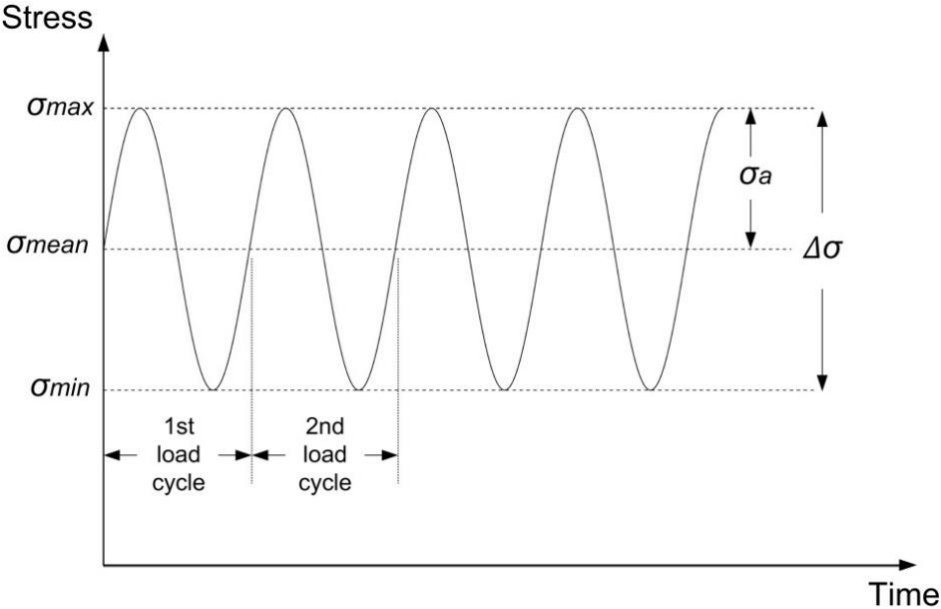
Figure 3 – Harmonized stress variation

Different stress ratios R, implies different load situations. The stress ratio varies from ∞ to -1. See Figure 4 – Stress ratio [3]. A stress ratio R, between 0 and 1 implies a tension-tension configuration which means that the entity of the cycle is pulsating in tension. See the table for depiction of the other configurations.
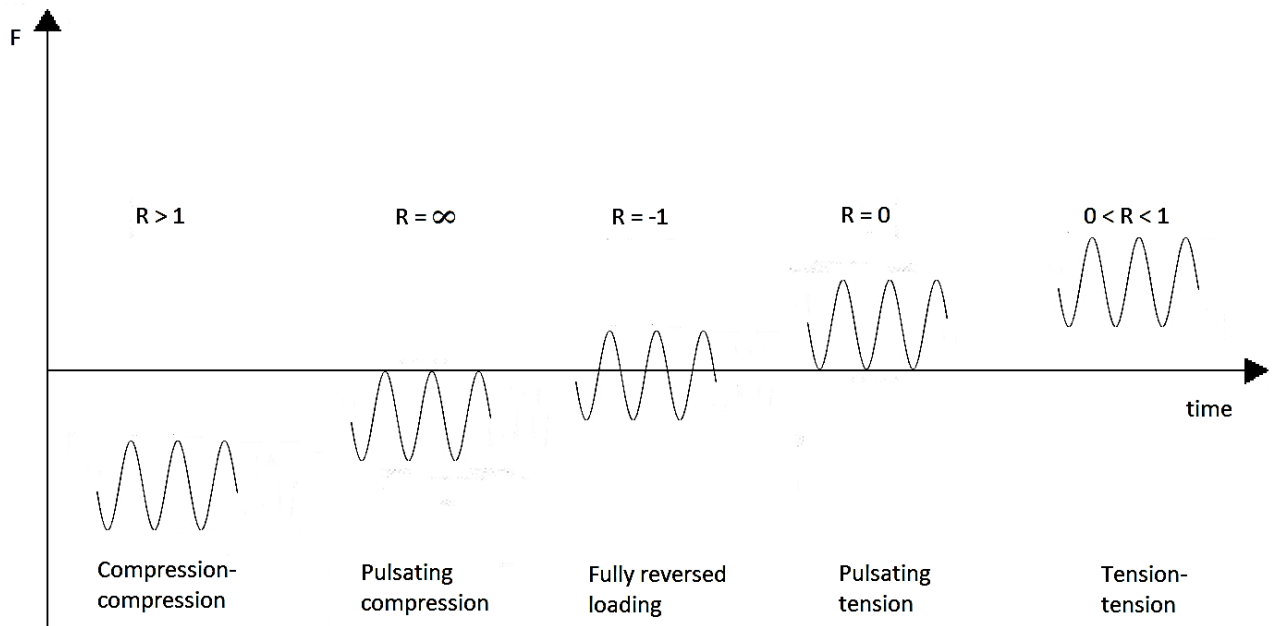
Figure 4 – Stress ratio [3]

The sinusoidal wave is expressed by the following formula:

$$y(t) = C + Asin(2\pi ft + \varphi) \hspace{4cm} (5)$$

Where

C	A constant defining a mean level
A	Amplitude, peak deviation from zero
f	Frequency (Hz), or oscillations per second
φ	Phase, specifies the location of the cycle at t=0 in radians.
t	Variable expressing time

Tsai and Ansell [9] investigated the effect of stress ratio R, and found that a reversed loading lead to the shortest fatigue life. This affect can be described by looking at the microstructure. Loading wood in compression past the fatigue limit cause local buckling of the microfibrils in the cell wall. This effect also accounts for the lower ultimate compression capacity. In tension the helically wounded microfibrils in the secondary wall will unfurl which creates internal shear interaction between the neighboring layers of microfibrils. In compression-compression sub-critical micro-buckling of the microfibrils will accumulate. While in tension-tension, fatigue critical shear damage will accumulate. In reverse loading it is likely that tension will open up damages caused in the previous compression part of the cycle thus increasing the damage inflicted per cycle.[7] Reversed loading is therefore the most damaging loading configuration to timber. This was also concluded by Hacker and Ansell [10]. In their research, they investigated the fatigue life effect of tension-tension (R=0.1), compression-compression (R=0.1) and fully reversed loads (R=-1) for laminated Khaya specimens. The same results were also reached by Bond and Ansell [11, 12]. Their results also supported the claim that fatigue strength is species-independent. This independency is important for the comparison of research material conducted on different materials. The experiments in this thesis uses R=0.1 as this is the typical load situation for a brigde.
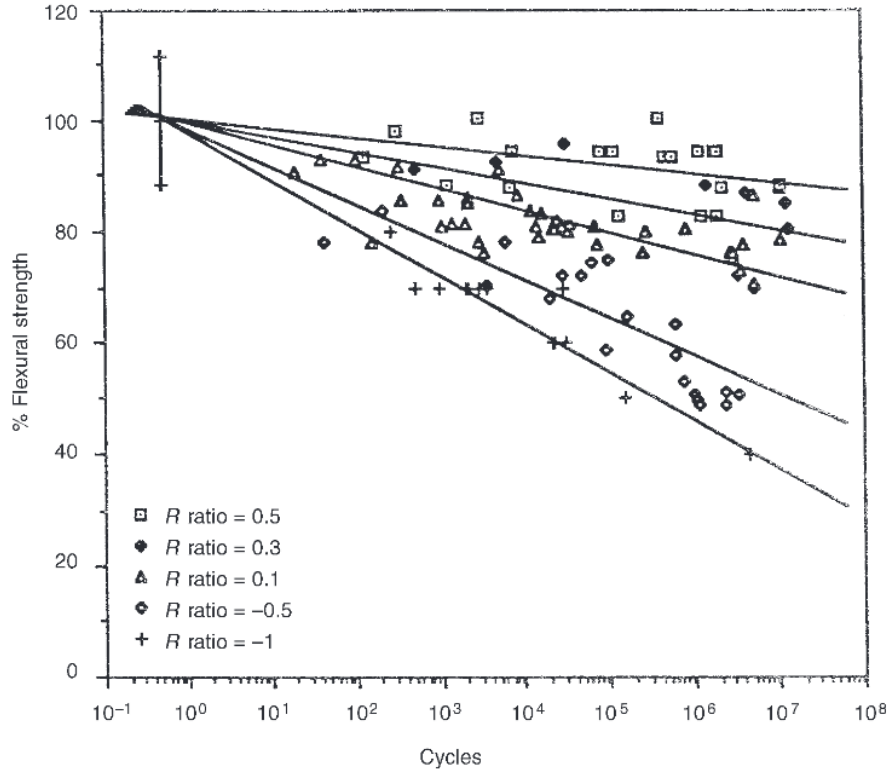
Figure 5 – SN-curve for different stress ratios R.

2.3.3 Normalized stress

To describe the rate of stress in reference to the ultimate static capacity, the normalized stress range is used. This means that normalized maximum stress (or just rate of stress) describes the maximum stress level in reference to the ultimate static capacity. This opens the possibility to compare specimens of different size proviso the use of similar conditions.

$$\Delta f = \frac{F_{max} - F_{min}}{F_{ref}} = \frac{\sigma_{max} - \sigma_{min}}{\sigma_{ref}} \tag{6}$$

$$f_{max} = \frac{F_{max}}{F_{ref}} = \frac{\sigma_{max}}{\sigma_{ref}} = \frac{\Delta f}{1 - R} \tag{7}$$

Where:

Δf	Normalized stress range
f_{max}	Normalized maximum stress (or just rate of stress)
F_{max}	Maximum applied load
F_{min}	Minimum applied load
F_{ref}	Static reference load

9

Knowing the rate of stress, which will be used in testing, the maximum and minimum values of the sinusoidal wave can be described, together with the mean value, which might cause DOL-effect see chapter 2.3.5.

$$F_{max} = f_{max} * F_{ref} \qquad (8)$$

$$F_{min} = F_{max} - f_{max}(1 - R) * F_{ref} = f_{max} * F_{ref} * R \qquad (9)$$

$$F_{mean} = \frac{F_{max} - F_{min}}{2} \qquad (10)$$

Thus, expression (5) can be rewritten as:

$$(11)$$

$$y(t) = C + Asin(2\pi ft + \varphi)$$

$$= F_{mean} + (F_{max} - F_{mean})sin(2\pi ft)$$

2.3.4   Frequency

Another aspect to consider when reviewing harmonized waves, is the influence of frequency on fatigue life. Several studies have investigated the effect of frequency for a variety of parameters. And in some cases, the influence of higher frequencies than 5 hertz has proven to give a longer fatigue life. Other studies has shown no influence of frequency [13]. The most comparable tests are Clorius et al [14].

Clorius et al [14] investigated the effect of frequency (0.01, 0.1, 1 and 10 Hz) when using square waves for compression load in 80% of quasi-static capacity on Norwegian spruce. The result was significantly different fatigue lives where the highest frequency gave the longest fatigue life. The heat increase was also noticeable.

In another research Clorius et al investigated the fatigue life of Norwegian spruce subjected to tension in the tangential direction, perpendicular to grain. Parameters subjected to study were frequency (00.1 Hz, 0.01 Hz), stress level (50% and 65%) and RH (65% and 85%), DOL, R=0. The results showed no influence of frequency at 65 % stress level and 65% RH. But influence was noticeable for 50% stress level and 85% RH. This suggests a strong influence of DOL.

2.3.5   Duration of load

Duration of load (DOL) can have a large influence on the fatigue life as investigated by Clorius. A high duration of load, or sustained load, will cause creep in timber structures due to timbers rheological properties. However, this effect is not investigated in this thesis as we assume a shorter duration of time, see 1.4 Limitations.

The effect of DOL in combination with fatigue, can be seen on the hysteresis loop as a horizontal movement along the compressive strain axis, see Figure 6. This is reasonable when considering that fatigue imposes a mean stress with a fluctuation around it on the specimen. In the same sense, a creep test can be seen as a fatigue test with zero amplitude (R=0).

(a)
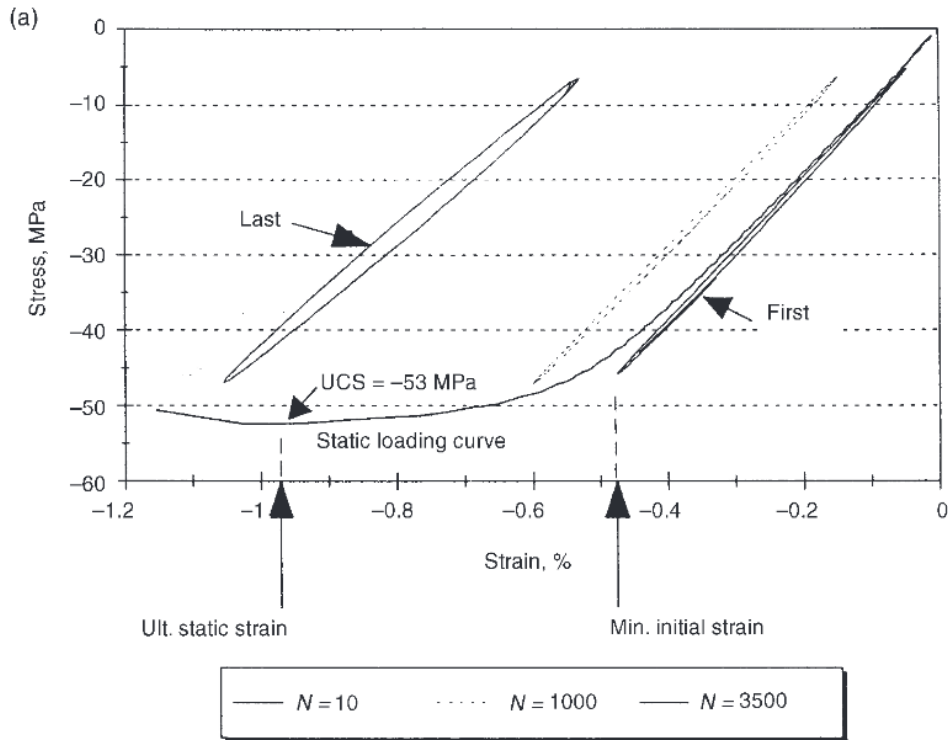
Figure 6 – hysteresis loop for khaya laminate. Captured at R=10 with σmax=-47.5 MPa after 10, 1000, and 3500 cycles with static loading curve for comparison. [7]

In this thesis, a frequency of 3 and 5 Hz is used, based on the test machines capabilities. The temperature of all specimens was measured and no noticeable increase in temperature was detected on the surface.

2.3.6 Load controlled or displacement controlled load-cell

Load controlled or displacement controlled rigs, are perhaps not a parameter in fatigue life in the normal sense, but it is of importance to the hysteresis loop and is therefore included here. In the hysteresis loop, a load controlled rig may give dynamic creep. While a displacement controlled rig may give dynamic stress relaxation.[7] Therefore this property is important when interpretation the hysteresis loop.

Tsai (1987) [7] which has published detailed reviews on fatigue of various wood species and wood laminates. Comments in his work that much information on fatigue testing methods are absent or vague in published work, especially whenever the testing is conducted as load or displacement controlled. Another issue which makes comparison difficult is the large variety of loading configuration.

2.4 Moisture content and temperature

The water chemically bound in the cell walls plays a major role in the stiffness and strength of wood, and thereby also the fatigue life of wood. When dried past the saturation point, the stiffness and strength of timber increases, and thereby also the fatigue life. This effect is also investigated in [9] (Tsai KT, Ansell MP), they concluded that increasing moisture content (MC) reduced the fatigue life. This can be seen in Figure 7 – SN-curve for variation of moisture content in Khaya laminates in fatigue at R=0.1 in flexure loading. [7]

11
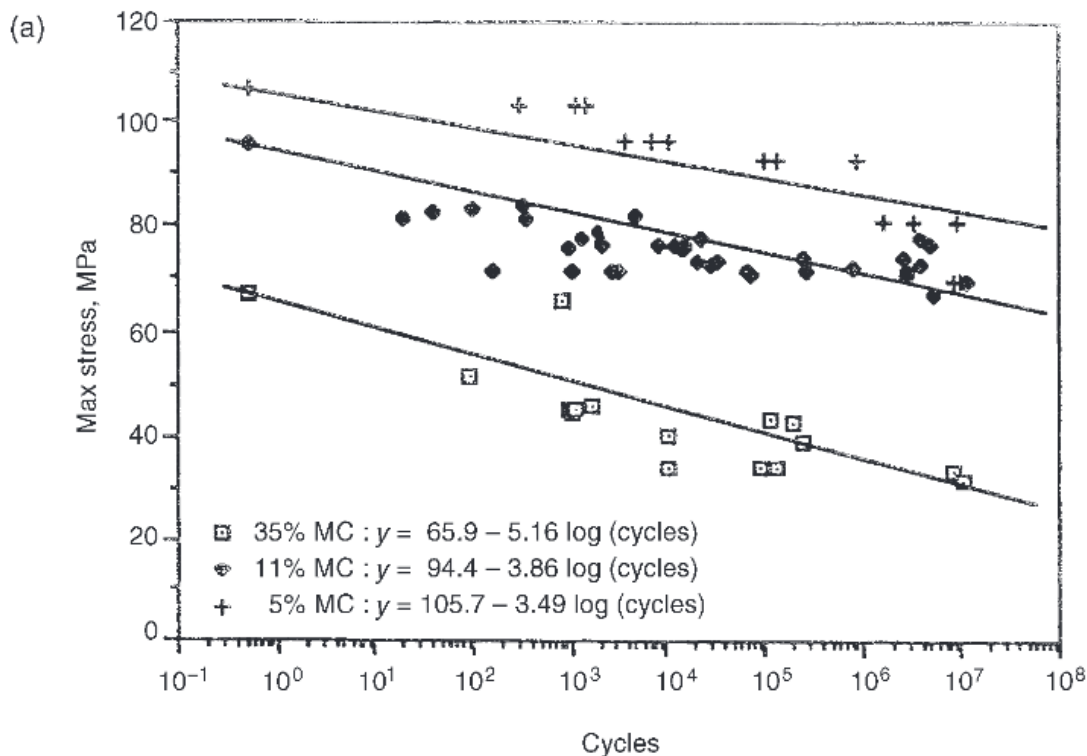
Figure 7 – SN-curve for variation of moisture content in Khaya laminates in fatigue at R=0.1 in flexure loading. [7]

2.5   Other considerations

2.5.1   Size effects

Spera et al conducted an extensive experimental investigation on veneer-laminated Douglas-fir [4]. They found that fatigue strength is characterized by a size-effect. Such an investigation is not conducted in this thesis. But should be mentioned as it might be observed.

2.5.2   Solid timber and laminated timber

This thesis focuses on Glulam, but, a lot of research has been conducted on solid timber. However, the research on solid timber can be used for comparison as it appears that fatigue life in sold timber and fatigue life in laminated timber is quite similar. The choice of raisin can have a minor effect.[7]

2.6   Fatigue life prediction

2.6.1   S-N curves

The fatigue life of materials is classically represented in the form of SN-curves. These curves represent the logarithmical number of cycles N before failure along the x-axis, and a stress level or stress range S along the y-axis. In this thesis, a normalized maximum stress (f_{max}) is displayed along the y-axis. Malo [15], argued that for R=0,1 both f_{max} and Δf gave equally good fitting to the results, but that f_{max} seemed the most reasonable for alternating loads. To express the results in the form of load level is also a possibility but this makes comparability obscure. Therefore, in this thesis, f_{max} is chosen based on comparability to other research. See Figure 7 and Figure 10 for examples of classical SN-curves, see also Figure 11 for a normalized SN-curve.

12

2.6.2 European standards

Fatigue verification according to Eurocode 5 (EC5) [16] is based on a simplified design method. The method uses an equivalent constant amplitude fatigue load to represent the entire fatigue load spectrum. To determine whenever a fatigue verification is needed the dimensionless ratio κ can be used.

$$\kappa = \frac{|\sigma_{d,max} - \sigma_{d,min}|}{\frac{f_k}{\gamma_{M,fat}}} \tag{12}$$

Where:

$\sigma_{d,max}$	Numerically maximum design stress
$\sigma_{d,min}$	Numerically minimum design stress
f_k	Characteristic quasi-static strength
$\gamma_{M,fat}$	Material partial factor

This can be compared to ratio κ to the limit values in EC5-Part 2 6.2(3), see Table 2.3. If the ratio κ is larger than the limit values, an extended verification is needed.

Type of loading or joint	Limit value
Members in compression parallel or perpendicular to grain	0.60
Members in bending or tension	0.20
Members in shear	0.15
Connections with dowels	0.40
Connection with nails	0.10
Other connections	0.15

Table 2.3 – limit values for the ratio κ from [16].

From EC5 table 2.1 the fatigue safety factor $\gamma_{M,fat} = 1.0$ can be found. The extended verification is given in EC5-A.3. The verification criterion is as following:

$$\sigma_{d,max} \leq f_{fat,d} \tag{13}$$

$$f_{fat,d} = k_{fat} \frac{f_k}{\gamma_{M,fat}} \tag{14}$$

$$k_{fat} = 1 - \frac{1-R}{a(b-R)} \log(\beta N_{obs} t_L) \geq 0 \tag{15}$$

Where:

$f_{fat,d}$	The design fatigue strength

k_{fat}	Factor for reduction of strength depending on number of cycles (N)
N_{obs}	The number of constant amplitude stress cycles
t_L	Design lifetime of structure according to EN 1990
β	Factor for consideration of failure consequence
a, b	Coefficients form EC5 table A.1.

The factors a and b does not correspond to fatigue of rod, however the closest values are constructional elements in shear. Which gives a=6,7 and b=1,3. These values are also applicable for the shear specimen. The factor for consideration of failure consequence can be taken as $\beta = 3$ for substantial consequences or $\beta = 1$ for non-substantial consequences.[16] Based on equation (15), the equation for the reduction factor can be we rewritten as;

$$k_{fat} = 1 - A * \log(N) \tag{16}$$

Where

$$A = \frac{1 - R}{a(b - R)} \tag{17}$$

$$N = \beta\, N_{obs} t_L \tag{18}$$

 This expression can be used to compare the Eurocode design criteria to SN-curves derived from testing.

Part II – Static and fatigue testing of axially loaded threaded rod in small rod to grain angles

1 Introduction

This part considers axially loaded threaded rods in 0 and 5-degree to the grain direction. Both static and fatigue properties will be experimentally investigated. In the following, what little research that exist and are relevant is summarized.

2 Literature

2.1 Withdrawal capacity of threaded rods embedded in timber elements.[17]

This journal article was conducted by post doctor Haris Stamatopoulos and professor Kjell Arne Malo, both from the department of structural engineering at NTNU. Both Stamatopoulos and Malo are supervisors for this thesis.

In this journal article the withdrawal capacity of threaded rods are studied by theoretical and experimental approach. The theory is based on Volkersen classical theory and assumes a bi-linear constitutive law. The experimental results are presented for a wide range of rod to grain angles and embedment depths. A near linear relation between embedment depth and withdrawal capacity was observed.

For their experimental testing, Malo and Stamatopoulos used a push-pull configuration with Norwegian glulam L40c which corresponds to GL30c (CEN2013), same as in this thesis. The rod which they used had a constant core diameter of 15 mm which also deviates from this thesis. The temperature and relative humidity is the same. This thesis concerns 180mm embedment depth while Malo and Stamatopoulos used 100 mm and 200 mm. We can use linear interpolation and compare the results. However, the results might not be comparable due to different setups. This will be investigated.
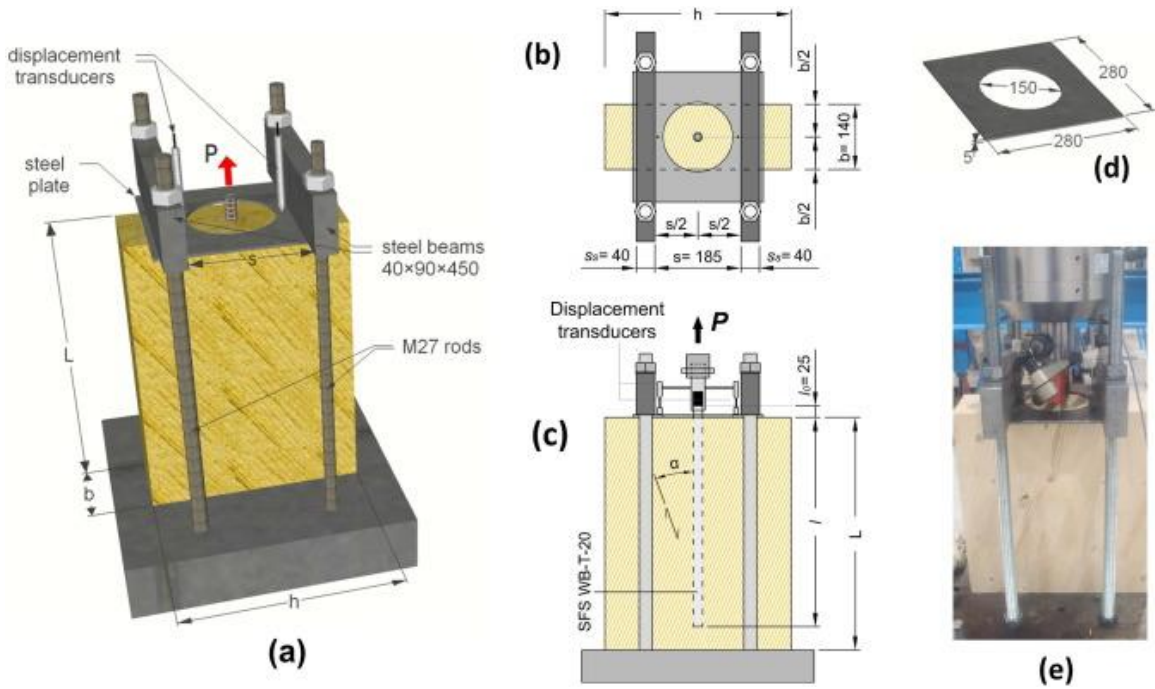
Figure 8 – Experimental set-up for Malo and Stamatopoulos. [17]

2.2   Fatigue performance of bonded-in rods in glulam, using three adhesive types. [1]

This journal article is published as part of the EU GIROD project, which was a collaboration between several nations to draft an acceptable standard for Glued in rods as part of the EC5-part 1.

Testing was conducted to experimentally investigate the fatigue behavior of different adhesives. Especially the two component polyurethanes was toughly investigated, because it showd tendency of a less brittle fracture. Two different specimen geometries were tested, one for 8mm rod and one for 16mm rod. Rods were inserted parallel to grain whit axial load at a frequency of 1 Hz with stress ratio R=0.1. Four failure mechanisms were observed; failure in adhesive, failure in rod, failure in intersection zone, failure in wood. There was sufficient variation to confirm that failure could result in any of the failure modes.
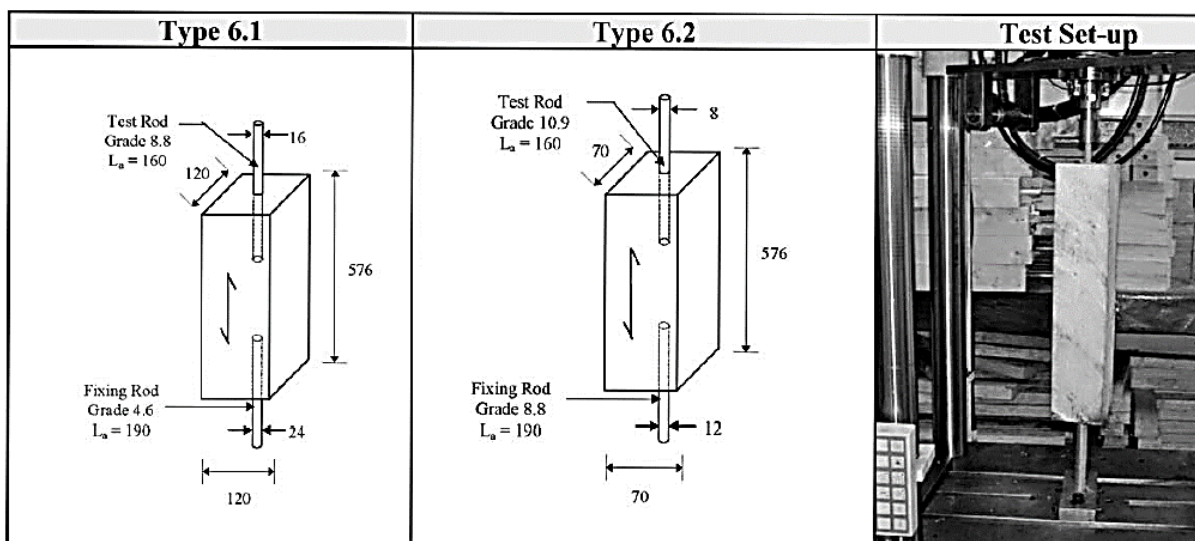
Figure 9 – Two different specimen geometries [1]

The results yielded better fatigue strength for epoxy than PUR and PRF.
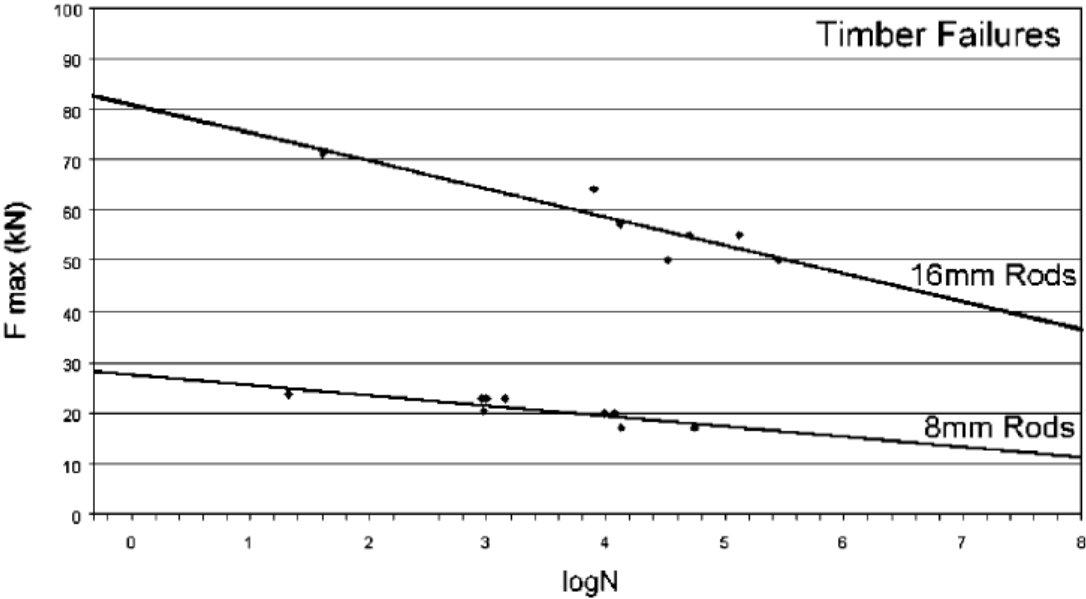
Figure 10 – Fatigue performance for the specimens that yielded fatigue in the timber.

The setup in this experiment is quite similar to what is used in this and the results for fatigue in timber might be comparable.
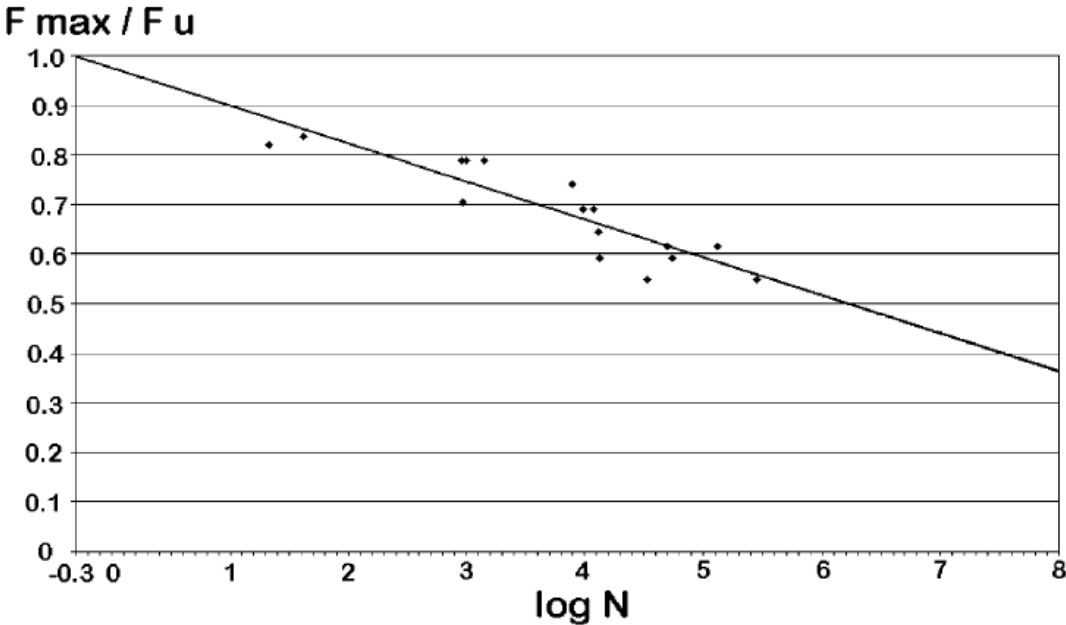
Figure 11 – Normalized values for all specimens with fatigue failure in timber [1]

2.3   Fatigue of threaded rods subjected to axial load [3]

"Fatigue of threaded rods subjected to axial load" is a master thesis written by master student Nina Løkken. The aim of her thesis was experimental investigating of threaded rods. She used the same setup as Stamatopoulos and Malo [2], however, the rod was different, and is similar to the rod used in this thesis. Testing were conducted for 90 and 45 degrees' specimen. Løkken conducted 5 static tests including both 90 and 45 degrees. In fatigue, she conducted 5 specimens for 90 degrees and 6 specimens for 45 degrees. Results were limited by unexpected

problems, and the number of tests were not adequate to make any conclusions. Most of the specimens failed due to fatigue in steel. And this was the tendency she concluded with, that fatigue for penetration depth of 330 mm in timber did not seem to be a problem as fatigue in steel occurs first.

Although the results were inconclusive, Løkkens thesis provided a good literature basis for future work on similar investigation, such as this thesis. Also, the experience from her thesis made it possible to avoid many of the same problems as she experienced. Her thesis provided the basis for the embedment depth chosen in this thesis; 180mm. Although a different setup was used, we will compare results with Løkken, because her objective was closely connected to this thesis.

2.4   Fatigue Strength of Dowel Joints in Timber Structures

This paper is conducted by professor Kjell Arne Malo at the department of structural engineering at NTNU. The paper reviews the fatigue performance of dowel connections in timber structures. The connection considered and the setup is simulating a truss on the Evenstad timber bridge. The report investigates different load ratios R=0,1 and R=-1 and different normalized loads. Both the setup and the load parameters are quite similar to this report, and a comparison will be conducted in the analysis

Figure 12 – Specimen in test rig, by Malo [15]

3   Method

Laboratory testing was conducted to experimentally investigate the fatigue properties of threaded rods embedded in glulam. Glulam is chosen based on the different applications of threaded rods, see introduction. The applications imply fatigue life in the HCF range. Objectivity is highly prioritized and no data is considered more valuable than other. This is underlined by the understanding of safety and knowledge of the vast variety in application of threaded rods where some results may be favorable in some situations but unfavorable in other.

3.1   Materials

The specimen consists of Norwegian spruce Glulam GL30c and Threaded steel rods, see appendix A and B for manufacture documentation.

3.1.1   Glulam

The material classification is GL30c with cross sectional dimensions 140x360 mm, made from 45 mm lamellas.

The classification GL30c implies:

GL	Glue laminated timber
30	Characteristic bending capacity
C	Combined glulam

Combined glulam implies that a portion of the outer lamellas contains a zone (h/6) with stronger properties than the core. For height 360 mm, the two outmost lamellas contains a zone of strength class T22 while the inner part contains a zone of T15, see [18].

Several orders for beams were placed, due to large quantities of specimen. The specimen was produced continuously for both shear specimen and rod specimen. Thus, an ideal sample distribution of specimen in the material is achieved.

All ordered beams had the same cross-section and properties. However, the length was varying.

Beam number	Description	Length
A	Spruce 140x360 GL30c	5000
B	Spruce 140x360 GL30c	5000
C	Spruce 140x360 GL30c	5000
D	Spruce 140x360 GL30c	5000
E	Spruce 140x360 GL30c	5000

F	Spruce 140x360 GL30c	2850
G	Spruce 140x360 GL30c	3050
h	Spruce 140x360 GL30c	3050
I	Spruce 140x360 GL30c	3258
J	Spruce 140x360 GL30c	3850
k	Spruce 140x360 GL30c	3740
L	Spruce 140x360 GL30c	5200

Figure 13- Beam number and lengths

3.1.2 Threaded steel rods

The threaded steel rods are hot-dip galvanized. The top or the stud is M20 8.8, metric threaded and the bottom part is threaded as in Figure 14 with a pitch of 8 mm and outer diameter 22,4 mm. The core or the groves, are slightly angled as shown in the figure. The geometry of the pitch and the cross-section of the rod can be found in appendix A or in the figure bellow.

This rod is used based on request and availability, it was in stock at the laboratory, and requested by the supervisors.
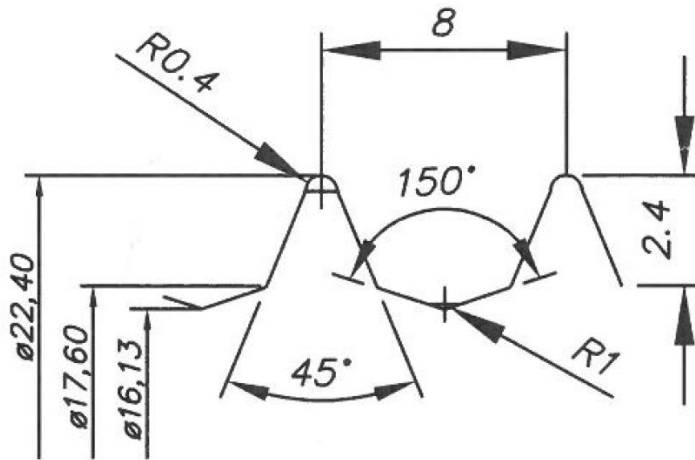
Figure 14 – Pitch and geometry of rod, see appendix A for further information.

3.2 Geometry of specimens

Several specimen geometries and setups were considered. The experience from Løkkens work was that her setup expressed a lot of flexural motion under cyclic loaded. Such a motion can cause bending of the rod and ultimately produce severe fatigue damage. Another aspect was whenever the test expressed pure pull-push conditions or if there was a degree of 3-point bending involved. Based in these experiences it was decided to investigate alternative setups. Two criterions were considered when investigating alternative setups. Experience and similarity to structural application. After consideration of several setups. The choice fell on the well-known setup that is used in [1], "Bonded-in rod connections for timber structures—development of design methods and test observations". The embedment depth of the 16 mm

20

rod is 180 mm. This corresponds very well with the threaded rod whom has an embedment depth of 150 mm and core diameter 16,13 mm. This type of setup was also used by Malo [15] in fatigue tests of dowel joints in timber structures. Malo chose this setup to simulate a truss in the Evenstad timber bridge. This complies well with the intention of this thesis.

The geometry of the specimen is depicted in appendix L and below.
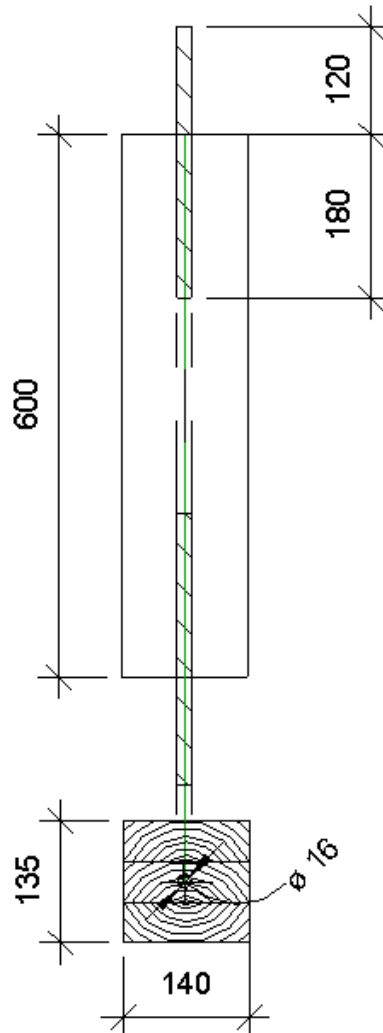
Figure 15-Specimen geometry

The initial cross-section measurements were a result of several considerations:
- The specimen used in [1]
- Availability on timber beams of GL30c 140*360 from shear testing.
- Material optimization with regards to the beams.
- Control of possible failure modes

The initial length of the beam was a result of the following considerations:
- The embedment depth of the rod.
- Material optimization.

- Creating multiple results from the same specimen. By having two equal ends, one will fail before the other based on variation in capacity. To get results from both rods we have to lock the already failed end. This can be done by clamping or insertion of dowels. But this will change the initial conditions. To avoid this, a longer specimen was created. This way, after initial failure of one end. The failed end could be cut off and a new rod could be inserted in that end. Now the other end will most likely fail. Thus, we gain two results from each specimen. The last rod was given the same embedment depth for easier production and to avoid problems with failure on the same side twice, a longer rod could be used but this would be a waste of material.

3.3   Production of specimen

The specimens were produced at the timber laboratory at NTNU. Due to large quantities of specimen most of the workload was conducted by the author and the laboratory personnel gave good assistance when needed. This resulted in a positive experience but also a consistency in the production of specimens with few variations in production methods and technique.

Upon arrival, the beams were quickly moved to a temperature and humidity controlled storage. Containing a constant 65 % relative humidity (RH) and a temperature of 20°C. This gives approximately 12% moisture content (MC) which is climate class 1.[19] The plastic wrapping which is used to prevent exposure during transportation were quickly removed to reintroduce abovementioned conditions.

The production of specimens was tested in advance on a couple of dummies to gain experience and develop a good production proses. The focus of the proses was accuracy and time to avoid drying cracks. The MC was measured during production with an electromagnetic moisture meter. As a result of the dummy production, the production was divided into several steps to reduce dry climate exposure. After finished production, the specimens were stored in the controlled storage for a minimum of 3 days before testing occurred to insure complying MC and temperature.

The specimen were, not visually graded before production as any deficiencies was difficult to detect. However, some lamellas had large drying cracks running through the entire beam, it was avoided to place the rod in the center of these lamella, see Figure 17.

The finished specimen had a smooth surface, the accuracy of specimen was a following:

specimen	Geometric parameter	Geometric measurement	Accuracy
0-degree specimen	h (height)	140	±3mm
	b (breath)	140	±3mm
	d (depth)	640	±5mm
	l (penetration depth)	180	±2mm
5-degree specimen	h (height)	140	±8mm
	b (breath)	140	±8mm
	d (depth)	640	±8mm

l (penetration depth)	180	±2mm

The embedment depth of the rod is 180mm. However, the thread height is declining towards the stud of the rod, see figure below. After production, it was noticed that the embedment depth was not b2 as depicted below, but somewhat bigger. The length of the rod in timber with full thread height were measured to 150 mm, while the full embedment depth was 180mm. To be conservative, 180mm is used in the following.
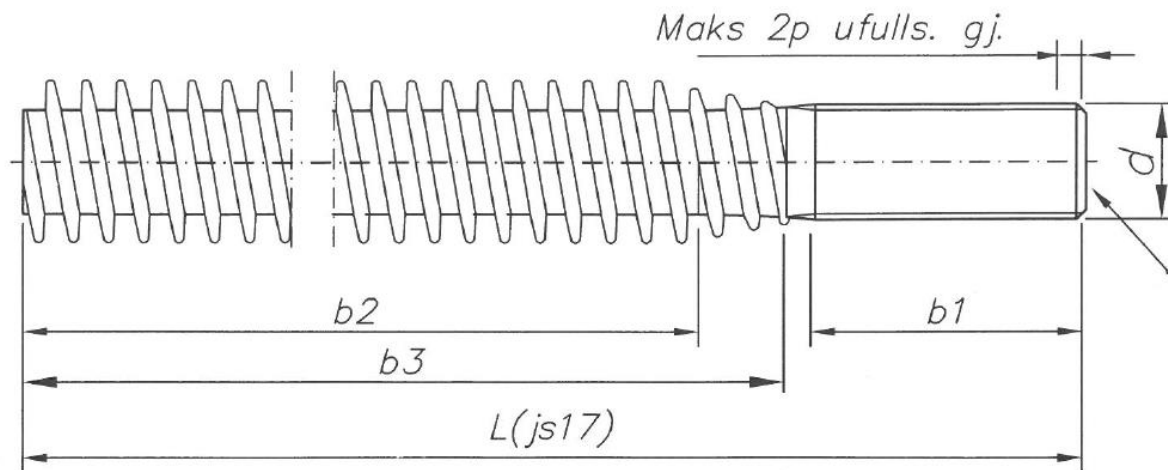
Figure 16- effective embedment depth (b2) and penetration depth (b3)

The fatigue calculations are however not affected, as the load is taken as 75% of the ultimate static capacity.

3.4 Specimen identity
Specimen are identified by informative names to keep track of important information related to the specific specimen. An example is specimen "F0-E7-345". Which implies:

Information type	Part	Alternatives	Description
Information related to test type	F	S, F	S stands for static test and F stands for fatigue test
	0	0, 5	0 is a 0-degree specimen and 5 is a 5-degree specimen
	-		break
Information on beam and placement in beam	E	A-L	All beams are named by letters in the order they arrived. "A" is the first beam and the first specimen produced come from this beam
	7		All beams were divided into cross sectional pieces. To keep track of which specimen lie in the vicinity of each other, all cross-sectional pieces were numbered from 1 at the start of the beam.
	-		break

23

Information on lamellas	123	1-8	Containing lamella 123. Where 2 is the lamella which the rod is inserted in. The numbering of the lamellas are done from the lamella which has the annular rings oriented in the opposite direction to the other lamellas, see Figure 17, here we can see that the upper lamella has the annular rings oriented opposite to the other lamella, therefore the numbering of the lamella in the cross-section of the beam, starts here.

Figure 17 – numbering of specimen, number starts at lamella with annular rings oriented in opposite direction.

3.5 Conditioning of specimen

As mentioned in chapter 2 Fatigue, state of the art. The moisture content along with the microstructure and the load parameters are the predominant factors that determine both static and fatigue properties. The conditioning of specimen are hence of great importance and several measures were implemented to achieve close to ideal conditions.

3.5.1 Conditions during storage and production

The following conditions were measured in the facilities that were used during production and storage. The conditions in the controlled storage follows the standard atmosphere 20/65 according to ISO 554.

Situation/location	RH [%]	Temperature [°C)
Controlled storage/ Ideal class 1 conditions	65	20
Laboratory hall	25	20-25
Timber workshop	20-25	21-25

Table 3.1 – Approximate RH and Tempt in facilities

Some problems occurred with the controlled storage. During Easter break, there was a power outage which broke the RH and temp controller unit. This was not detected until a week later. Therefore, some of the specimen show a bit lower MC, the affected specimen could be excluded or a reduction factor could be implemented. However, this was not done due to the MC variation being quite small, and that such a consideration would take up precious time. This is however a non-conservative assumption because lower MC will give stronger specimen.

3.5.2 Conditions during testing

As shown in Table 3.1, the conditions during testing in the laboratory hall, were not ideal. A vapor barrier was therefore used, inspired by building physics. The ends were taped around the rods. The specimen was tested for temperature increase due to the high frequency. The temperature was measured using an infrared thermometer. No temperature increase was measured.

Figure 18 – Plastic bags used as vapor barriers, clamping in top and bottom

3.5.3 Weighing and drying of specimen

The specimen was weighed and dried to determine their moisture content and density in accordance with ISO 13061-1:2014 and ISO 13061-2:2014 respectively. The process for measuring the mass of the specimen are as described in chapter 3.10.1.

In the 5-degree specimen, the rods will be inserted into one lamella and cross though 2-3 different lamellas. This means that the lamellas surrounding the rod might have different density properties, as the rod can be inserted in a end-lamella with strength class T25 and

penetrate further into inner lamellas with strength class T14. Because of this variation in density in the lamellas surrounding the rod in the, the specimen has been weighed and drying in their entirety. This is to get a density representation of all the lamellas. This is done instead of taking samples like described in ISO 3129. The negative aspect of this representation is that nots and other defects will influence the density calculation. Because of this, the precision level chosen for weighing is $w, {}^0/_0 = 1,0$. Furthermore, no desiccator has been used as the specimen was weighed while they were still warm. For drying of specimen, a ventilated oven has been used with temperature $(103\pm2)°C$.

The oven is designed with a temperature sensor in top and the heating element in bottom. There was an issue concerning drying of one batch of specimen. The specimen was placed too close to one another, so a delay occurred between the heating in bottom and sensor control in top. Thus the lower row of specimen was exposed to greater heat than the top specimen. This could have been quite dangerous. Luckily the flaw was detected the next morning and corrected. Excessive heating might cause chemically bound water to evaporate and thus giving lower density and higher MC. This effect was limited by re-saturating specimen before they were dried again.

The density is calculated by the following formula.

$$\rho_W = \frac{m_W}{a_W \times b_W \, x l_W} = \frac{m_W}{V_W} \tag{19}$$

The surface of the specimen is even, however variations will occur, this might affect the density calculations.

3.6   Specimen setup for testing
To avoid problems with bending of the rods like Løkken had. Several measures were considered and implemented:
- The timber element of the specimen is drilled straight through, this way we minimize the risk of different angles in each end. This also complies well with the idea of having another rod inserted afterwards the first failure occurs.
- To further avoid bending of the rods, spherical hinges were considered in each end. But to keep the test-setup as simple as possible. Initial testing were started without this in order to gain experience. After initial testing it was found that bending of the rods were not a problem and the idea of spherical hinges were dropped.

Figure 19- Picture of setup

3.7   Testing equipment

3.7.1   Instron 1325 loadframe and loadcell with grips

For static and fatigue testing of threaded rods, Instron 1325 (500 KN) were applied, see appendix D for information and calibration curve.

During initial testing of the Instron 1325, a malfunction occurred. The machine created loud high-frequent noise and large load variations were observed in wavematrix^{TM}. The machine was quickly labeled as out of order. Testing did not resume before weeks had passed. The service technician from Instron recalibrated the machine and a malfunction in the settings were found and corrected. No results were recorded prior to service. After service, the machine behaved exceptionally well.

3.7.2   Recording and control of load procedure.

Both static and dynamic testing was conducted using Wavematrix^{TM}. Wavematrix^{TM} is a Instron product designed for dynamic and fatigue testing. The tests were constructed using steps for each part of the load procedure. The program controlled test procedure, waveform shape, control mode, data logging and test progress.

3.8 Static load procedure

The static testing follows EN 26891:1991 [20]. Which is a standard for determination of strength and deformation properties for timber structures containing mechanical fasteners. An estimated maximum load in needed to conduct the test. The withdrawal force is estimated from equation (20) with mean capacity from Stamatopoulos and Malo [2], which for 0 and 5 degrees are respectively

$$f_{ax,0,mean} = 13,81\ MPa \text{ and } f_{ax,5,mean} = 13,98\ MPa.$$

$$F_{est} = f_{ax,\alpha,est} \times d \times l_{eff} \tag{20}$$

Where:

F_{est}	Estimated maximum static failure load
$f_{w,est}$	Estimated withdrawal strength
d	Outer rod diameter
l_{eff}	Effective embedment depth

As concluded by Malo and Stamatopoulos, equation (20) will underestimate the static capacity.

The load procedure from ISO 6891:1983 is showed in the figures bellow with estimated loads for the different stages in the standard. After a constant rate of loading, up to $0,7 * F_{est}$, the loading goes from load controlled to displacement controlled, with a constant rate of slip. The test is completed when the specimen has reached 20 mm slip. This in order to easier determine on which side the failure occurred. It is important for failure to occur while in displacement control in order not to damage the loadcell.

There is little difference in the load levels for 0 and 5 degrees. See appendix E for calculations.
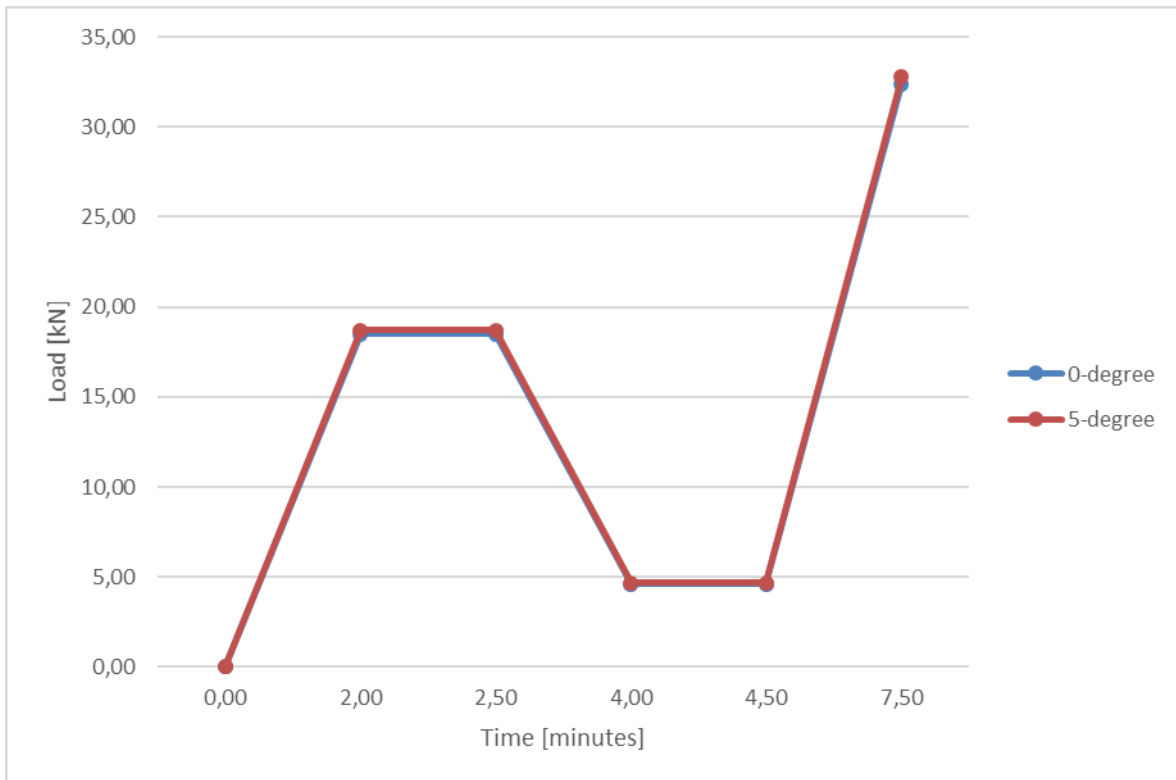
Figure 20 – Load procedure used during static testing of rod.

The load procedure is listed in the figure bellow.

Control	Load Stage	Load 0-degree [kN]	Load 5-degree [kN]	time elapsed[mm]
Load controled	0	0,00	0,00	0,00
	0,4*F$_{est}$	18,50	18,72	2,00
	hold for 30s	18,50	18,72	2,50
	0,1*F$_{est}$	4,62	4,68	4,00
	hold for 30s	4,62	4,68	4,50
	0,7*F$_{est}$	32,37	32,76	7,50
displacement controled	constant rate of slip for 3-5 min			11,50
	1,0*F$_{est}$			

Figure 21 – Load procedure in accordance with ISO 6891-1983

3.9   Cyclic load procedure

The load configuration for the cyclic loading is tension-tension with R=0.1. This to represent the application of appliance as accurate as possible. It is considered unlikely that trusses on timber bridges will experience reversing loads. The waveform is chosen as sinusoidal due to a gradual loading from traffic is the most likely, and due to enable comparison to other research. The frequency was originally 1 Hz due to comparison reasons. This was increased to 5 Hz due to time consuming testing. The high frequency migth affect fatigue life and temperature see literature chapter. No influence on temperature was found. Traditional hydraulic actuators were used, Instron 1325, 500 kN. The specimen was removed and placed while the machine was in load protect for HMS reasons.

The cyclic loading parameters are based on results from static testing. See chapter 2.3 for formulas used in calculations, and appendix F For calculations.

29

The loading procedure is divided in 3 steps:
1. Uploading to mean load with a constant rate of load.
2. Gradual increase in amplitude before target amplitude is reached, takes 3-5 cycles.
3. Cyclic load until failure, see figure bellow. The Instron 1325 is load controlled during the cyclic loading.

Load parameter	0-degree	5-degree
R	0,1	0,1
f_{max}	0,75	0,75
F_{ref}	39,01	41,11
F_{max}	29,2575	30,8325
F_{min}	2,92575	3,08325
F_{mean}	16,091625	16,957875
$F_{amplitude}$	13,165875	13,874625

Figure 22 – cyclic load parameters.
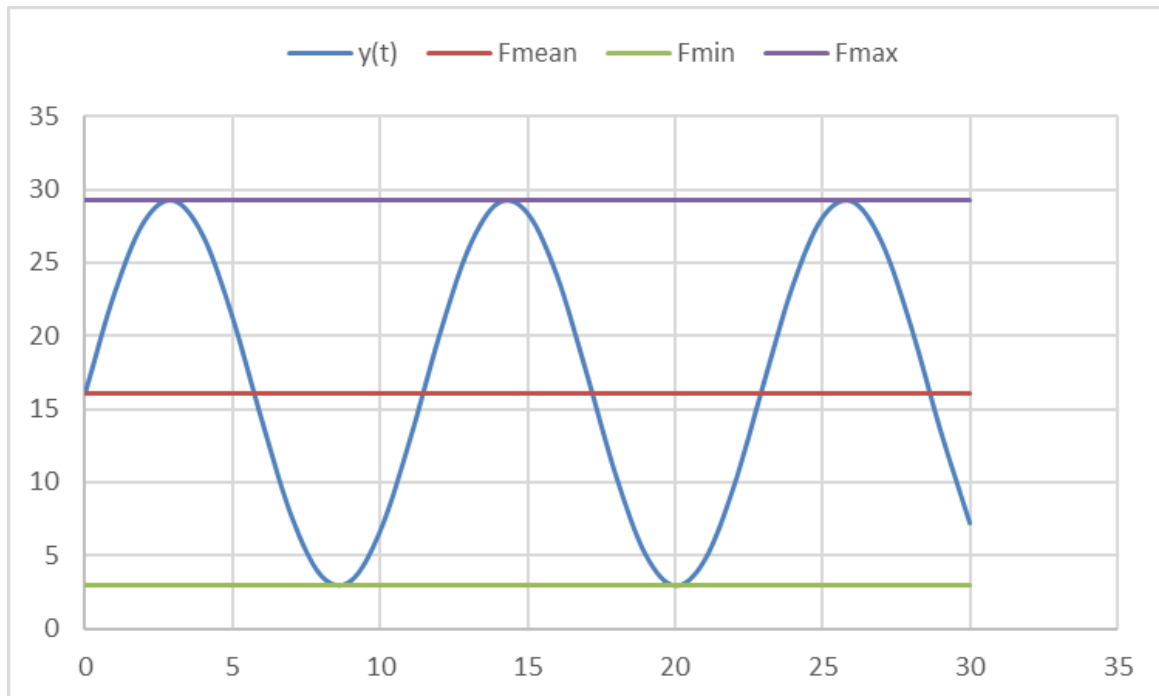
Figure 23 – cyclic load with parameters depicted

3.10 Testing procedure
The testing of both static and cyclic specimen was done according to procedure bellow. However, plastic bag was not used for all static tests due to shorter duration. The major difference in static and cyclic testing, is the programed load procedure in Wavematrix^{TM}.

1. Check that oil pressure in on "high" and that breaks on the traverse are fully pressurized, the gauge should show 220-250 bars.
2. Collect random specimen from storage and weigh immediately.
3. Place specimen in bag with rods sticking out through holes in each side of the bag.
4. Seal openings in plastic bag by taping the plastic bag around the holes onto the rods. Thereafter tape and sealing opening in bag by twisting the plastic and folding it before taping to ensure seal.

5. Switch Instron 1325 from computer control to console control. Set the console in displacement controlled mode and turn on load protect to +-2kN.
6. Place the rod on the specimen inside the lower grip.
7. Gradually adjust height on piston with console.
8. When grips are covering more than 2/3 of rods, lift specimen to ensure equal spacing on each side and then tighten grip to 200 bars.
9. Switch control from console to computer with wave-matrix installed.
10. Check limits in wave-matrix and make sure they are activated.
11. Start the testing procedure programmed in wave-matrix.
12. When test procedure ends (failure of specimen). Switch to console control mode. Place console in displacement control mode and turn on load protect to 2 kN.
13. Untighten grips at top and bottom.
14. Remove plastic bag and weigh specimen immediately.
15. Start from top (step 1).

3.10.1 Additional procedure for drying of specimen
1. Failed specimen are collected and placed in drying oven at 103°C. Insure a minimum of approximately 5 centimeters spacing in-between specimen, on all sides. 48x48 mm timber were placed diagonal between layers of timber to insure proper spacing.
2. After approximately 3 days, weigh samples of specimen. Place back into oven after weighing.
3. After a period of time (minimum 8 hours), weigh the same samples over again. If no change in mass is detected, the entire batch of specimen can be weighed.
4. Weigh each specimen in entire batch. Record data and calculate MC and density.

3.11 Specimen output
For each test specimen, the following data were recorded for further interpretation and analysis of test results:
1. Geometrical Dimensions
   a) Heigth H
   b) bredth b
   c) depth d

2. Mass of specimen:
   a) Mass before testing, m_1.
   b) Mass after failure m_2. recorded right after testing was completed (m2). However some specimen completed during the night. Mass was not measured until morning.
   c) Mass after drying, in compliant with ISO 13061-1[21]. However the mass of the entire specimen were measured, not a small clear wood specimen

3. After failure:
   a) Embedment depth l, and failure modes 1-3 are recorded after failure, by cutting the specimen. Document by photographing the failure zone.
   b) Visual inspection of failure zone for any deficiencies in failure zone.
   c) MC calculated
   d) Load and displacement curves are logged fore static testing.
   e) N for cyclic testing.

3.12 Statistical analysis

In this theory, the lognormal distribution is used to represent the results for both static and fatigue. Lognormal distribution is used in order to comply with NS-EN 14358:2016 [22] and also due to comparability to other results[3, 17]. However, Dahl [23] found that Weibull might give an even better fit for his shear results. This is not further investigated due to limited time.

$$f(x,\xi,\delta) = \frac{1}{\sqrt{2\pi} \cdot x \cdot \delta} \cdot e^{\left(\frac{1}{2}\left(\frac{ln(x)-\xi}{\delta}\right)^2\right)}, x \geq 0 \; and \; f(x,\xi,\delta) = 0, \; \text{x<0}$$

(21)

4 Results, static testing

4.1 Experimental results and failure modes

The experimental results for both 0 and 5-degree specimen are summarized in Table 4.1. Along with the moisture content, maximum load and failure modes. All static specimen that failed, failed in failure mode 1, see figure below. The average moisture content from static testing is 12.7% and the average density is 455 kg/m³.

Figure 24-Fracture mode 1

Name	MC	density (p12)	$F_{ax,\alpha}$	$f_{ax,a}$	Failure mode
	%	[kg/m3]	kN	MPa	[1/2/3]
S0-E2-678-1	12,61	426,33	38,9	9,82	Mode 1
S0-E2-678-2	12,61	421,32	38,9	9,82	no failure
S0-F2-123-1	12,56	437,14	26,28	6,64	Mode 1
S0-F2-123-2	12,56	437,14	26,28	6,64	no failure
S0-D8-678-1	11,89	420,13	64,23	10,43	Mode 1
S0-D8-678-2	11,91	420,21	64,23	10,43	no failure
S0-D8-345-1		438,07	66,84	10,85	Mode 1
S0-D8-345-2		438,07	66,84	10,85	no failure
S0-D1-678-1	15,54	486,06	38,61	9,75	Mode 1
S0-D1-678-2	15,54	486,06	38,61	9,75	no failure

S5-L2-5678-1	12,29	460,69	52,84	13,34	Mode 1 , knot and drying crack
S5-L2-5678-2	12,29	460,69	52,84	13,34	no failure
S5-L3-45678-1	12,32	473,01	47,13	11,90	Mode 1, with drying crack
S5-L3-45678-2	12,32	473,01	47,13	11,90	no failure
S5-L7-45678-1		459,73	39,29	9,92	Mode 1,
S5-L7-45678-2		459,73	39,29	9,92	no failure
S5-L2-2345-1	11,64	477,12	34,47	8,70	Mode 1
S5-L2-2345-2	11,64	477,12	34,47	8,70	no failure
S5-L6-45678-1	12,82	479,40	31,83	8,04	Mode 1
S5-L6-45678-2	12,82	479,40	31,83	8,04	no failure

Table 4.1- Static testing results

Due to few results, it is interesting to investigate the change in the lognormal distribution for each added specimen. As this indicates whenever a curve converges. The 0-degree specimen converge towards a higher capacity and the 5-degree specimen converge[3] towards a lower capacity than what is presented in Table 5.1

The relative displacement to force is depicted below, the specimen showed substantial capacity after failure occurred.
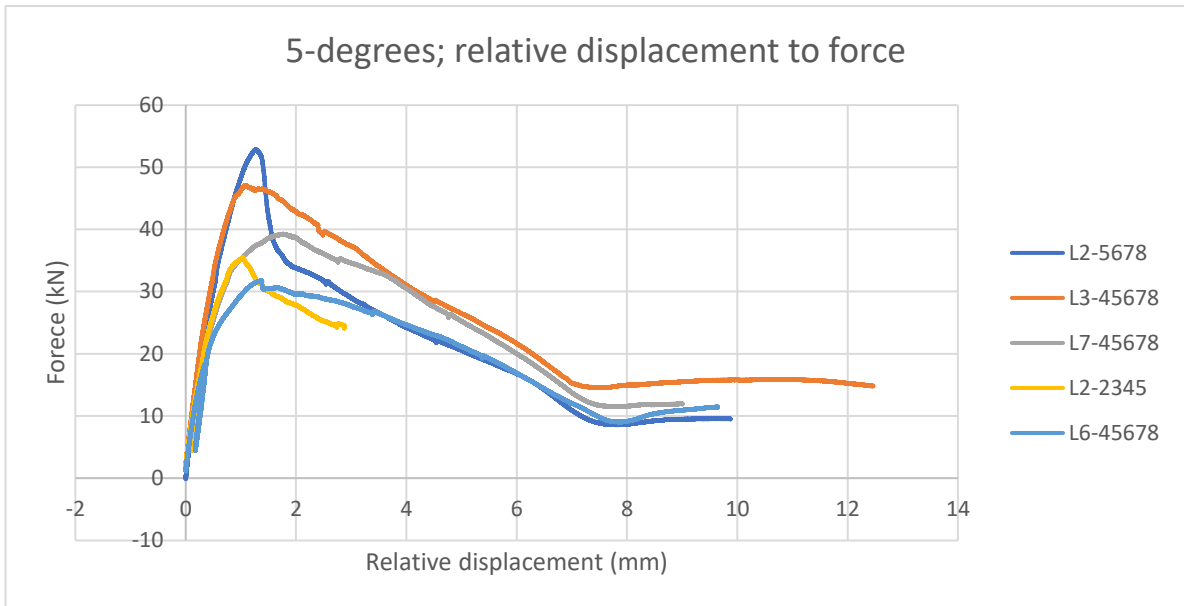
Figure 25-Relative displacement to force during static tested, measured directly from the loadcell.

---

[3] *If curve 10 is compared to curve 8, a relative reduction in inclination can be seen for the 5-degree specimen, which indicates that the variation in capacity in stabilizing. At the same time, the curve shifts slightly to the left, indicating that it converges but that it converges towards a lower capacity than given in the results. For the 0-degree specimen the same effect can be seen, however this is not inclining but increasing both with regards to spread in capacity but it also converges towards a higher capacity than given in the results.
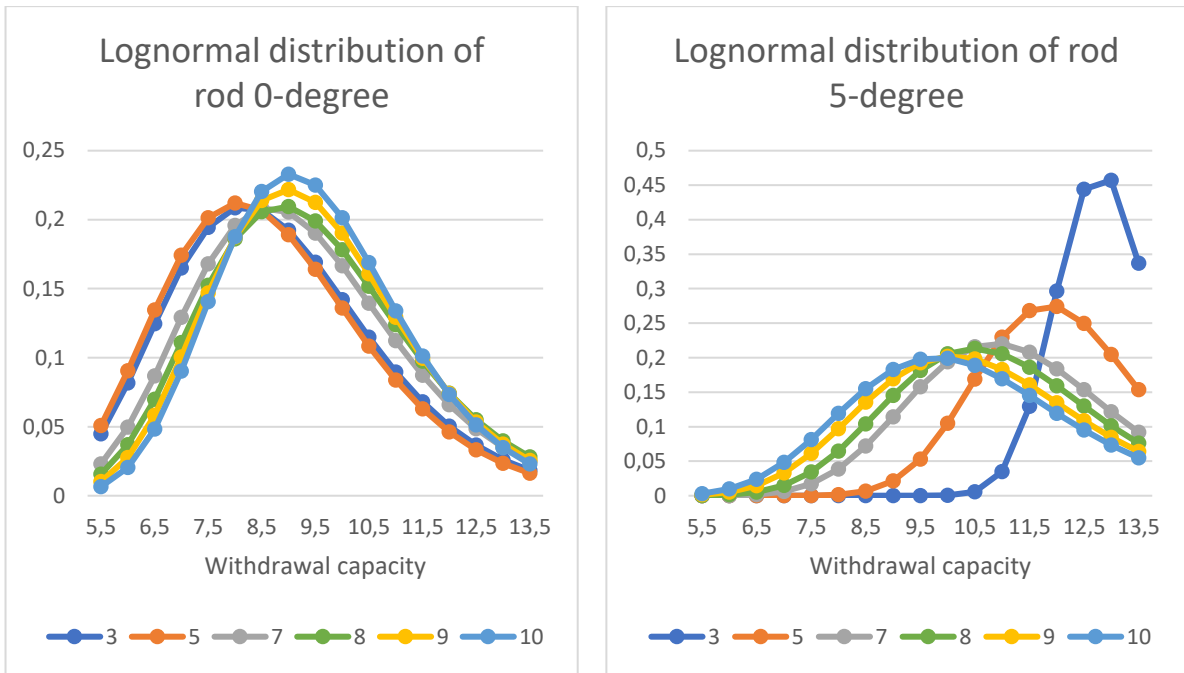
Figure 26- Change in the lognormal distribution as more specimen are added, the number describes amount of specimen included in the respective distribution.

The specimen were produced in such a manor that after failure, the failed side could be cut off and a new rod could be inserted in that part, this way results could be gained from both sides of the specimen. However, due to unexpected high cycle count, only one side of the specimen were tested, the opposite side of the specimen that didn't fail is therefore assumed to the same capacity, this is a conservative assumption as the specimen would probably have a higher capacity.

5 Analysis and discussion of static results

A lognormal distribution was used in this thesis see, chapter 3.12. The accompanying mean capacity, coefficient of variation (COV) and 5-percintile characteristic values are listed in the table below. The COV is especially low, partially due the conservative assumption of similar capacity yielding a lower spread in data. The data below describes both results from the conservatively assumed embedment depth of 180 mm. It also describes the results is only the full thread height is considered giving a effective embedment depth of 150 mm. More in this in the following.

Summary of results		mean	std	cov	char
		y	s		f0,05
		[N/mm2]	[N/mm2]		[N/mm2]
leff=180	0-degree specimen	9,46	0,1860	0,0832	6,33
	5-degree specimen	10,38	0,1992	0,0858	6,71
Leff=150	0-degree specimen	10,98	0,1675	0,0700	7,69
	5-degree specimen	12,46	0,1992	0,0796	8,05

Table 5.1- Statistical evaluation of rods.

5.1 Comparison to Stamatopoulos [17]

The static experimental results are compared to Stamatopoulos in order to evaluate the results. As seen in table 5.1. the mean capacity yielded at 9.46 and 10.38. This is low compared to Stamatopoulus. Results from Stamatopoulos can be seen in the table below. The setup is depicted in the literature part

		$f_{ax,\alpha} = \frac{F_{max}}{d*l_{eff}}$ [MPa]			
α	number of specimen	mean	COV	Median	5%-fractile
0,00	25	13,8100	0,15	13,79	10,19
10,00	22	14,1400	0,17	13,9	10,06

Table 5.2- Results from Stamatopoulos [2]

Since the setup in this thesis only yields the lowest of two results, a montecarlo simulation was created to evaluate if this could explain the difference in the results.

The montecarlo simulation is made using the data from Stamatopoulos. The simulation is performed by generating two random number, and finding their representative capacity by the mean and cov from Stamatopoulos results. The lowest of these walues are saved. After 10 000 such simulations the mean static pullout capacity was found as 12.63 N/mm2. This simulation probably overestimate the deviation in results from each end due to the fact that lognormal distribution takes into account deviation that occurs between different lamellas and different beams, while the setup used here tests more or less the same lamella in the same vicinity.

Other reasons for the deviation in pullout capacity can be due to the rod. In this thesis, the rod as an inclining thread height on the end which is assumed to give full capacity in a conservative manner. However, it's possible that this part has a lower contribution. If this part of the rod is completely neglected and the effective penetration depth is assumed to be only

150 mm. Then the capacity changes like described in the table5.1. However, to assume to contribution from the other part seems unlikely and the more probable assumption would be something in between 150 – 180. However, no documented or theoretical model is present and as such this assumption cannot be defended. Therefore, an effective penetration depth of 180 mm is assumed in a conservative manner.

If both montecarlo and the non-conservative embedment depth of 150 mm is considered. Then the values of 10,98 MPa for 0-degrees and 12,46 MPa for the 5-degrees comes quite close to the 12,46 found by montecarlo.

Another reason for difference in capacity can also lie the boundary conditions and the stiffness of the setup. Stamatopoulos used a pull-push configuration while this thesis uses a pull-pull configuration.

6   Results, fatigue testing

The load configuration is described in detail in chapter 3, and is summarized in Table 6.1.

Conditioning	Climate class 1: RH=65% and T=20°C
Stress ratio R	0,1 (tension-tension)
Frequency	5 Hz
Normalized maximum load	$f_{max} = 0,75$

Table 6.1 – Summarized load parameters

The results from 11 fatigue tests are listed in the table below with accompanying MC, density, number of cycles and failure mode, see appendix G for documentation of failure modes. The specimen was weighed before and after testing to investigate the effectiveness of the vapor barrier. The results yielded 26,69 grams in average loss of mass., which corresponds to 0,7% average loss in MC during the fatigue testing. The average fatigue testing time was 79 hours per specimen. Even though the frequency is quite high, no temperature increase were measured on the surface of the specimen during testing. The density p_{12} is based on the average mass during testing and is the mean density of the specimen, see chapter 3.5.3 for more information. See appendix H for more information and results on fatigue testing.

Specimen	MC	Reduction in mass	p12	Number of cycles	Failure mode
	%	[g]	[kg/m3]	N	
F0-E7-345	14,5	77,9	429,0	165000	Mode 1
F0-E7-678	13,0		420,8	42740	Mode 1
F0-D1-345		73,4	408,7	2780000	no failure, stop due to cycle count
F0-D7-678	12,1	1,4	449,2	139330	Mode 3, close to mode 1, but included a small layer of timber around rod.
F0-E8-456	11,9	12,2	393,6	2657532	Mode 2, block pullout, the block follows a drying crack
F0-E8-123	12,4	2,6	458,9	553002	Mode 3 with visible drying crack along the rod
F5-L1-45678				2500000	no failure, stopped due to cycle count
F5-L7-12345		28,9		2581639	no failure, stop due to cycle count
F5-L4-45678		36,1		3299982	Mode1
F5-L3-12345		25		251318	Mode1
F5-L5-5678		0,7		690400	Mode1

Table 6.2- Fatigue testing results see Appendix H for supplementary information.

The governing failure mode was the same as for static testing; a clear pullout of rod from timber in the rod-timber interface. However, 3 specimens showed deviation in failure mode, these are depicted in the figures below. Two of the specimen tore out timber bordering to a crack, see Figure 27and Figure 28. The last specimen tore fibers along the annular rings, see Figure 29.See Appendix G for more documentation on failure modes.
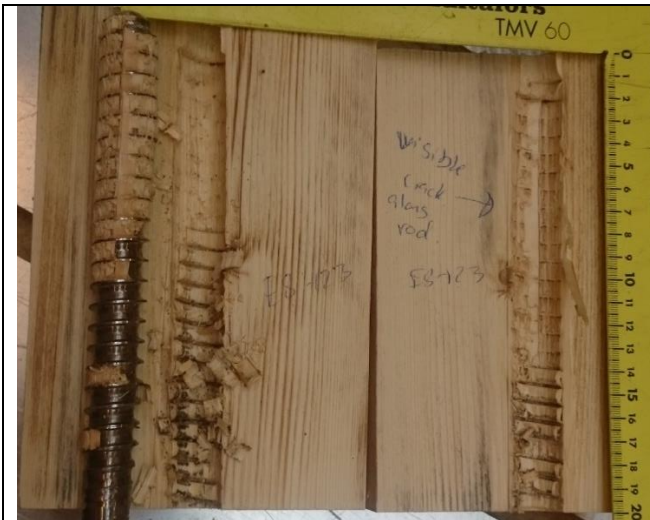
Figure 27-F0-E8-123 failure mode 3 and lower capacity due to crack
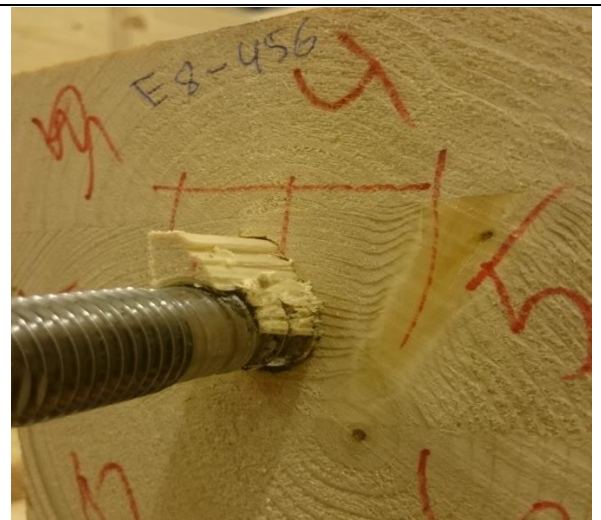
Figure 28-F0-E8-456 Failure mode 3, block tear-out, the block follows a radial crack on one side.

Figure 29-F0-D7-678, failure mode 3, follows intersection zone but deviates and tears out some fibers, it might seem to follow the annular rings..

After failure of the first rod, the specimen was put aside for further testing of the other rod. However, due to an unexpected high number of cycles this was not conducted, and the fatigue capacity is therefore assumed equal for both ends. This is a conservative assumption. However, Malo [15] found that the opposite side failed simultaneously or shortly after the first side, this is presumed due to testing of the same lamella in the same vicinity should yield approximately equal results. In this thesis, we assume that the opposite side has the same capacity in a conservative manner. All specimen are included in further analysis in order to obtain a realistic capacity.

A couple of specimen was terminated before failure occurred, due to a time consuming high number of cycles, see Table 6.2. These specimens were not dried as they were put aside for further testing as part of another thesis. Therefore, some data in the table is missing. Including these specimens in the analysis are particularly conservative, as none of the rods failed. However, in review of few specimen, it seems reasonable to include all specimen.

7 Analysis of fatigue results

All specimen were tested for $f_{max} = 0,75$. Thus, the logarithm of number of cycles can be evaluated as the statics results were. This evaluation is listen in the tables below. The 5-degree specimen is found to have a larger average number of cycles. The coefficient of variation is also substantially lower. This might be explained by the angle of the rod which should be less prone to drying cracks. This assumption might be supported by the lower coefficient of variation for 5-degree specimen.

Summary of results	mean N	mean Log(N)	standard deviation	coefficient of variation
	y	y	s	cov
	[N/mm2]		[N/mm2]	
0-degree specimen	1056267	5,60	0,13208	0,07699
5-degree specimen	1864668	6,11	0,08503	0,04838

Table 7.1-Statistical review of number of cycles. The distribution is based on log(N).
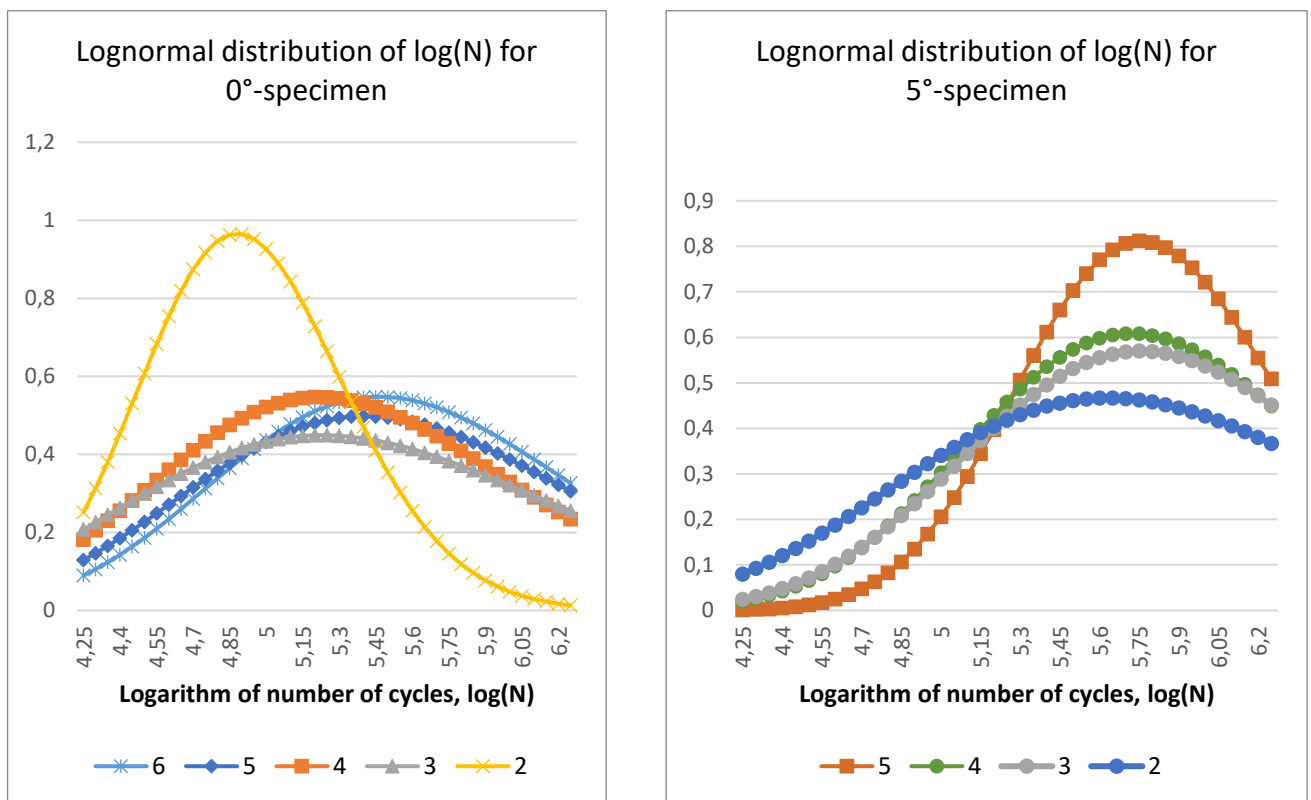
Table 7.2- The lognormal distribution of log(N) and it's relative change for each added specimen

Initially the goal was to test for $f_{max} = 0,75$ and $f_{max} = 0,60$. However, 0,6 would give an even higher number of cycles than for 0,75, which would produce less results. Therefore, it was decided to only do 0,75, and instead use the principle of a linear SN-curve to redistribute the specimen based on their cycle-count to a more probable normalized load. Such a method is somewhat unusual, and therefore, both redistributed SN-curve and the original SN-curve are presented in Figure 31. This will imply that we regard all specimen as having equal amounts of inherent damage as mentioned in chapter 2.1.

Following the classical assumption that timber has a linear SN-curve. It seems just to assume that there is a linear relationship between the capacity of a specimen and the logarithm of cycles it can handle. This can be expressed in the form of a liner equation.

$$y = b + a(x - c) \quad when \; x = [d, e] \tag{22}$$

Substituting gives:

$$f_{ax,\alpha} = f_{ax,\alpha,min} + \frac{f_{ax,\alpha,max} - f_{ax,\alpha,min}}{N_{max} - N_{min}} * (N - N_{min}) \tag{23}$$

Since there are 10 samples all with the same normalized stress level, the lognormal distribution for the logarithm of number of cycles can be found. Thereafter using the notation in NS-EN14358:2016 [22] the equation above can be rewritten to:

$$f_{ax,\alpha} = \left(\bar{y}_{f_{ax,\alpha}} - s_{f_{ax,\alpha}} * u_{0,05}\right) + \frac{s_{f_{ax,\alpha}}}{s_N}\left(N - (\bar{y}_N - s_N * u_{0,05})\right) \tag{24}$$

Where

$f_{ax,\alpha}$	The static withdrawal capacity
N	Number of cycles
$\bar{y}_{f_{ax,\alpha}}$	Mean of the withdrawal capacity
$s_{f_{ax,\alpha}}$	Standard deviation for withdrawal capacity
$u_{0,05}$	The 5-percentile value of
$\bar{y}_N$	Mean of the logarithm of number of cycles
s_N	Standard deviation for number of cycles

The equation will then be a linear relation between the logarithm of number of cycles and the withdrawal capacity. The linear relationship is fitted to start at the 5-percentile value of withdrawal strength and logarithm of number of cycles.
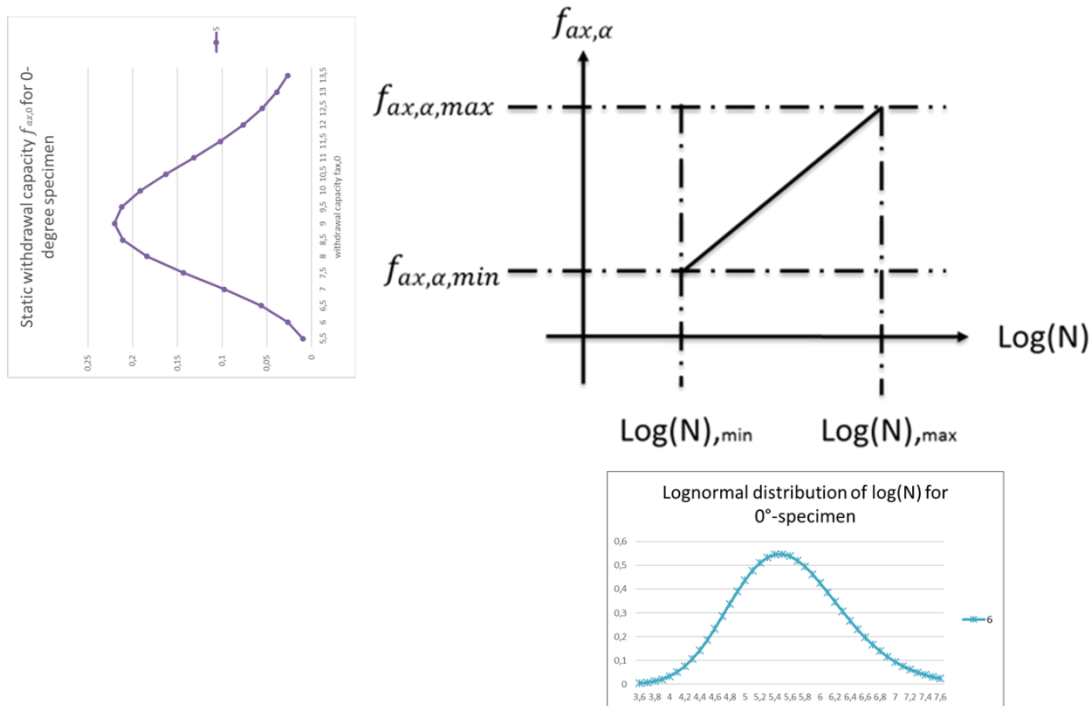
Figure 30- linear relation between capacity and the logarithm of number of cycles.

Both the redistributed and the original curves are presented in the figures bellow. The data have been fitted to the linear equation using linear least square (SSE), the squared residual and the parameters are presented in the table below.

$$\bar{f} = A log(N) + B \tag{25}$$

0-degree not redistributed		0-degree redistributed	
A	-0,0398	A	-0,0411
B	0,9756	B	0,9851
Σ(R^2)	0,1276	Σ(R^2)	0,1407
5-degree not redistributed		5-degree redistributed	
A	-0,0374	A	-0,0402
B	0,9531	B	0,9558
Σ(R^2)	0,1765	Σ(R^2)	0,2011

Table 7.3-Results from fitting data to linear SN-curve based on least square method.

The results are compared to EC5-2[16], Løkken [3] and Malo [15] in Figure 31 . The equation used for the linear line is not similar for all sources, as can be seen in the table below, this has been accounted for Figure 31- Redistributed and non-redistributed SN-curves compared to other research

Source	Equation of line	Parameters	
Løkken 45°	"-0,023Ln(x)+0,9738"	A	-0,023
		B	0,9738
Løkken 90°	"-0,022ln(x)+0,9694"	A	-0,023
		B	0,9738
EC5-2 shear	$k_{fat} = 1 - \dfrac{1-R}{a(b-R)} logN$	R	0,1
		a	6,7
		b	1,3
EC5-2 tension	$k_{fat} = 1 - \dfrac{1-R}{a(b-R)} logN$	R	0,1
		a	9,5
		b	1,1
EC5-2 dowels	$k_{fat} = 1 - \dfrac{1-R}{a(b-R)} logN$	R	0,1
		a	6
		b	2
Malo	"A*log(N)+B"	R	0,1
		A	-0,066
		B	0,96

Table 7.4- Parameters and equations for SN-curves.
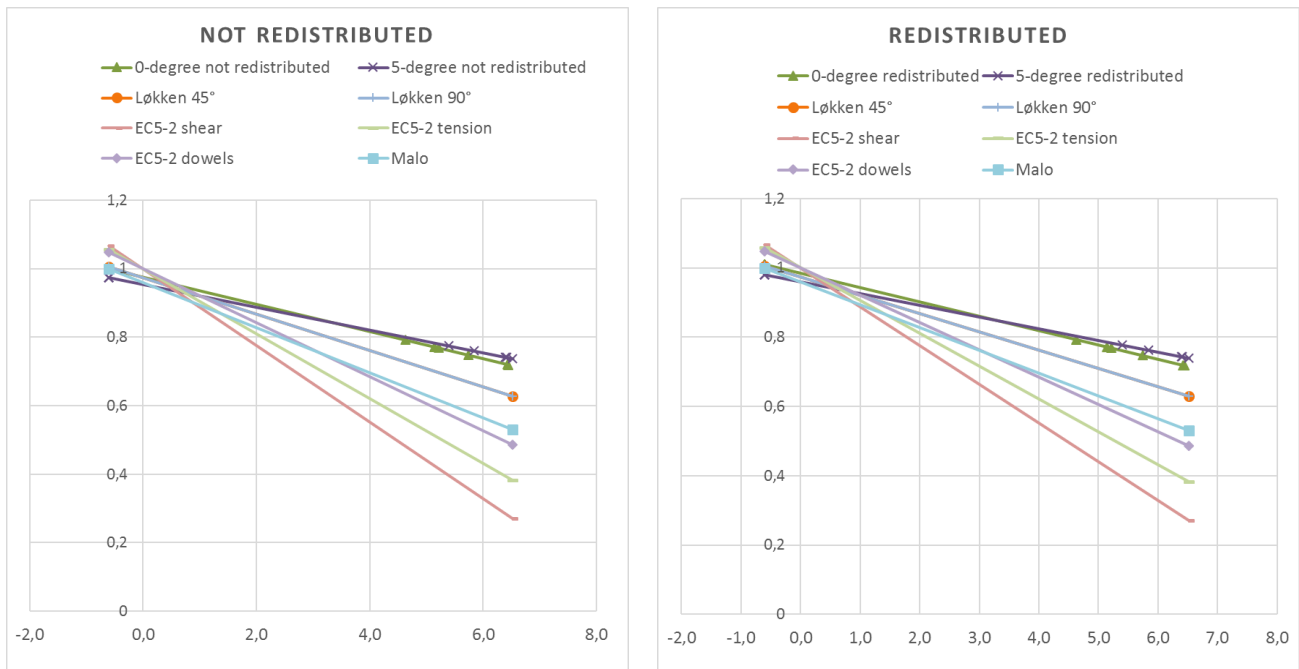
Figure 31- Redistributed and non-redistributed SN-curves compared to other research

The redistributed and non-redistributed SN-curves are shown in the table below.
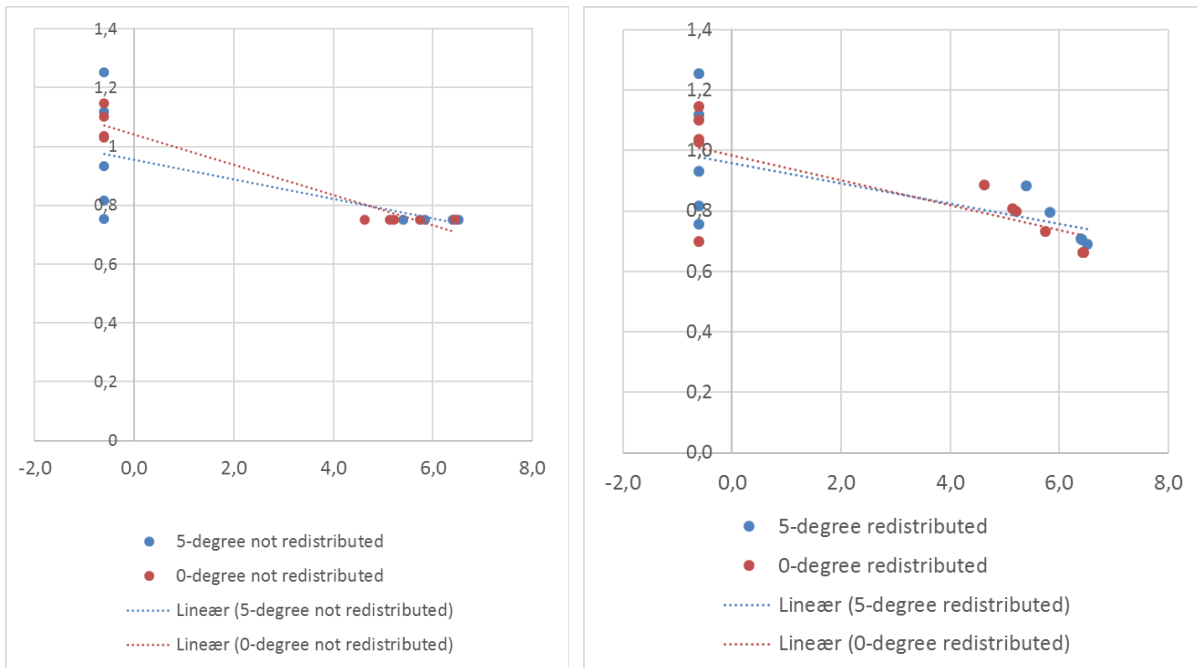
Figure 32-Comparison of redistributed Sn-curve and non-redistributed SN-curve

The slope of the curves is small compared to other results. The results are much better than anticipated. As discussed previously the results are also conservative, both with respect to static capacity and number of cycles. A higher frequency could result in a higher number of cycles as discussed in chapter 2.3.4. However, this should not amount to such a high capacity as given above.

8   Conclusion, remarks and future work

The static and fatigue strength of threaded rods subjected to axial loading have been tested. The results amount to 10 static tests and 11 fatigue tests which gives 20 static connections and 22 fatigue connections, this includes both 0 and 5-degree specimen. The following concluding remark are made:

- Structures with axial loaded rods in small rod to grain angles may experience fatigue damage for penetration depths lower than 180 mm.
- The fatigue strength of threaded rods seems to be quite high, the closest verification criteria in the Eurocode 5 part 2, seems to be dowels, but even this seem to underestimate the capacity, this must be further investigated.
- The test setup was easy to produce, worked efficiently, and gave a lot of results even though not all specimen failed. The setup produced conservative results. The results are quite even with a low coefficient of variation for both static and fatigue results.
- The effect of cracks was expected to have a larger impact on the threaded rods. However, most specimen failed in failure mode 1. Some were affected but still had a considerable capacity.

A couple of remarks:

- The static capacity is conservatively assessed due to an undocumented effect of reduced thread height. This is assumed to not affect the fatigue performance which is based on the ultimate static capacity found by static testing.

For future work, it is recommended to conduct more tests with varying penetration depth, stress ratios R, normalized maximum load f_{max} and several rod to grain angles. The effect of moisture content and frequency might also be investigated further.

Part III – Static and fatigue testing of longitudinal shear

1 Introduction

There are many shear tests which are used to determine the shear strength and stiffness of timber. The problem is that most of these tests induce stress perpendicular to grain, and some are less applicable to fatigue testing. A selection of tests is presented in the following.

ISO13910:2014 [24] describes two test methods for measuring the shear strength parallel to grain. The first test, is a beam setup, and the second test is a setup using glued steel plates. The Standard itself states that the glued steel plate test might give one-third greater capacity than the beam test.
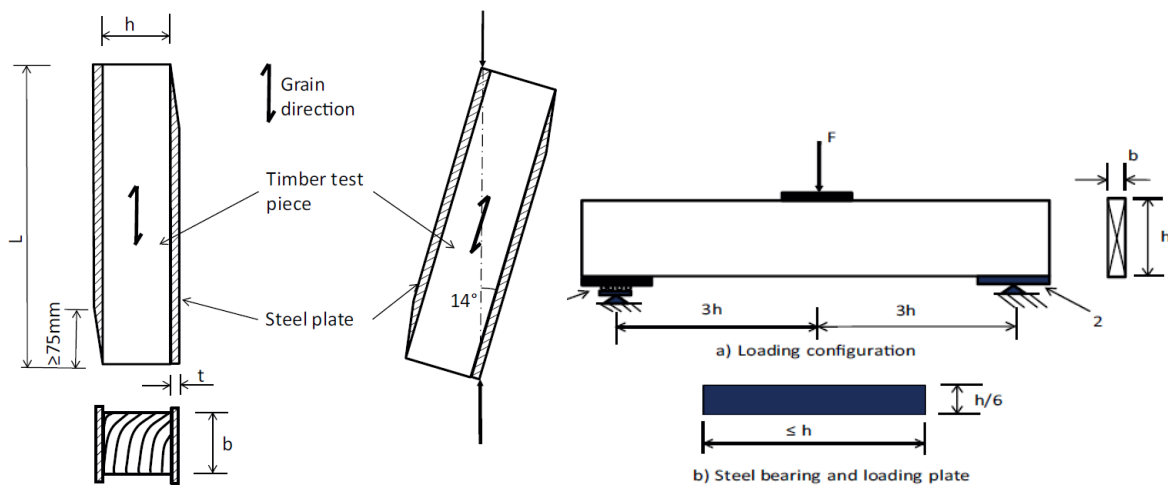
Figure 33- Shear tests according to ISO13910:2014

Another shear test is the Losipescu shear test, see figure below. This test has proven to give acceptable shear moduli for timber, as the fixture is loaded it produces zero bending moment in the critical zone while the shear forces are non-zero. However, although the shear moduli are acceptable the shear capacity is inaccurate due to bending in the non-critical zone, especially for longitudinal shear.[23]

The specimen which Dahl and Malo [23] found to be the most appropriate is the Arcan shear test. This test consists of a butterfly shaped fixture that allows the loading to result in a pure shear stress situation. All material planes can be tested and the test is also applicable for testing of linear and nonlinear parameters.
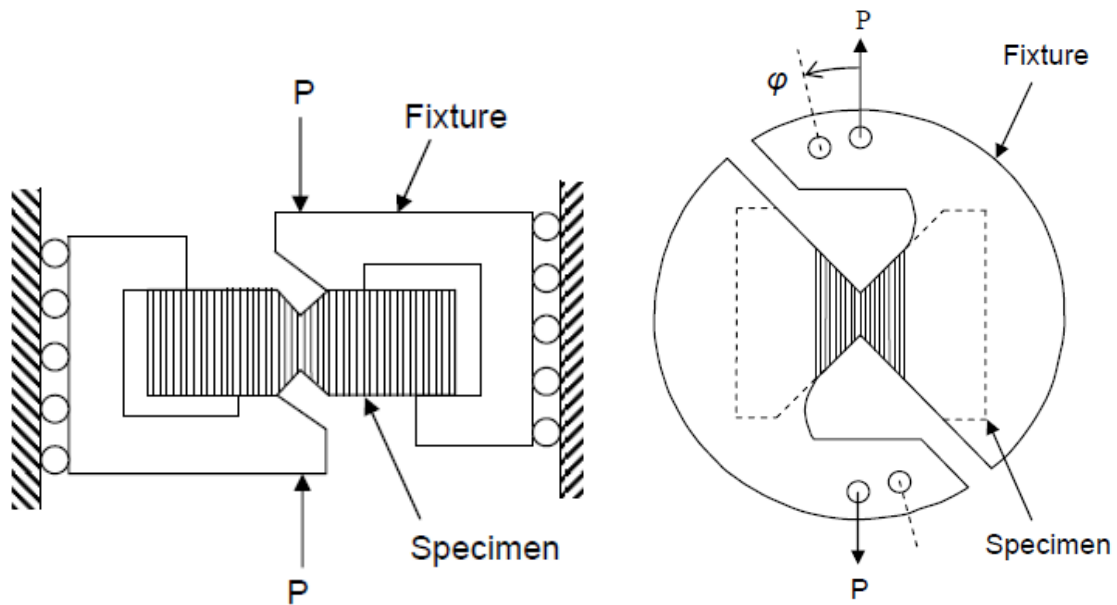
Figure 34-Losipescu shear test on the left and Arcan shear test on the right.

Based on the Arcan and Losipescu tests, Professor Kjell Arne Malo at the department of structural engineering at NTNU[4], developed the theory behind a new shear test which also is applicable to fatigue testing.
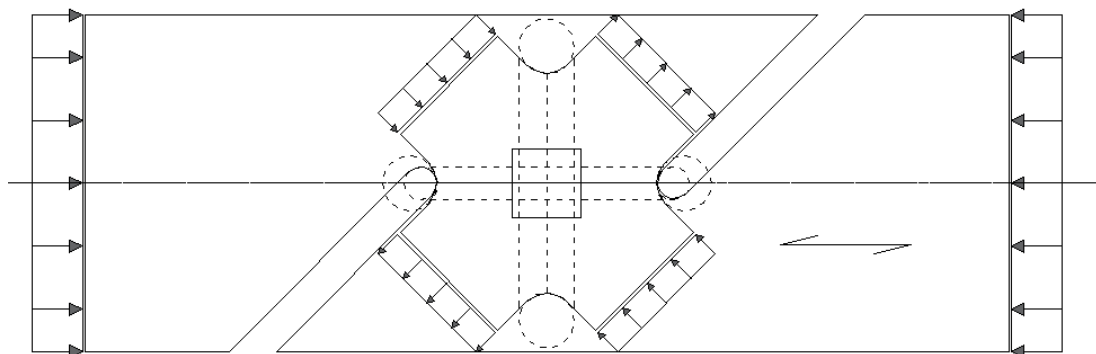
Figure 35-Shear specimen developed by Kjell Arne Malo.

The specimen was previously subject of study by MSc student Line Sigbjørnsen[5] in her master thesis. However, she concluded that further optimization was necessary. The specimen is therefore first optimized before achieving the aim of this this part; Experimental investigation of static and fatigue properties of Glulam GL30c in longitudinal shear. A review on Sigbjørnsens work is given in chapter the litterature. However, Sigbjørnsen only considered specimen of RL orientation, this thesis will focus on specimen with both RL and TL orientation, with both static and fatigue testing. Other informative sources have been Dahl and Malo [23] whom investigated the shear properties of spruce softwood.

The optimization has been a collaboration with PhD -student Katarzyna Ostapska-Luczkowska[6]. Whom has been an important contributor to this thesis.

1.1 Background of shear specimen

The general idea behind the design is illustrated in the figure below. The pure shear situation is rearranged into a cruiceform test specimen, the final design emerges as timber is cut away around the cruicefrom.
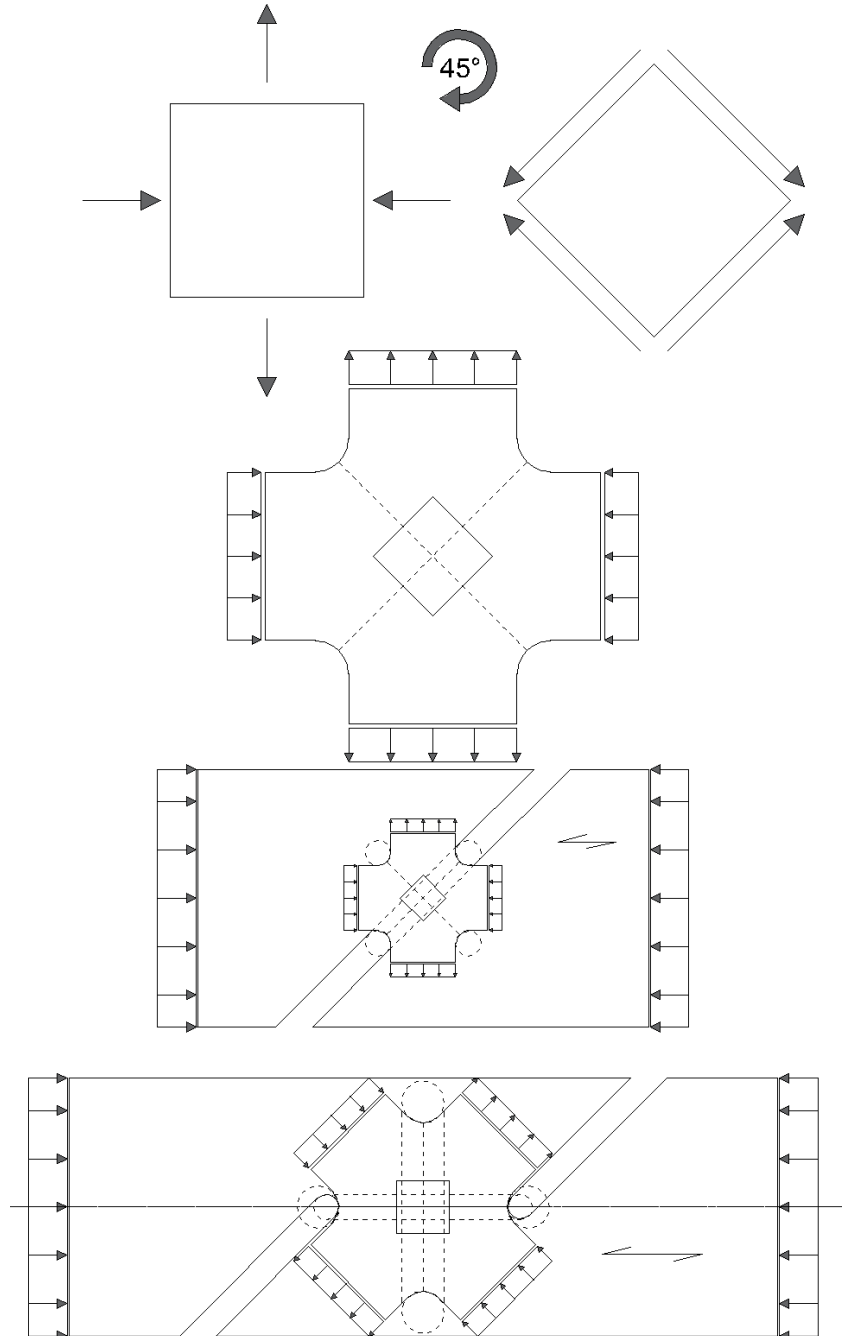
Figure 36 – Development of shear test, illustrated by Katarzyna Ostapska- Luczkowska.

During her work, Sigbjørnsen [25] optimized the spezimen by the use of experimental testing with Aramis and modeling in Abaqus. She found that there were a correlation between the height of the specimen and the height of the shear zone. She also investigated the breadth of the specimen and the depth of the cuts. The resulting specimen fractured from either shear, tension perpendicular to fibers or a combination. From her optimization, she concluded that

the shear capacity was probably underestimated and the G-moduli were quite high. No correlation between density and shear capacity were found. Her thesis has been important in the following work.

2 Method

The experimental work took place at the laboratory part of the department of Structural Engineering at NTNU.

The specimen was produced out of Norwegian GL30c beams, see Appendix B for documentation. The beams were chosen with a width of 140 mm in order to obtain material with a minimum of annular ring curvature. Upon arrival at the laboratory they were quickly moved to a temperature and moisture controlled storage facility with ideal class 1 conditions implying 65% relative humidity and 20°C. There the timber was re-saturated to obtain approximately 12% moisture content for several days before production. See part 1 for more information on climate conditions.

Due to dry conditions in the woodworking laboratory, a series of dummy tests were produced to optimize the production with regards to time and accuracy. The final accuracy of the specimen is approximately described in the table below. After production and re-saturation, the "as is" measurements of each specimen were documented. The critical height h and depth d of the shear zone was measured using a slide caliper to get as accurate data as possible. See chapter 2.9 for more information on documented properties of specimen.

Geometric parameter	Geometric measurement [mm]	Accuracy [mm]
H	600	± 4
w	140/135	± 3
d	135/140	± 3
h	65/66	± 2
t	12	± 3

Table 2.1 - Accuracy of specimen

2.1 Optimization using finite element analysis

The optimization was conducted using finite element analysis hereafter FEA, and Python scripting. The FEA model was created by PhD-student Katarzyna Ostapska- Luczkowska.The model is parametrized with regards to the geometrical inputs. Based on these parameters, it runs a optimization loop, using scripting in Python, in order to obtain least tension perpendicular to grain. This model will presented by Katarzyna in hear PhD and is therefore not further discussed herein.

From optimization, the geometry presented in Figure 37 was found. However, the initial detailing of the notch was rejected when presented, due to difficulty of production. Because of this an experimental production was first conducted in order to device a possible geometry. The result of this is the Notched-90 deign. However, after experimental investigation of the Notched-90 design was completed, another possible design was devised which resembled the initial design, this is the notched-45 design. Therefore, a second experimental investigation was conducted. Although the second design resembles the initial optimized design the most, it is not necessarily the best design. Even though the optimization and production was conducted in two parts, it is hereafter presented as a simultaneous investigation. This is done to simplify the structure of the thesis. The complete geometry of the specimen and cut design from beams can be found in Appendix L.

2.2   Specimen

Two types of specimen were produced for each design, corresponding to the RL and TL material planes. Although the specimen was produced from 140 mm wide lamella, it was impossible to obtain specimen with Cartesian material axes. So, in order to obtain the pure LT and LR shear properties, a theoretical differentiation must be conducted, this is discussed more in chapter 4.2.

With respect to representable material qualities, the specimen was sorted as to avoid the larges macroscopic defects like knots and finger jointing in the shear zone. However, a complete reduction in apparent inhomogeneities were not chosen.

Specimen were produced with the geometries depicted in the Figure 37. For each geometry two specimen types were created denoted $ij\ where\ i = (R, T)and\ j = L$. Rolling shear is thus not considered. The first index i assigns the normal vector of the load plane and the second index j assigns the direction of the test load. Notice that this is opposite to the definition used for material parameters. Thus, the specimen ij corresponds to the shear property τ_{ji}. See Figure 37 general geometry of shear specimen and Figure 38 for geometry of notches.
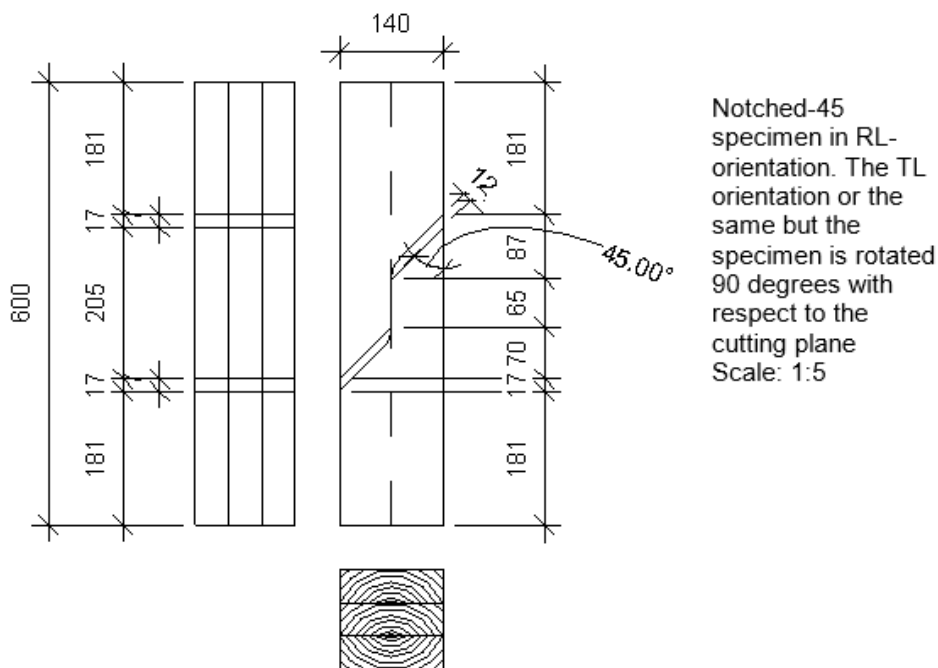
Figure 37- General geometry of shear specimen, depicted is N45-RL

The name notched 45 and notched 90 comes from the angle of the notch. The specimen on the right in Figure 39, has a notch which is a 90-degree cut. While the other specimen has a 45-degree cut, se figure bellow.
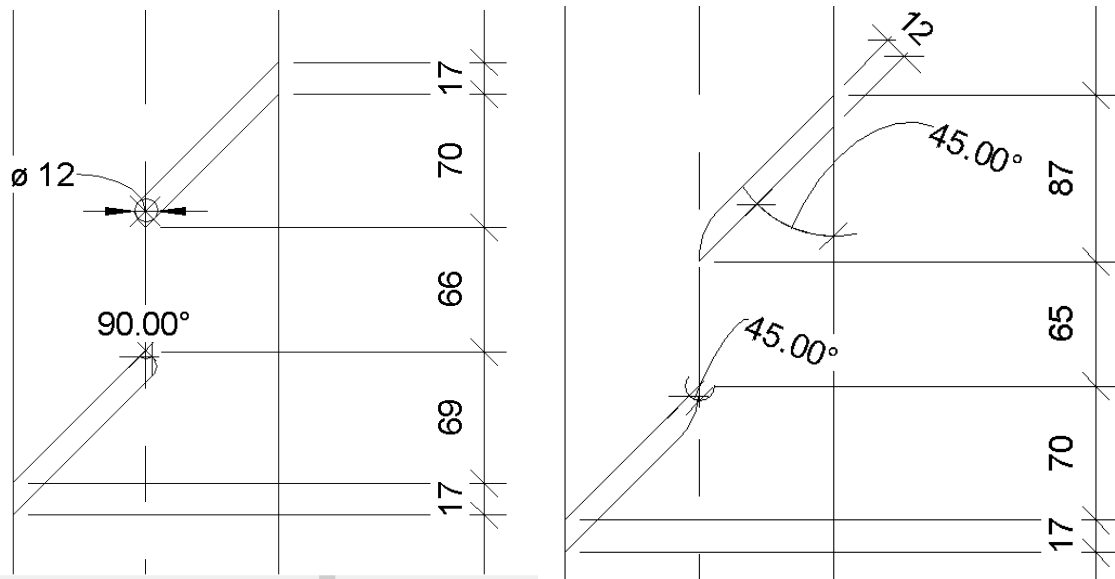
Figure 38- Notched 90 and Notched 45 geometry

The notched design specimen is mainly produced with a table saw and a floor-standing drill. This produces even and smooth surfaces, the transition zone requires extra attention from a file. The sharp design specimen is produced with a bandsaw. The bandsaw blade has a depth of 7 mm which is quite small. This enables the possibility of cuts with smaller radius.

For both type of specimen, special attention has been devoted to getting even and parallel end surfaces, to avoid eccentricity which would cause bending of specimen, and thus producing tension perpendicular to grain, contribution to failure mode 2. The parallel position of the notches is also important.
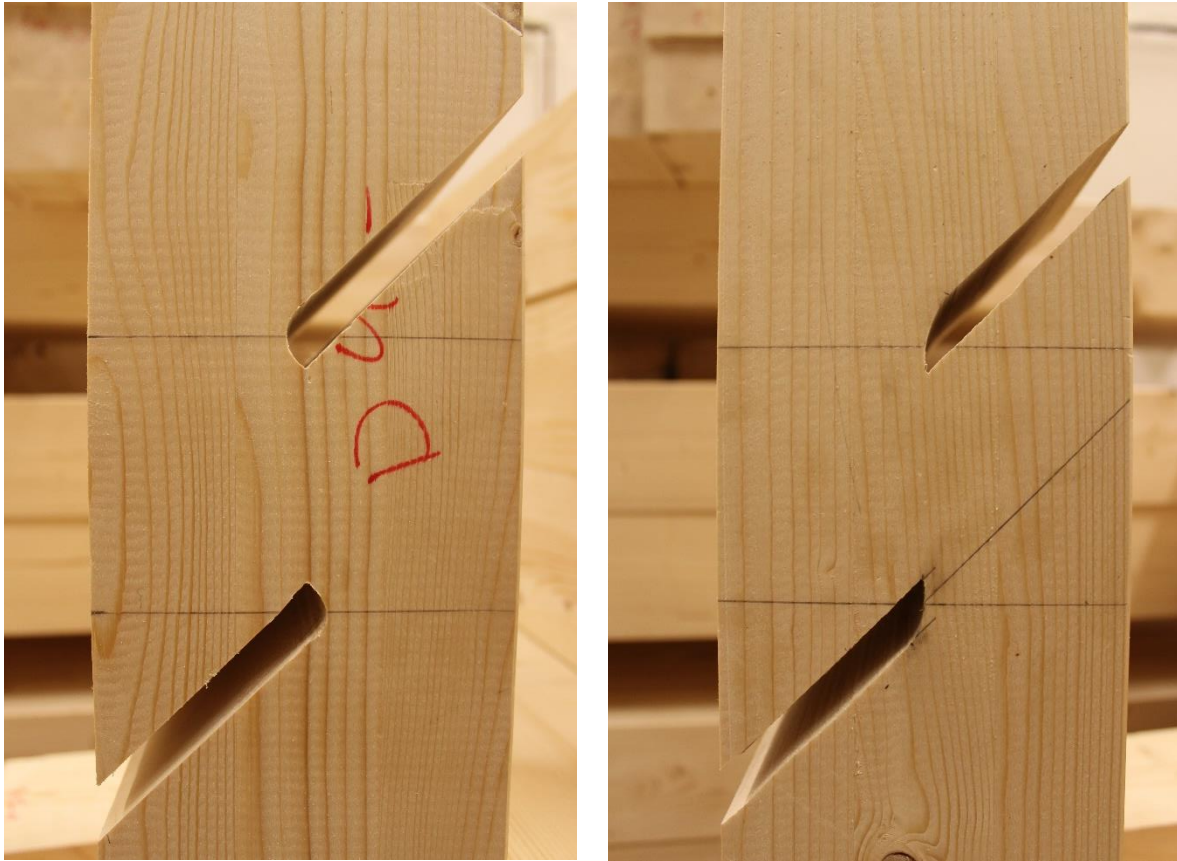
Figure 39 – picture of notched-90 TL design on the left and notched-45 TL design on the right, the only difference from Figure 38 is that the timber is rotated 90-degree with respect to the cutting.

2.3 Specimen identity

As for rods, the shear specimen is given informative names in order to keep track of the most important information related to the specimen. An example is F90-TL-E1-123

Information regarding:	Part:	Options	Description:
Specimen and test type	F	F, S	F for fatigue tested F for static tested
	90	45, 90	90 for notched-90 45 for notched -45
	-		
Orientation	TL	TL, RL	TL – tangential longidutional shear zone RL – Radial Longitudional shear zone
	-		
Section	E	A-L	Which beam the specimen were taken from
	1	1-8	Where in the length of the beam the specimen originate from
	-		
Lamellas	123	1-8	Which lamellas are included in the specimen. 1 starts at the lamella with annular rings in opposite orientation than the other.

2.4 Boundary conditions

To obtain uniform compression, the specimen is placed between two 35 mm thick steel plates, which are clamped in the hydraulic rig, see Figure 41.

The specimen is also fixed in the horizontal plane by 22 mm thick plywood brackets. These are only necessary for the fatigue testing but are used for static tests as well in order to gain equal stress situations with regards to the comparison and creating of SN-curves. See Figure 40 for plywood brackets.
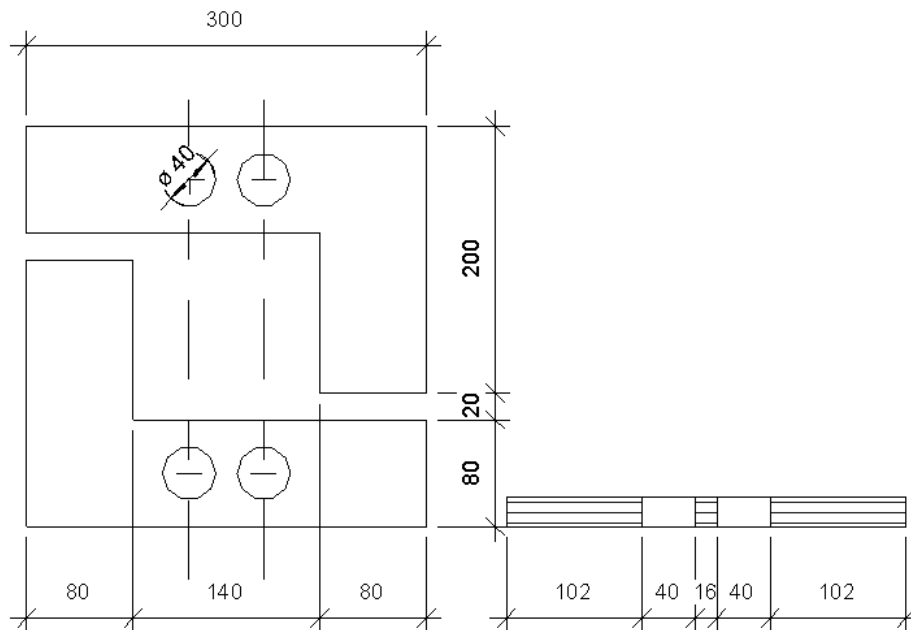
Figure 40-Plywood brackets

2.5 Load procedure and data recording from loadcell

The load procedure used for static testing follows NS-ISO 6891 [20] and failure is reached within $300 \pm 120 \; sek$ as defined in ISO 13910:2014 [24]. See Appendix k for load procedure used for static testing. For the static testing the load parameters was based on a shear capacity of $f_{v,g,k} = 3,5$ taken from NS-EN 14080. [26] The loading procedure runs to 40% of estimated capacity before unloading to 10% and thereafter 70% before displacement controlled failure. This enables the possibility of investigating ultimate capacity but also elastoplastic behavior. Herein only the linear behavior is treated.

The fatigue test procedure is the same as described in appendix F, and is adjusted according to the specific geometry of every specimen. The mean shear capacity τ_{LR} and τ_{LT}, used for computing the fatigue load parameters, is taken from static testing of N90 and N45 and their RL and TL orientationThe most important load parameters are given in the table below.

Frequency	3,5 Hz
f_{max}	0,6-0,75
R	0,1

Table 2.2- Load parameters used in cyclic testing of shear specimen.

Two different hydraulic rigs are used for experimental testing, see table below. Wavematrix™ was used to control and program the load procedure for both static and cyclic loading. The data recording of displacement and load was carried out by Aramis for static loading. This was done in order to automatically input these data in the calculation of strain and stresses. For cyclic loading, another computer was used for logging load, displacement and cycle count. This was done because Wavematrix™ had a recording limit of 1000 cycles.

Hydraulic press	Static capacity	Problems	More information
Instron 1325	500 kN	Load variation and load noise, see chapter 3.7.1.	Appendix D
Schenk treble	1000 kN for loadcell and 6000 kN for frame.	Oil leakage	Appendix C

Table 2.3 – Hydraulic presses used in shear testing

The tests were run in the laboratory hall see part 2 for climate conditions. Therefore, a vapor barrier with thickness of approximately 2 μm was used to prevent the specimen from drying out, see Figure 41. The vapor barrier was folded to form a continuous layer against the pressure plates to avoid eccentricity.

The Schenk Treble hydraulic rig Figure 42 had an oil leak, due to a damage in the grip plates. The oil leakage was absent for static testing but evident for the fatigue testing. The vapor barrier protected most of the specimen. However, some specimen was exposed to small amounts in the lower ear of the specimen. This is assumed to not affect their behavior, see Appendix J.

Figure 41-Vapor barrier used during testing
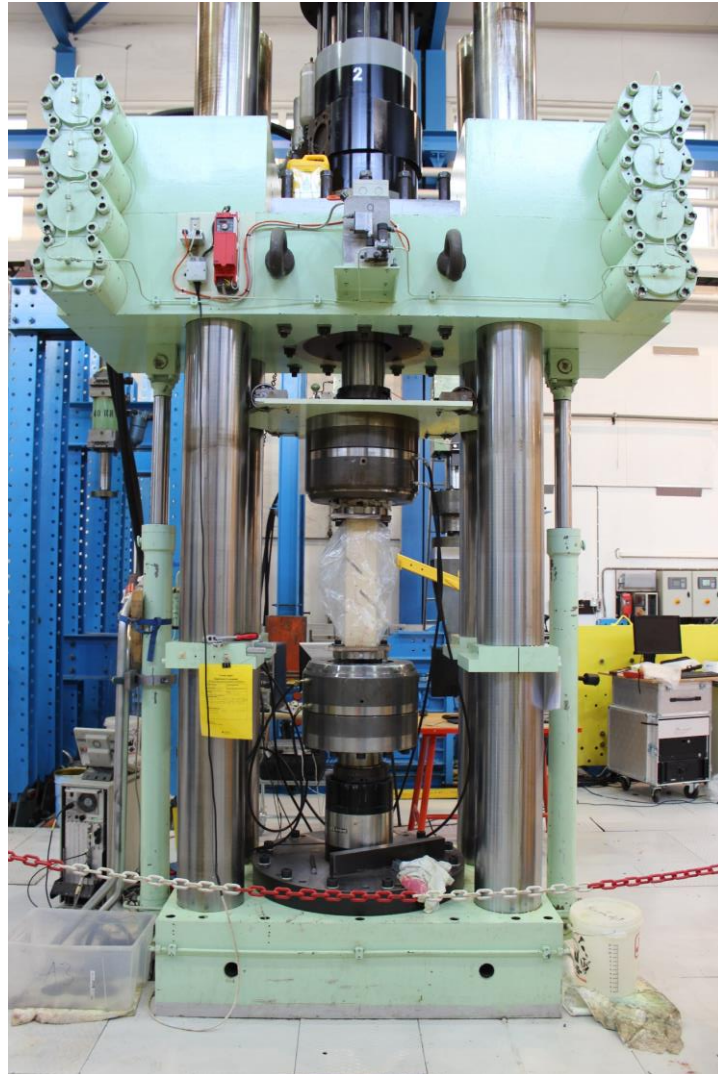
Figure 42-Schenk Treble

2.6 Aramis and Video extensometer

Video extensometer was used to measure the strains on the surface of the static specimen. The program and hardware used was produced by GOM® for the ARAMIS software. The software works by mapping a stochastic sprayed pattern with facets and assigns coordinates to these points. The software then measures the change of these coordinates in relation to one another and together with load and displacement data input from the loadcell, computes strains and stresses. The mapping itself is sensitive to light, measuring size, exposure time and spray pattern. Measuring size and exposure time are given, so the light and stochastic pattern must be adjusted accordingly. Several dummies were produced to get the right light intensity and stochastic pattern.

The system was calibrated with the full calibration process before each static test series, in accordance with the system manual.

The settings were as following:

Measuring volume	200x150 mm	Meassuring distance	290 mm
Lens	20 mm A1 (Titanar)	Slider distance	102 mm

	4M (4 million pixels)		
Camera angle	25,2°	Calibration object	CP20 175x140

The measurement deviation after calibration is documented in the worksheet for each specimen. The deviation ranged between 0,02-0,04 px.

2.7 Highspeed camera

Highspeed camera was used to measure the fracture propagation. The resolution on the highspeed camera was 254x384 pixels with a recording speed of 20 000 pps. The recording was stopped manually. Unfortunately, the recording speed was too low to capture the fracture propagation.

2.8 Weighing and drying

After failure, the specimen was dismounted and weighed before the shear zone was visually inspected for macroscopic deficiencies like knots and cracks. See Appendix k.

The mass of the specimen was found both prior m_1 and post m_2 to testing. This was done to determine the efficiency of the vapor barrier as well as determining the average mass during testing m_{avg}. The volume V_w of the specimen was calculated from the geometry. A slide caliper was used to measure the critical measurements.

The moisture content and density was measured according to ISO 13061-1:2014 [21] and ISO 13061-2:2014 [27]. However, the entire specimen was measured as a mean instead of 20mm cubes in contradiction to the standards. The precision level 1,0 in accordance with ISO13061-1:2014. Desiccators were not used. The dry mass m_{dry} of the specimen was found by drying the specimen at $103°C \pm 2°C$ for at least 3 days, before two successive weighing of samples were conducted with a minimum of 8 hour intervals to determine whenever constant mass was achieved. The formulas are listed in chapter 3.5.3.

2.9 Output

For each of the specimen in the series, the following data were extracted for further conclusions and interpretation of test results:
1) Date of testing
2) Geometrical parameters:
   a) Height H
   b) Breath b
   c) Depth d
   d) Distance from edge to notch on lower cut, b_1
   e) Distance from edge to notch on upper cut, b_2
   f) Shear zone height h
   g) Cut thickness t_1 and t_2
   h) Cuts' distance l
   i) Calculated volume V
   j) Calculated shear zone area A
3) Moisture content (MC)measured by digital wood moisture tester right
4) Mass right before test, m_1

5) Mass right after ended testing, m_2
6) Mass after drying, m_{dry}
7) MC resulting from mass measurements
8) Visible inspection
   a) Knots; size, orientation, location,
   b) Drying cracks after testing; size, orientation, location.
9) For static loading the calibration deviation was also documented
10) For static and cyclic loading, all load parameters were documented.

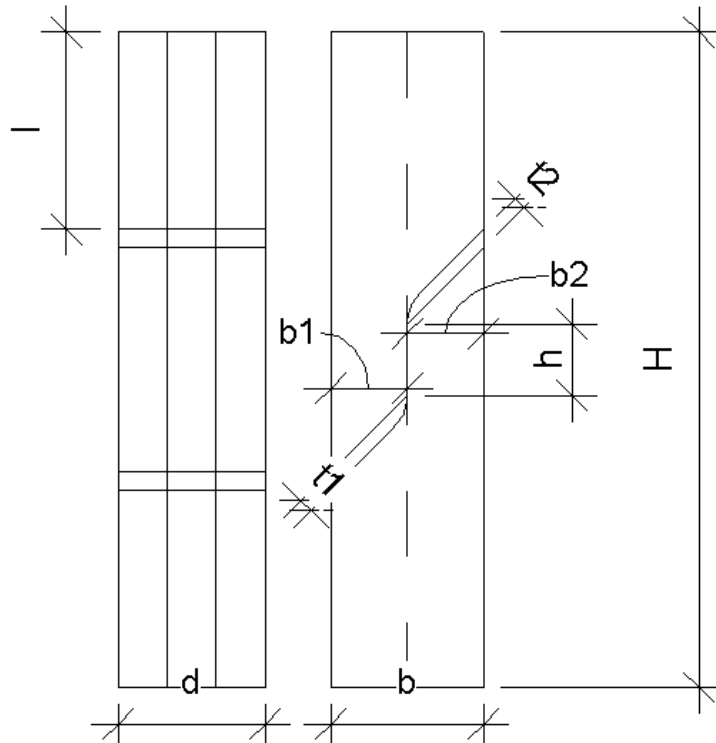The definition of the geometrical parameters can be seen in the figure below.

Figure 43- Definition of geometrical parameters

3 Static results

The following amount of specimen is tested:

Design	Mode	Orientation	nr. tests
Notched-90	Static	Radial	14
		Tangential	12
	Fatigue	Radial	13
		Tangential	12
Notched-45	Static	Radial	14
		Tangential	14
	Fatigue	Radial	11
		Tangential	12
Sum			102

3.1 Static testing results

The results from 51 static tests are listed in the table below with accompanying MC, density, number of cycles and failure modes, see appendix k for typical failure modes. There are 26 notched-90 specimens (see Tabell 3-2) and 25 notched-45 specimens (see Tabell 3-1), including both RL and TL orientation.

The accuracy of calibration for Aramis is also included, the acceptable limit for accuracy is 0,040. The specimen was weighed before and after testing to investigate the effectiveness of the vapor barrier. The results yielded 1,6 grams in average loss of mass., which corresponds to 0,04% average loss in MC during the static testing. The density p_{12} is based on the average mass during testing and is the mean density of the specimen, see chapter 3.5.3 for more information.

Orientation	Name	Accuracy of calibration	Failure mode	MC	measured density p_{12}	Max load F_{max}	Max stress τ_{max}
			[1,2]	[%]	[kg/m3]	[kN]	[N/mm2]
RL	S45-RL-C7-678	0,034	1	12,6	472,2	49,1	5,63
	S45-RL-I6-345	0,037	1	13,5	429,5	33,2	4,09
	S45-RL-H6-123	0,037	2	12,0	433,0	36,9	4,34
	S45-RL-I5-345	0,037	1	11,7	447,2	35,3	4,01
	S45-RL-I1-345	0,037	1	13,2	411,2	52,4	6,02
	S45-RL-H3-123	0,037	1	12,7	412,4	46,4	5,42
	S45-RL-H4-123	0,037	1	12,7	421,2	57,8	6,62
	S45-RL-H5-123	0,037	1	12,0	412,9	48,2	5,71
	S45-RL-H1-678	0,037	1	11,2	480,4	43,9	5,03
	S45-RL-I5-678	0,035	1	12,7	443,4	50,1	5,71
	S45-RL-C8-678	0,035	1	11,5	472,3	45,0	5,48
	S45-RL-xx-xxx7	0,035	1	10,8	419,5	37,1	6,70

	S45-TL-C7-345	0,034	2	11,6	365,2	53,9	5,97
	S45-TL-C8-123	0,034	1	13,1	419,4	45,0	5,13
	S45-TL-H2-345	0,037	1	11,6	395,3	48,8	5,42
	S45-TL-H2-678	0,035	1	11,6	481,3	68,7	7,35
	S45-TL-I2-123	0,035	1	13,7	434,0	70,2	7,71
	S45-TL-I1-678	0,035	1	12,8	431,4	59,7	6,52
TL	S45-TL-I4-678	0,035	1		425,5	62,7	6,90
	S45-TL-H4-456	0,035	1	11,7	453,9	58,1	6,41
	S45-TL-H5-456	0,035	1	11,8	450,4	58,1	6,39
	S45-TL-H3-678	0,035	1	11,5	484,5	73,4	8,25
	S45-TL-H1-234	0,035	1	12,9	396,8	48,6	5,70
	S45-TL-I3-678	0,035	3	12,4	418,7	46,0	5,14
	S45-TL-I6-678	0,035	1	12,5	431,9	55,4	6,27

Tabell 3-1- Static results of notched-45 specimen

Orientation	Name	Accuracy of calibration	Failure mode	MC	measured density	Max load	Max stress
					p_{12}	F_{max}	τ_{max}
				[%]	[kg/m3]	[kN]	[N/mm2]
	S90-RL-B2-123	0,04	2	13,1	475,8	37,7	4,72
	S90-RL-B3-123	0,04	1	12,9	473,1	38,0	4,56
	S90-RL-B7-234	0,04	1	13,3	464,8	46,5	5,24
	S90-RL-B1-123	0,037	2	12,8	487,9	35,6	4,25
	S90-Rl-B2-456	0,044	1	12,7	432,4	37,3	4,38
	S90-RL-B7-567	0,044	1	13,0	460,1	36,2	4,21
RL	S90-Rl-B4-654	0,04	1	13,0	433,2	36,0	4,41
	S90-Rl-B6-234	0,04	2	12,3	486,0	45,3	5,26
	S90-RL-B4-321	0,04	2	12,9	461,6	49,6	5,59
	S90-Rl-B6-567	0,04		12,8	443,4	30,8	3,52
	S90-RL-B8-567	0,04	1	12,5	455,5	36,2	4,27
	S90-Rl-B9-123	0,04		12,5	490,3	43,4	5,04
	S90-Rl-B5-567	0,034	1	12,8	450,3	26,0	3,03
	S90-TL-A3-456	0,04			442,3	28,0	2,88
	S90-TL-A2-543	0,031	1	13,5	416,3	37,1	4,19
	S90-TL-A1-234	0,04	2	10,1	405,1	51,1	5,77
	S90-TL-A6-345	0,04	2	14,0	425,8	40,1	4,39
TL	S90-TL-A6-678	0,04	1	13,0	413,9	41,4	4,88
	S90-TL-A3-123	0,04	2	13,7	452,4	34,2	4,02
	S90-TL-A1-567	0,04	2	13,1	421,9	42,8	4,91
	S90-TL-A4-123	0,04	2		457,3	51,1	5,52
	S90-TL-A5-678	0,04	1	12,8	412,7	46,8	5,11

S90-Tl-A4-678	0,04	2		436,4	44,6	4,90
S90-TL-C2-123	0,034	1		419,5	44,4	5,07
S90-TL-C1-456	0,034	2	11,2	395,8	35,5	4,00
S90-TL-C2-456	0,034	1	10,6	400,2	40,0	4,54

Tabell 3-2-Static results for notched-90 specimen.

The two dominant failure modes are failure mode 1 which is fracture in a single shear plane, and failure mode 2 which is fracture in two shear planes. Mode 2 is assumed to be caused by exceeding of tension capacity perpendicular to grain. Other influences are eccentricity caused by cracks or knots producing larger bending of specimen and therefore increased tension perpendicular to grain. This influence can be seen in the figure below for specimen D1-12

Figure 44-failure mode 2 due to drying cracks in shear plane causing deviation of fracture-plane.

A interesting observation was made regarding the RL specimen, the 3 lamella specimen and 2-lamella specimen does not fracture the same way. The lamellas in a 2-lamella specimen are more prone to behaving separately, the two lamellas can fracture independent of each other, see figure bellow. While the 3-lamella specimen fractured as a whole.

61

Figure 45-Partially Independent fracture of a 2 lamella specimen, notice the change in fracture over the adhesive zone.

3.2 Aramis results

Aramis was used to calculate the strains over the shear zone. Not all specimen was computed as there was a problem with the server, on witch Aramis ran. The power was cut by a default by other students in the laboratory, and the files saved on the Linux server are yet to be recovered as the computer cannot restart due to storage related issues. The IT department concluded that due to the formatting of the drives, a Linus expert should be involved, due to time limitations no such person is yet to be engaged. Computation is quite time consuming as well. The stress-strain curves computed from Aramis can be found in Appendix I. An example is shown below. The computation of results in Aramis was handled by Katarzyna Ostapska- Luczkowska.
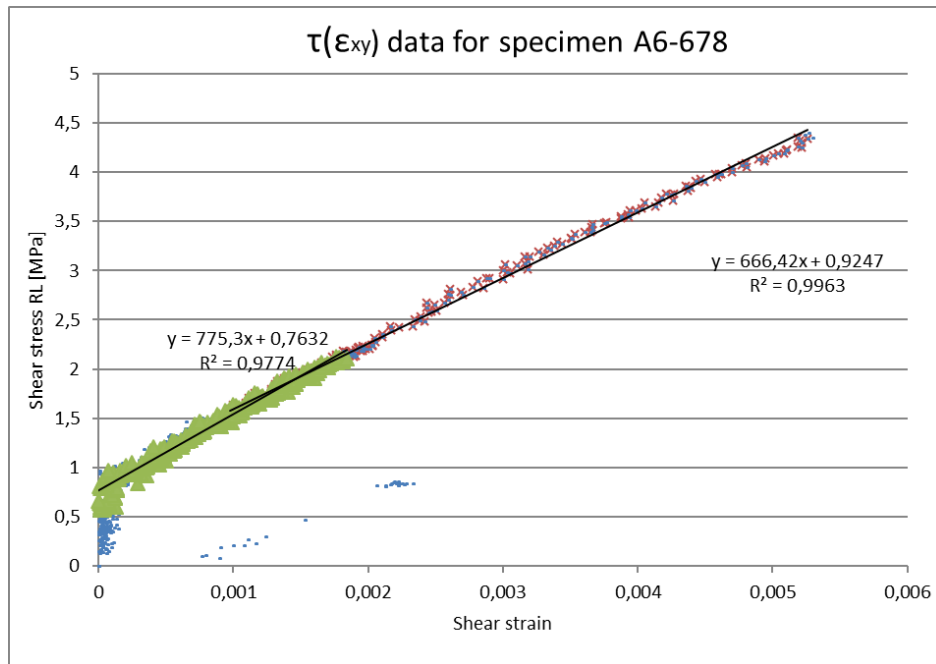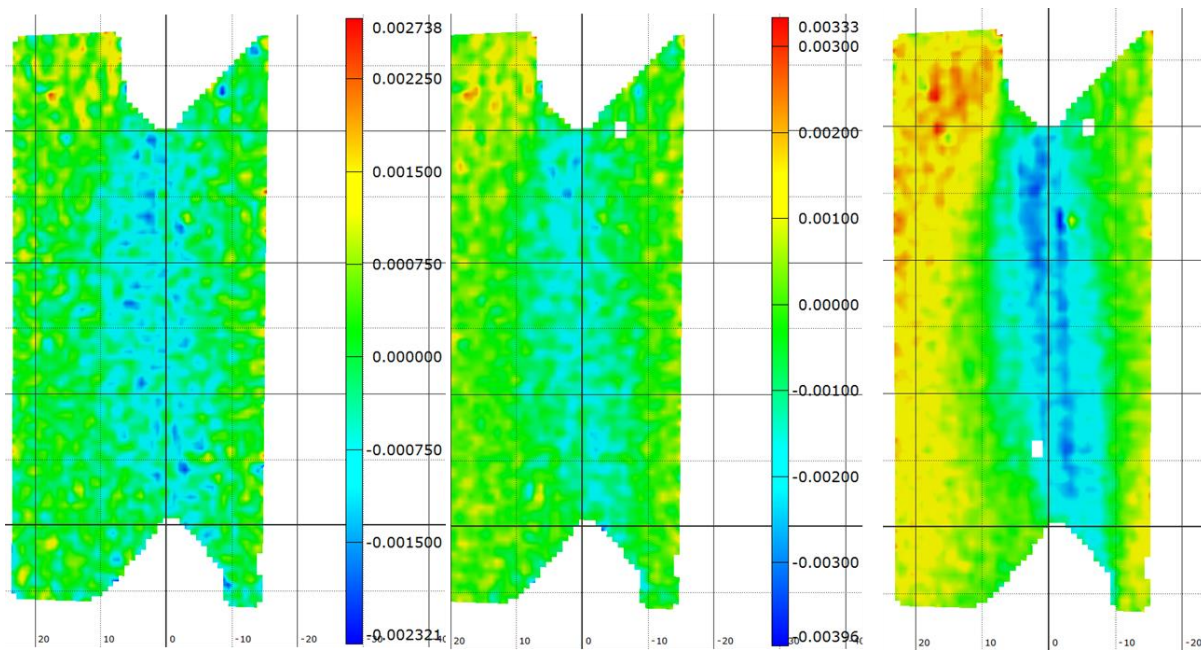
Figure 46-Stress-strain curves from Aramis

Figure 47-Shear distribution from Aramis

As the digital image correlation (DIC) in Aramis computed quite slowly, the area of interest was narrowed to focus on the shear strains as shown in Figure 47. This was done in order to finish the computation of the G-moduli. As such, the conclusion of optimization with regards to tension perpendicular to grain is not included in this thesis due to time limits, and thus it will be presented by Katarzyna Ostapska- Luczkowska.

4 Analysis of static results

4.1 Analysis of static testing

In accordance with 14358:2016[22], the lognormal distribution of static results yielded the mean, cov and characteristic values, presented in the figure below. The coefficient of variation is acceptable in the range of 0,08-0,12. The characteristic values comply well with NS-EB 14080:2013[18]. The notched-90 design gives a considerable lower capacity than the notched-45 design. This might be partially explained by fracture, the notched-90 design allows a less directed propagation of fracture and therefore the fracture can propagate onto weaker zones. The specimen might also produce less tension perpendicular to grain, this is yet to be fully investigated.

The TL specimen can also be observed to have a larger capacity for both designs. This might be explained by drying crack in the radial direction, this will severly reduce the capacity for RL specimen.

Summary of results		Mean	Standard deviation	Coefficient of variation	Characteristic value
		y	s	cov	f0,05
Design	Orientation	[N/mm2]	[N/mm2]		[N/mm2]
Notched-45 specimen	RL	5,40	0,17	0,10	4,29
	TL	6,40	0,15	0,08	5,34
Notched-90 specimen	RL	4,50	0,17	0,11	3,51
	TL	4,63	0,18	0,12	3,56
Combined Notched-45	TL and RL	5,92	0,18	0,10	4,11
Combined Notched-90	TL and RL	4,56	0,17	0,11	3,24
Combined designs	RL	4,93			
	TL	5,51			
	all	5,23			

Figure 48- Mean shear capacity, coefficient of variation, Standard deviation, Characteristic values.

4.2 Differentiate between LR and LT shear capasity

As cartesian material axes was impossible to obtain even with 140mm lamellas. The pure LT and LR shear properties must be found by a theoretical differentiation if this is desirable. It can be argued that the combined material properties of LT and LR, found herein, is more realistic with regards to some practical applications, as it is considered unlikely that a completely cartesian orientation of fibers will occur in practical applications. However, if desirable, two possible ambiguous methods are discussed in the following.

To differentiate between the shear capacity in LR and LT direction, two methods were devised. Little experience is known from such differentiations and as such, this should be considered as only supplementary information to the results above.

To differentiate, the area distribution between LR and LT must be known for the specimen. The specimens were 3D scanned in order to find the specific LR and LT areas, however to

due to lack of time, the script for analysis of areas were not made and therefore the specific areas are not known. The following calculations are therefore based on a presumed area of 1/3 in LT and 2/3 in LR.

The first method is based on solving the equation below as a simultaneous set of two equations, the specimens are paired together to solve for τ_{LR} and τ_{LT}. The mean, cov and characteristic values are calculated from these pares.

$$A_{LR,1} * \tau_{LR} + A_{LT,1} * \tau_{LT} = F_1 \qquad (26)$$
$$A_{LR,2} * \tau_{LR} + A_{LT,2} * \tau_{LT} = F_2$$

The results from this method is as following

two sets of equations	Notched 45 specimen	f_{RL}	8,71
		f_{TL}	4,45
	Notched 90 specimen	f_{RL}	6,32
		f_{TL}	3,57

The other method is based on non-linear least squared, and the equation is the same as above. But now the mean is found by reduction of the residual R^2 based on the difference in force F, see the equation below.

$$R = (F_{testing} - F_{mod,equation}) \qquad (27)$$

The results from this method is as following

Linear least square	Notched 45 specimen	f_{RL}	6,51
		f_{TL}	5,65
	Notched 90 specimen	f_{RL}	4,43
		f_{TL}	4,63

This method does not behave as expected, however it might behave different with a more realistic area distribution. This differentiation is not further discussed. The results should only be reviewed as supplementary information. The methods are only included on an informative basis for future testing.

4.3   G-modulus from Aramis computation

Aramis was used to calculate the strains over the shear zone. The G-modulus for the computed specimen are as following. See Appendix I for more information on stress-strain curves. As mentioned not all specimen were computed, unfortunately, no notched-45 specimen was computed, see chapter 3.2.

S90-RL-B4-654	TL	1370,6
S90-TL-A1-567	TL	1170,8
S90-TL-B2-123	RL	946,6
S90-RL-B7-234	RL	463
S90-RL-B3-123	RL	520
S90-RL-B4-321	RL	1720

Straigth-RL-C6-123	RL	691
S90-TL-C2-456	TL	1699
S90-TL-C2-123	TL	1015
S90-TL-C1-456	TL	1049
S90-TL-A6-678	TL	670,3
S90-TL-A6-345	TL	1020
SRound-A5-345	RL	615,19
S90-A4-TL-123	TL	1191
Average	RL	619
	TL	1148

Table 4.1-G-modulus for RL and TL specimen

Dahl and Malo [23] in their testing using the Arcan shear test for testing of specimen in LR and LT found the following results for the G-modulus.
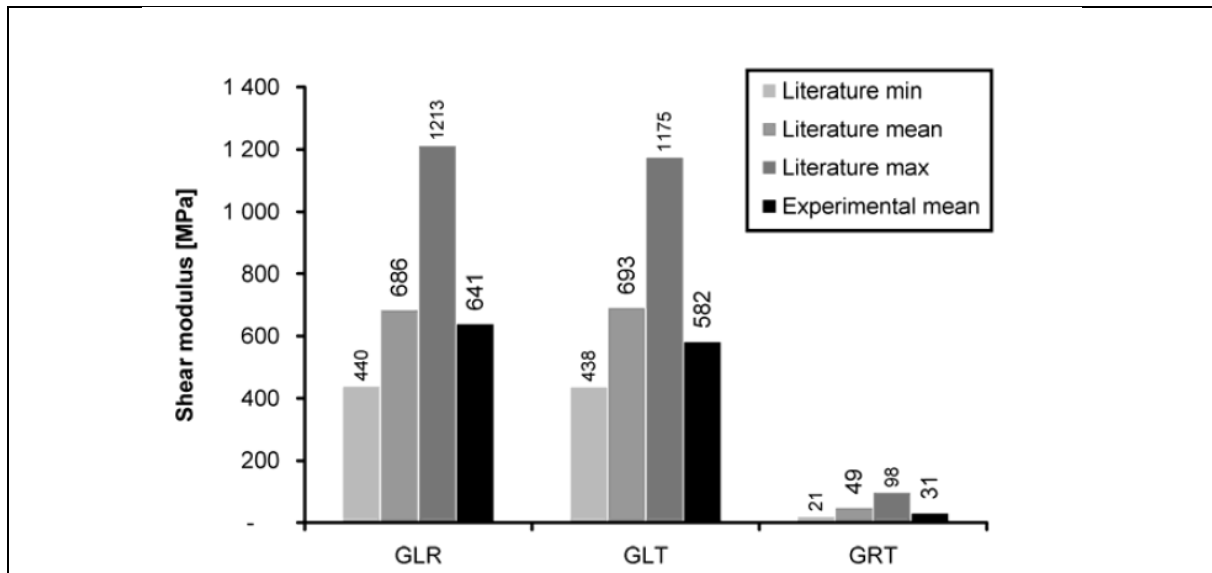

Figure 49- Average shear moduli from literature and experimental values from Dahl and Malo [15]

The average G-moduli of 619 complies well with Malo and Dahls investigation. The average G-moduli for the TL specimen of 1148 is however quite high. This might be due to the fact that the TL G-moduli is a combination of RL and TL and a transformation should be conducted, this will give a lower value for the TL. This transformation is not conducted due to shortness of time.

5   Fatigue results

The object was to experimentally evaluate the fatigue properties of timber in shear. As no conclusion had been made with regards to design. Both specimen was experimentally investigated in fatigue, this has also served as a comparison to investigate if the design would impact the fatigue property of the specimen.

The results from 48 fatigue tests are listed in the table below with accompanying MC, density, number of cycles and failure modes, see figure appendix k for typical failure modes. The specimen was weighed before and after testing to investigate the effectiveness of the vapor

barrier. For the specimen with registered mass reduction, the average loss in MC was 0,1%. However, 17 % of the specimen had an average increase in mass of 1 gram, due to oil leakage, or approximately 0,3% increase in mass. This is regarded as satisfactory results considering the average fatigue testing time was 5,2 hours per specimen. Temperature measurements uncovered no temperature increase for the 3,5 Hz frequency. The density p_{12}, is based on the average mass during testing and is the mean density of the specimen, see chapter 2.8 for more information.

	Name	Failure mode	MC	Density, p12	Crack lengt	Fmax - corrected	N	Fmax - uncorrected
			[%]	[kg/m3]	[mm]	[%]		[%]
F90-TL	F90-TL-C5-xxx	2,0	12,7	441,3		70,1	23182,0	70,1
	F90-Tl-D3-123	1,0	12,5	459,5		66,3	104419,0	66,3
	F90-TL-D4-123	1	11,1	437,4		65,9	282451	65,9
	F90-TL-C1-123	1	12,3	413,1		66,2	700	66,2
	F90-TL-E4-678	1	12,4	403,9		65,7	20089	65,7
	F90-TL-D6-456	1	11,5	371,3		65,8	27544	65,8
	F90-TL-E5-123	1	13,1	441,9		65,3	74351	65,3
	F90-TL-unknown1	2	11,5	402,5		61,9	104301	61,9
	F90-TL-E1-123	1	12,4	422,4		68,4	51943	68,4
	F90-TL-D5-123	1		417,8		68,4	112903	68,4
	F90-TL-D7-123	1	11,2	442,8		68,4	79224	68,4
F90-RL	F90-RL-D2-123	1	11,7	436,8	44,0	98,3	103	67,0
	F90-RL-E4-123	1	12,4	417,1	31,0	96,8	5	74,2
	F90-RL-E6-567	1	12,9	443,2		72,1	29708	72,1
	F90-RL-C3-123	1	11,8	428,4	30,0	92,8	1663	71,7
	F90-RL-E6-123	1	13,3	426,1	69,0	138,3	427	69,2
	F90-RL-C3-678	1	12,7	435,8	22,5	86,3	94	71,6
	F90-RL-unknown	1	11,8	405,1		71,6	97712	71,6
	F90-RL-D2-456	1	11,9	373,5	31,0	93,0	330	71,4
	F90-RL-D4-456	1	11,7	360,5		71,1	49490	71,1
	F90-RL-C4-123	1	12,3	431,3		71,9	150851	71,9
	F90-RL-D5-456	1	11,2	360,4		72,1	7	72,1
	F90-RL-noName	1	11,6	412,7		71,3	581	71,3
	F90-RL-D6-123	1	10,8	435,6		70,8	291915	70,8
F45-TL	F45-TL-E1-678	1	11,5	424,8		49,5	8	49,5
	F45-TL-I4-678	1	19,1	449,1		56,7	33815	56,7
	F45-TL-J3-678	1	11,4	434,9		56,8	10564	56,8
	F45-TL-K5-678	1	10,8	405,7		56,9	24423	56,9
	F45-TL-K4-678	1	10,5	414,7		56,9	338433	56,9
	F45-TL-J1-345	1	10,6	461,3		56,8	67438	56,8
	F45-TL-J4-456	1	10,8	450,6		56,9	8544	56,9
	F45-TL-K3-567	1	11,0	409,9		56,8	5606	56,8
	F45-Tl-k2-678	1		428,4		56,8	46889	56,8
	F45-TL-K2-345	1	10,8	395,9		56,9	53611	56,9
	F45-TL-K1-678	1		407,9		57,0	41460	57,0
F45-RL	F45-RL-E7-12	1	12,2	442,6		57,4	136537	57,4
	F45-RL-E3-45	2	12,5	444,6	0,0	56,8	301694	56,8
	F45-RL-D1-12	2	17,9	438,4	81,0	798,4	112	63,5

F45-Rl-E5-78	2	13,0	430,1	0,0	57,4	52070	57,4
F45-RL-D5-78	2	11,3	420,9		56,6	182820	56,6
F45-RL-C8-45	2	11,6	351,0		94,9	19	94,9
F45-RL-E4-45	2	11,8	442,6		62,3	71847	62,3
F45-RL-C1-78	1	12,4	441,5		62,7	1446	62,7
F45-RL-unknown4	2	11,6	430,8		62,4	23960	62,4
F45-RL-I2-567	2		441,9		62,4	47	62,4
F45-RL-C7-12	2	11,8	433,2		62,4	26456	62,4
F45-RL-K5-123	1		494,8		63,4	150996	63,4
F45-RL-J3-345	1		449,9		63,5	41617	63,5

Table 5.1- Fatigue results from shear testing

The average density is 424 kg/m3 and the average number of cycles is approximately 65100. Correlation between density and number of cycles were not investigated due to lack of time. Several specimens had substantial cracks upon investigation. This was taken into account and two different SN-curves were devised, see analysis.

Figure 50-Pictures of fracture patterns in shear

.

6 Analysis of fatigue performance

6.1 Number of cycles, statistics.

The number of cycles were investigated using the lognormal distribution for the logarithm of number of cycles. The fit of the distribution was not investigated due to shortness of time. The results are described in the figures bellow.

Summary of results, number of cycles		mean	Mean (log)	std	cov
		y	y	s	
		N			
Notched-45 specimen	RL	76125	4,016	0,489	0,377
	TL	57345	4,173	0,494	0,365
Notched-90 specimen	RL	47914	3,190	0,662	0,666
	TL	80101	4,635	0,173	0,114

Table 6.1- Statistical distribution of N for Shear specimen

An interesting observation can be seen from the Notched-45 design; The RL orientation has more cycles in average than the TL orientation, this is somewhat unexpected. For the Notched-90 deign this is opposite. This might be explained as the RL design is more directing with regards to the fracture path and perhaps less tension perpendicular to grain.
The coefficient of variation is very high for the Notched-90 RL specimen, again this probably due to drying cracks. Per contra, the coefficient of variation for Notched-45 RL is in the range of the TL configurations. This supports the assumption that the Notched-90 design allows for a less directed shear fracture which means the fracture propagates onto the weaker zones. The coefficient of variation is quite low for the Notched-90 TL design. This is understandable when looking at the results in table Table 5.1. This might be explained as the TL orientation has less influence of cracks and the Notched-90 allows for a less directed fracture path, producing more even results.

6.2 SN-curves

The parameters for the SN-curves are listed in the table and follows equation 28.

$$\bar{f} = Alog(N) + B \qquad\qquad (28)$$

Two sets of equations were made for each specimen. The adjusted equation was made by correcting the normalized load level after inspection of cracks. This means that the adjusted equation gives the fatigue strength when there are no cracks. The "not adjusted" equation gives the fatigue strength of timber with cracks. From the table below it is seen that it is the RL equations that are affected the most by this adjustment. This is quite simply because several of the specimen had drying cracks in the RL directions, while few TL specimen had drying crack in the shear plane, see also table Table 5.1 column 8.

	A	-0,0621
N90-Tl: adjusted	B	0,9585
	R^2	0,6556
	A	-0,0621
N90-Tl: not adjusted	B	0,9585
	R^2	0,6556

69

N90-RL: adjusted	A	-0,0527
	B	0,9646
	R^2	0,5084
N90-RL: not adjusted	A	-0,0568
	B	0,9296
	R^2	0,4817
N45-TL: adjusted	A	-0,0815
	B	0,9284
	R^2	0,7008
N45-TL: not adjusted	A	-0,0815
	B	0,9285
	R^2	0,7008
N45-RL: adjusted	A	-0,0745
	B	0,9672
	R^2	0,6413
N45-RL: not adjusted	A	-0,0747
	B	0,9607
	R^2	0,6278

The results for both static and fatigue results are plotted in the figures below for the different orientations.
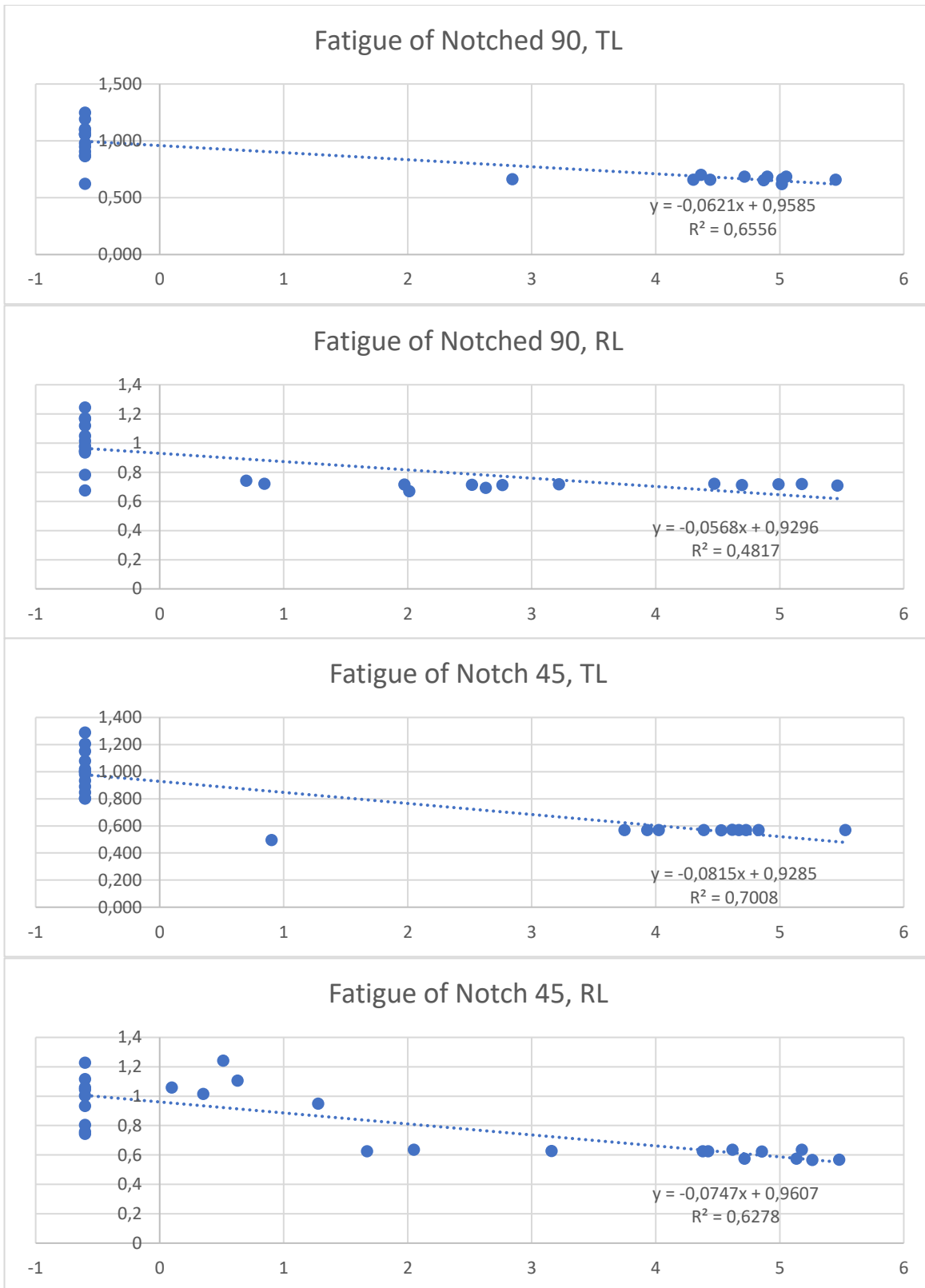
Figure 51-SN-curves with plots for static and fatigue results for both N90 and N45 in RL and RL orientation.

A interesting observation is made from the SN-curves; The N90 design gives a less steep slope for the RL orientation compared to the N45 design.
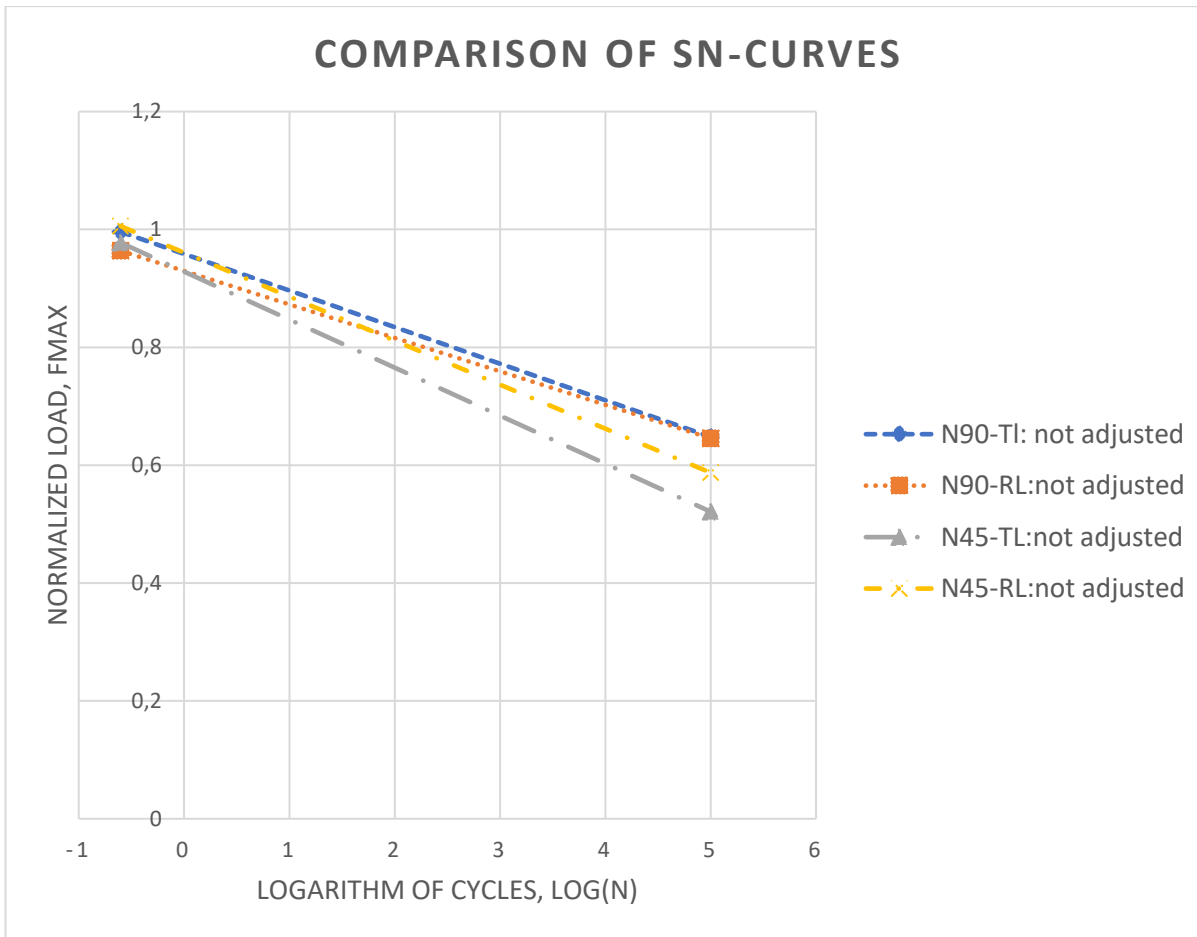
Figure 52-Comparison of the resulting SN-curves

The Following literature with equation and parameters are compared to the SN-shear curves found herein, in Figure 54.

Kvittingen rod 0 - not redistributed	"A*log(N)+B"	A	-0,0398
		B	0,9756
Kvittingen rod 5 - not redistributed	"A*log(N)+B"	A	-0,0374
		B	0,9531
Løkken 45°	"-0,023Ln(x)+0,9738"	A	-0,023
		B	0,9738
Løkken 90°	"-0,022ln(x)+0,9694"	A	-0,023
		B	0,9738
EC5-2 shear	$k_{fat} = 1 - \dfrac{1-R}{a(b-R)} logN$	R	0,1
		a	6,7
		b	1,3
EC5-2 tension	$k_{fat} = 1 - \dfrac{1-R}{a(b-R)} logN$	R	0,1
		a	9,5
		b	1,1
EC5-2 dowels	$k_{fat} = 1 - \dfrac{1-R}{a(b-R)} logN$	R	0,1
		a	6
		b	2

Malo	"A*log(N)+B"	A	-0,066
		B	0,96

Figure 53- Equations and parameters for comperable SN-curves

From the figure below it can be seen that the resulting SN-curves compare well with literature. Compared to the rods in part 2. The fatigue life is substantially lower, but compared to the conservative Eurocode for bridge design [16] it is somewhat higher, as expected. Other literature sources have ranged in the area of 0,075 to 0,090 for the inclination parameter A. This is not further investigated due to shortness of time.
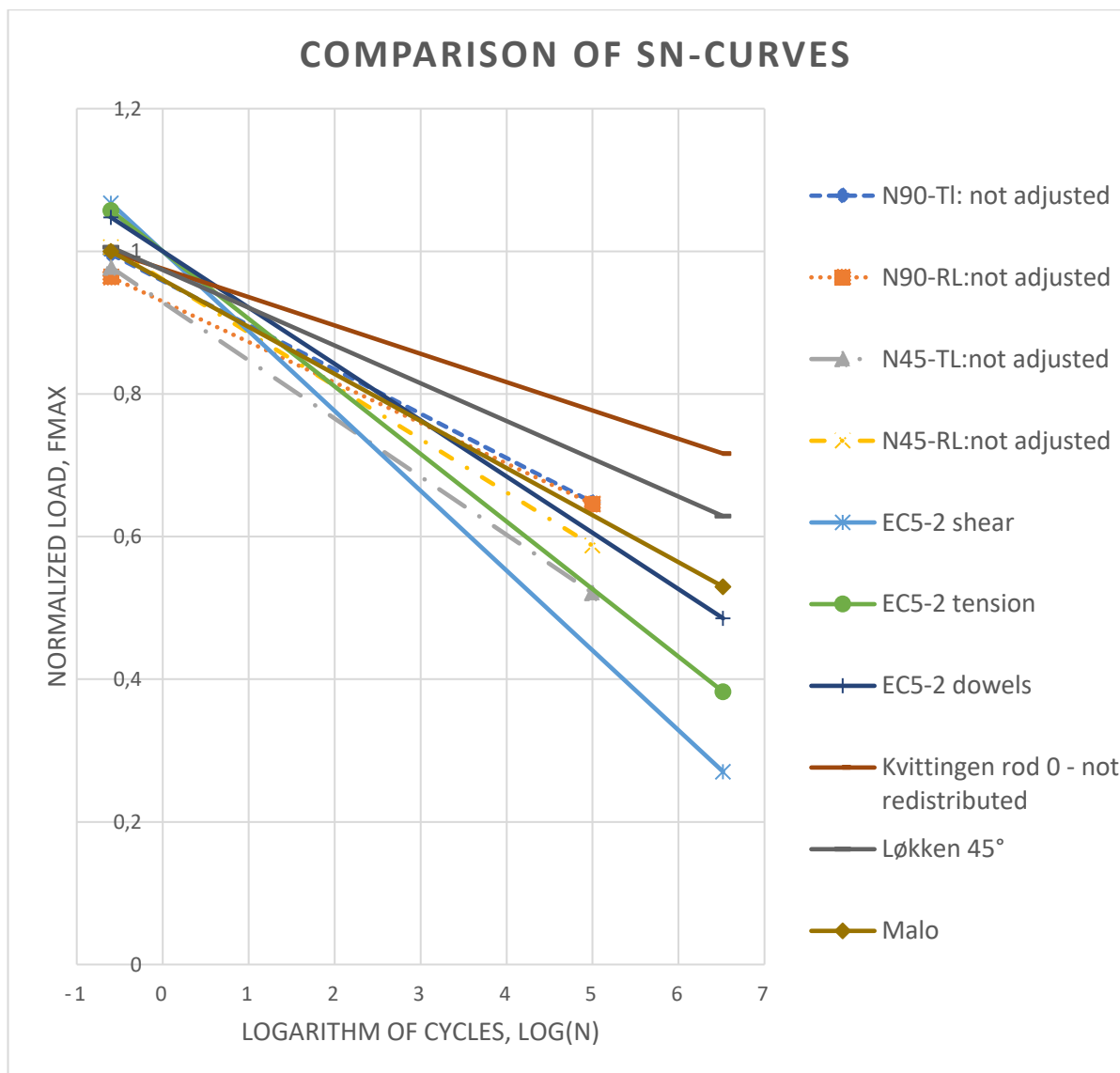
Figure 54-Comparison of resulting shear SN-curves to literature.

7   Conclusion, remarks and future work

The static and fatigue strength of the shear test have been investigated for two different designs Notched-90 and Notched-45, each for the two orientation RL and TL. The results amount to a total of 99 valid test specimens, 51 static specimens and 48 fatigue specimens. The following concluding remark are made:

73

- Structures subjected to shear loading with a normalized load of 0,75 may experience fatigue damage.
- The fatigue strength of timber in RL and TL for both designs seem conservative with regards to the Eurocode.
- The test setup was easy to produce, and easy to test, the vapor barrier work efficiently.
- The effect of drying cracks has a significant effect on the fatigue strength, especially for the RL orientation.
- Further analysis of data is necessary to determine the effectiveness of the shear test.
- The Notched-45 design gives larger capacity for both RL and TL in static.
- For fatigue life, the SN-curve is steeper for both RL and TL with Notched-45 design.

A couple of remarks:
- The G-moduli for LT found herein is quite high as it is a combination of both TL and RL properties, see chapter 4.3.
- Different literature have indicated an increased fatigue life with frequencies above 1 Hz, herein a frequency of 3,5 is used.

For future work the following should be further investigated:
- The differentiation discussed in chapter 4.2.
- Recalculate the G-moduli for as discussed in chapter 4.3.
- The investigation and computation of all datasets from Aramis as discussed in 3.2.
- Further investigate the tension perpendicular to grain and the effectiveness of design.
- Investigate a density-shear parameter correlation effect for existing results.
- Calculate hysteresis loop.
- Consider duration of load effect.
- Continued testing for other parameters such as R=-1, frequencies of 1.0 , 0.1 and 0.01, and maybe other climate classes.

8 Refrences

[1]   R. Bainbridge, C. Mettem, K. Harvey, and M. Ansell, "Bonded-in rod connections for timber structures—development of design methods and test observations," *International Journal of Adhesion and Adhesives,* vol. 22, no. 1, pp. 47-59, 2002.

[2]   H. Stamatopoulos and K. A. Malo, "Withdrawal Properties of Threaded Rods Embedded in Glued-Laminated Timber Elements," ed: NTNU, 2016.

[3]   N. Løkken and K. A. Malo, "Fatigue of Threaded Rods Subjected to Axial Load," ed: NTNU, 2016.

[4]   M. Gougeon, J. B. Esgar, D. A. Spera, and M. D. Zuteck, "Structural properties of laminated Douglas fir/epoxy composite material - NASA-RP-1236 - DOE/NASA/20320-76," ed: Sponsoring Organization: NASA Lewis Research Center, 1990.

[5]   I. Smith, E. Landis, and M. Gong, *Fracture and fatigue in wood*. Chichester: Wiley, 2003.

[6]   P. K. Larsen, *Dimensjonering av stålkonstruksjoner*, 2. utg. ed. Trondheim: Tapir akademisk forl., 2010.

[7]   B. Harris, *Fatigue in Composites : Science and Technology of the Fatigue Response of Fibre-Reinforced Plastics* (Woodhead Publishing Series in Composites Science and Engineering). Boca Raton: Woodhead Publishing, 2003.

[8]   L. Li, M. Gong, I. Smith, and D. Li, "Exploratory study on fatigue behaviour of laterally loaded, nailed timber joints, based on a dissipated energy criterion," *Holzforschung,* vol. 66, no. 7, pp. 863-869, 2012.

[9]   K. Tsai and M. Ansell, "The fatigue properties of wood in flexure," *Journal of Materials Science,* vol. 25, no. 2, pp. 865-878, 1990.

[10]   C. Hacker and M. Ansell, "Fatigue damage and hysteresis in wood-epoxy laminates," *Journal of Materials Science,* vol. 36, no. 3, pp. 609-621, 2001.

[11]   I. Bond and M. Ansell, "Fatigue properties of jointed wood composites Part II Life prediction analysis for variable amplitude loading," *Journal of Materials Science,* vol. 33, no. 16, pp. 4121-4129, 1998.

[12]   I. Bond and M. Ansell, "Fatigue properties of jointed wood composites Part I Statistical analysis, fatigue master curves and constant life diagrams," *Journal of Materials Science,* vol. 33, no. 11, pp. 2751-2762, 1998.

[13]   C. Astle *et al.*, "Timber for small wind turbine blades," *Energy for Sustainable Development,* vol. 17, no. 6, pp. 671-676, 2013.

[14]   C. O. Clorius, M. U. Pedersen, P. Hoffmeyer, and L. Damkilde, "Compressive fatigue in wood," *Journal of the International Academy of Wood Science,* vol. 34, no. 1, pp. 21-37, 2000.

[15]   K. A. Malo, W. Nordic, and P. Nordic Timber Bridge, *Fatigue tests on dowel joints in timber structures*. Stockholm: Nordic Timber Council AB, 1999.

[16]   Pronorm, *Eurokode 5: Prosjektering av trekonstruksjoner : Del 2 : Bruer*. Lysaker: Pronorm, 2005.

[17]   H. Stamatopoulos and K. A. Malo, "Withdrawal capacity of threaded rods embedded in timber elements," *Construction and Building Materials,* vol. 94, pp. 387-397, 2015.

[18]   *Timber structures - Glued laminated timber and glued solid timber - Requirements*, NS-EN 14080:2013+NA:2016, 2013.

[19]   *Eurokode 5: Prosjektering av trekonstruksjoner = Eurocode 5: Design of timber structures. Part 1-1: General common rules and rules for buildings : Del 1-1 : Allmenne regler og regler for bygninger* (Eurocode 5: Design of timber structures. Part 1-1: General common rules and rules for buildings). Lysaker: Standard Norge, 2010.

[20]   *Timber structures - Joints made with mechanical fasteners - General principles for the determination of strength and deformation characteristics (= EN 26891:1991) (ISO 6891:1983)*, NS-ISO 6891:1983, 1991.

[21]   *Physical and mechanical properties of wood — Test methods for small clear wood specimens — Part 1: Determination of moisture content for physical and mechanical tests*, ISO 13061-1:2014, 2014.

[22]   *Timber structures - Calculation and verification of characteristic values*, NS-EN 14358:2016, 2016.

[23]   K. B. Dahl and k. Norges teknisk-naturvitenskapelige universitet Institutt for, "Mechanical properties of clear wood from Norway spruce," 2009:250, Norwegian University of Science and Technology, Faculty of Engineering Science and Technology, Department of Structural Engineering, Trondheim, 2009.

[24]   *Timber structures — Strength graded timber — Test methods for structural properties*, ISO 13910:2014, 2014.

[25]   L. Sigbjørnsen, K. A. Malo, and F. F. I. O. T. I. F. K. Norges Teknisk-Naturvitenskapelige Universitet, "Shear Properties of Nordic Glulam CE L40c," ed: Institutt for konstruksjonsteknikk, 2012.

[26]   *Timber structures - Glued laminated timber and glued solid timber - Requirements*, NS-EN 14080:2013+NA:2016, 2016.

[27]   *Physical and mechanical properties of wood — Test methods for small clear wood specimens — Part 2: Determination of density for physical and mechanical tests*, ISO 13061-2:2014, 2014.

Appendix A – Threaded rod documentation

DOKKA FASTENERS

Vår ref / Our ref	Dato / Date	Sertifikatnr. / Certificate No.
Hilde Loeng	11. April, 2016	**548122**

Kunde / Customer	Produksjonsordrenr / Production Order no.	Salg-eksp.-no
NTNU/ Kjell A.Malo / Odd Nerdal	548122	Sales-exp. No 161513

Institutt for konstr.teknikk, Port 1	Kundens ref./ Customers ref.
Rich.Birkelandsv.1a, 7491 Trondheim	117319

NORGE	Kundens tegning / Customer drawing

Kund.det.nr./ Customer part no.	Artikkelnr., benevning / Part no., part name
	77 pcs Stud bolt, M20 x 1900, cl. 8.8 , DFS 1626

Omfang / extent

INSPECTION CERTIFICATE   EN 10204 - 3.1

It is hereby certified that the products covered by this certificate has been tested and is compliant with the requirements of the order.

Product standard DFS 1626 pos.1

Mechanical properties: ISO 898-1:2013, Cl. 8.8.

Threads: M. tol. cl. 6az. ISO 965-4:1998, before hot dip galv.

Product marking: DF 8.8U 122

Foreskrevet materiale / Prescribed material	Levert materiale / Supplied material
acc. to. ISO 898-1	GERDAU 32 CrB4

MATERIALANALYSE / CHEMICAL COMPOSITION

Charge nr.	C	Si	Mn	P	S	Cr	Ti	B	Al	Cu
176201	.33	.20	.82	.009	.003	1.09		.0033		.15
Analysekrav / min	.30	.12	.70			1.05		.0020		
Specification max	.34	.25	.90	.015	.015	1.20		.0050		.25

VARMEBEHANDLING / HEAT TREATMENT

Hardened and tempered

MEKANISKE EGENSKAPER / MECHANICAL PROPERTIES

Prøve på ferdig produkt / test on manufactured product	Krav / Specification		Prøveres. / Test results		Prøveantall / Number .of samples	Anmerkning / Note
	Min. !	Max	Min. !	Max		
Zn belegg / Zncoating μm						
Strekkfasthet/Tensile strength Rm N/mm²						
$R_{p0.2}$ på hel bolt / $R_{p0.2}$ on full size bolts N/mm²						
Hardhet / Hardness HB	250	331	264	277	5	Average 271
Spesiell strekkprøving / Special tensile test Strekkfasthet/Tensile strength Rm N/mm²	830		938	966	3	Prøvestaver iflg. / Test pieces acc to Ø 12.6
Flytegrense / Yield stress Rel Rp₀.₂ N/mm²	660		855	889	3	
Forlengelse / Elongation A₅ %	12		14	15	3	
Kontraksjon Z %	52		62	65	3	Average 63
Skårslagprøve / Impact test kV 300 Joule						Prøvestaver iflg. / Test pieces acc to EN 10045-1
Slagseighet / Impact strength Joule	27 J		121	138	3	Test pieces: 10x10x55 Single values: 138 – 121 – 131 J
Prøvetemperatur / Test temp. °C	- 20°					

Kvalitetskontrollavdeling / Quality Control Department

Hilde Loeng   Phone: 61 11 30 30   Fax: 61 11 30 03

Maks 2p ufulls. gj.

d

b2

b3

b1

L(js17)

R0.4

8

150°

2.4

ø22,40

ø17,60

ø16,13

45°

R1

DF   8.8U

***

Charge mrk.
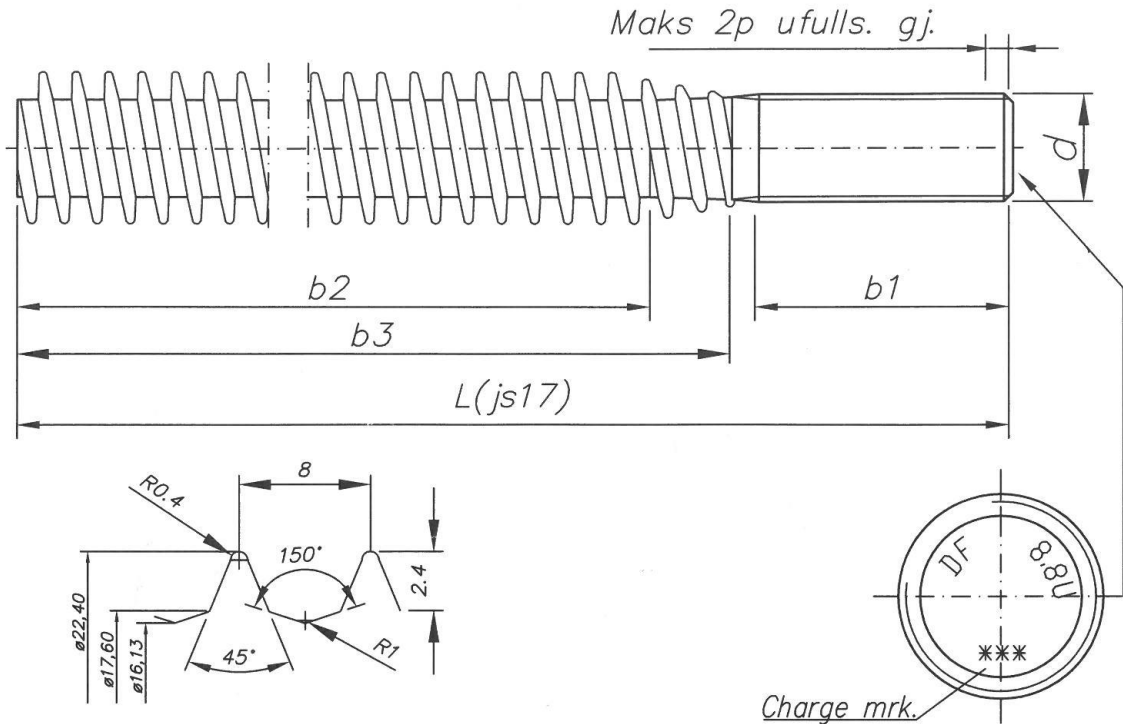
Gjenger: M, tol kl. 6az iflg DF-SP-693-51 før vfz. ISO 965-4(6az)
Mek. egensk. iflg. ISO 898-1:2013 kl 8.8.
Form og beliggenhetstol ifl DIN ISO 4759-1 utf. kl. B
Overflate: Varmforsinkes ISO 10684, høytemp skal benyttes (530-560℃)

Pos.nr.	1		2		3		4		5	
Gjenge d	M20									
P	2.5									
	min	maks	min	maks	min	maks	min	maks	min	maks
Materialdiam.	17,966	18,050								
b1	90	95								
b2	1750	–								
b3	–	1800								
L	1892,5	1907,5								
Bruddgr. N/mm2	830									
Flytegr. N/mm2	660									
Forlengelse, A5%	12									
Slagseighet J.	27									
Test temp.℃.	-20									
Kunde	NTNU									
Kundetegn.	Mail 16.12.15									

Stk. antall	Gjenstand	Pos.nr.	Materiale	Emnesm?l–Modell nr.	Netto Vekt–kg	Tegn.nr.–Anmerkninger

Forandr.

AVDELING: _____

Gruppe   SALGSVARER

Undergr. _____

Delgruppe _____

TITTEL: Pinbolt, spes. gjenger for tre
          i ene enden. NTNU

Målestokk
—

Dato   Navn
Tegn. 16.12.15 T.Låksrud

Kontr.

Godkj: 16/12-15 EL

Erstatn. for:

DFS-1626-1

Erstattet av:

DOKKA FASTENERS

For 1 stk.

2

Appendix B – characteristic strength and stiffness properties

MOELVEN

KARAKTERISTISKE
FASTHET - OG STIVHETSEGENSKAPER
FOR GRAN OG TRYKKIMPREGNERT LIMTRE

Egenskap	Symbol	Enhet	CE merket Limtre GL30C	S-bjelken	Smalt Limtre
Bøyning	$f_{m,k}$	N/mm²	30	28	24**
Strekk	$f_{t,0,k}$	N/mm²	19,5		
	$f_{t,90,k}$	N/mm²	0,5		
Trykk	$f_{c,0,k}$	N/mm²	24,5		
	$f_{c,90,k}$	N/mm²	2,5 (5,5*)		
Skjær	$f_{v,k}$	N/mm²	3,5		
Rulle skjær	$f_{r,k}$	N/mm²	1,2		
Elastisitetsmodul	$E_{0,\ mean}$ deformasjonsberegning	N/mm²	13 000	12 500	
	$E_{0,\ 05}$ stabilitetsberegning	N/mm²	10 800		
	$E_{90,\ mean}$ deformasjonsberegning	N/mm²	300		
Skjærmodul	$G_{0,\ mean}$	N/mm²	650		
Rulle skjærmodul	$G_{r,\ mean}$	N/mm²	65		
Densitet	ρ_k styrkeberegning	kg/m³	390		
	ρ_{mean} lastberegning	kg/m³	430		

Karakteritiske fasthetsverdier for styrkeklasse GL30C er i.h.t NS-EN 14080:2013 tabell 4

S-bjelken og *Smalt-limtre* er limtrebjelker som er splittet i fra et emne med styrkeklasse GL30C.

Karakteritiske fasthetsverdier for *Smalt-limtre* er i.h.t NS-EN 14080:2013 punkt 5.1.7.
(bredde ≥ 38mm; høyde/bredde ≤ 8)

*) skal <u>kun</u> benyttes sammen med beregningsregler gitt i rapport nr. 86 fra Norsk Treteknisk Institutt (www.treteknisk.no). Dette som alternativ metode til EK5 pkt. 6.1.5.

**) for *Smalt-limtre* som <u>kun</u> er splittet i to deler fra emne er $f_{m,k}$ = 28 N/mm2

Gode rom

Desember 2015

Kalibreringsskjema, Schenk 1000 kN

NKT nr.	
Modell	Schenk
F. nr.	
Type	1000 kN
Følsomhet(mV/V)	2 mV/V
Kalibrator	NKT-102

Sporbarhet	MarinTek
Akkreditert	
Kalibreringsdato	16.09.2013
Neste kalibrering	16.09.2015

Kalibreringskurve

$y = -0{,}9935x + 0{,}29$
$R^2 = 1$

X-values: Instron
Y-values: Loadcell

kalib. kurve
Linear (kalib. kurve)

Instron	Kal. Cel	Kal. Cel	Gj.snitt	Linear
1000	-989,9	-990,1	-990	-993,5
900	-892,7	-891,1	-891,9	-894,15
800	-793,7	-791,7	-792,7	-794,8
700	-695,8	-693	-694,4	-695,45
600	-597,8	-594,8	-596,3	-596,1
500	-499,7	-496,7	-498,2	-496,75
400	-401,1	-398,4	-399,75	-397,4
300	-301,6	-299,7	-300,65	-298,05
200	-201,6	-200,3	-200,95	-198,7
100	-101,2	-100,1	-100,65	-99,35
0	0	0	0	0
-100	101	100,3	100,65	99,35
-200	201,5	200,9	201,2	198,7
-300	300,6	299,8	300,2	298,05
-400	399,2	397,6	398,4	397,4
-500	497,9	496,7	497,3	496,75
-600	597,2	596,3	596,75	596,1
-700	696,5	695,8	696,15	695,45
-800	795,8	795,3	795,55	794,8
-900	895	894,8	894,9	894,15
-1000	994,3	994,3	994,3	993,5
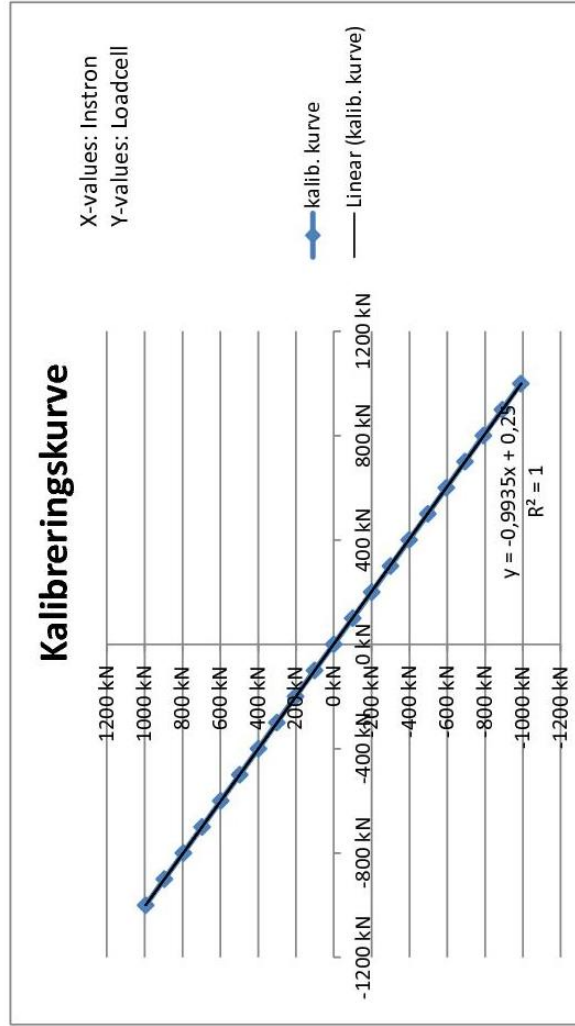
Underskrift: Dato:

Appendix D

Kalibreringsskjema, Instron 500 kN

NKT nr.		
Modell	Instron	
F. nr.		
Type	500 kN	
Følsomhet(mV/V)	2 mV/V	
Kalibrator	Kalibreringslastcelle	

Sporbarhet	Lille prøvesal
Akkreditert	Zwick Roell
Kalibreringsdato	12.06.2014
Neste kalibrering	12.06.2016

Kalibreringskurve

$y = -1,0072x + 0,11$
$R^2 = 1$

X-values: Instron
Y-values: Loadcell

◆ kalib. kurve
— Linear (kalib. kurve)

Underskrift: Dato:

Kal. Celle	Instron	Instron	Gj.snitt	Linear
-500	502	500,9	501,45	503,6
-450	452,6	451,4	452	453,24
-400	403	401,8	402,4	402,88
-350	353,4	352,3	352,85	352,52
-300	303,5	303	303,25	302,16
-250	253,5	253,3	253,4	251,8
-200	203	203,4	203,2	201,44
-150	152,3	153	152,65	151,08
-100	101,6	102,3	101,95	100,72
-50	50,8	51,3	51,05	50,36
0	0	0	0	0
50	-50,6	-51,3	-50,95	-50,36
100	-101,2	-102,1	-101,65	-100,72
150	-151,8	-152,7	-152,25	-151,08
200	-202,3	-203	-202,65	-201,44
250	-252,6	-253	-252,8	-251,8
300	-302,8	-302,7	-302,75	-302,16
350	-352,5	-352	-352,25	-352,52
400	-402,1	-401,2	-401,65	-402,88
450	-451	-450,2	-450,6	-453,24
500	-499,7	-499,1	-499,4	-503,6

5

Appendix E

Load procedure used during static testing in compliance with ISO 6891-1983.

0-degree

Parameters		
l_eff	149,5	mm
d	22,4	mm
f_mean,0-degrees	13,81	Mpa
F_max,0-degrees	46,246928	kN

Control	Load Stage	load [kN]	load rate	interval [min]	time [mm]
Load controled	0	0,00		0	0,00
	0,4	18,50	9,249	2	2,00
	hold for 30s	18,50	9,249	0,5	2,50
	0,1	4,62	9,249	1,5	4,00
	hold for 30s	4,62	9,249	0,5	4,50
	0,7	32,37	9,249	3	7,50
displacement controled	3-5 min			3-5 min	11,50
		46,25		4	7,50
	rate of load last stage:				3,47

5-degree

Parameters		
l_eff	149,5	mm
d	22,4	mm
f_mean,5-degrees	13,975	Mpa
F_max,5-degrees	46,79948	kN

Control	Load Stage	load [kN]	load rate	interval [min]	time [mm]
Load controled	0	0,00		0	0,00
	0,4	18,72	9,360	2	2,00
	hold for 30s	18,72	9,360	0,5	2,50
	0,1	4,68	9,360	1,5	4,00
	hold for 30s	4,68	9,360	0,5	4,50
	0,7	32,76	9,360	3	7,50
displacement controled	3-5 min			3-5 min	11,50
		46,25		4	7,50
	rate of load last stage:				3,37

Load procedure used during static testing in compliance with ISO 6891-1983.
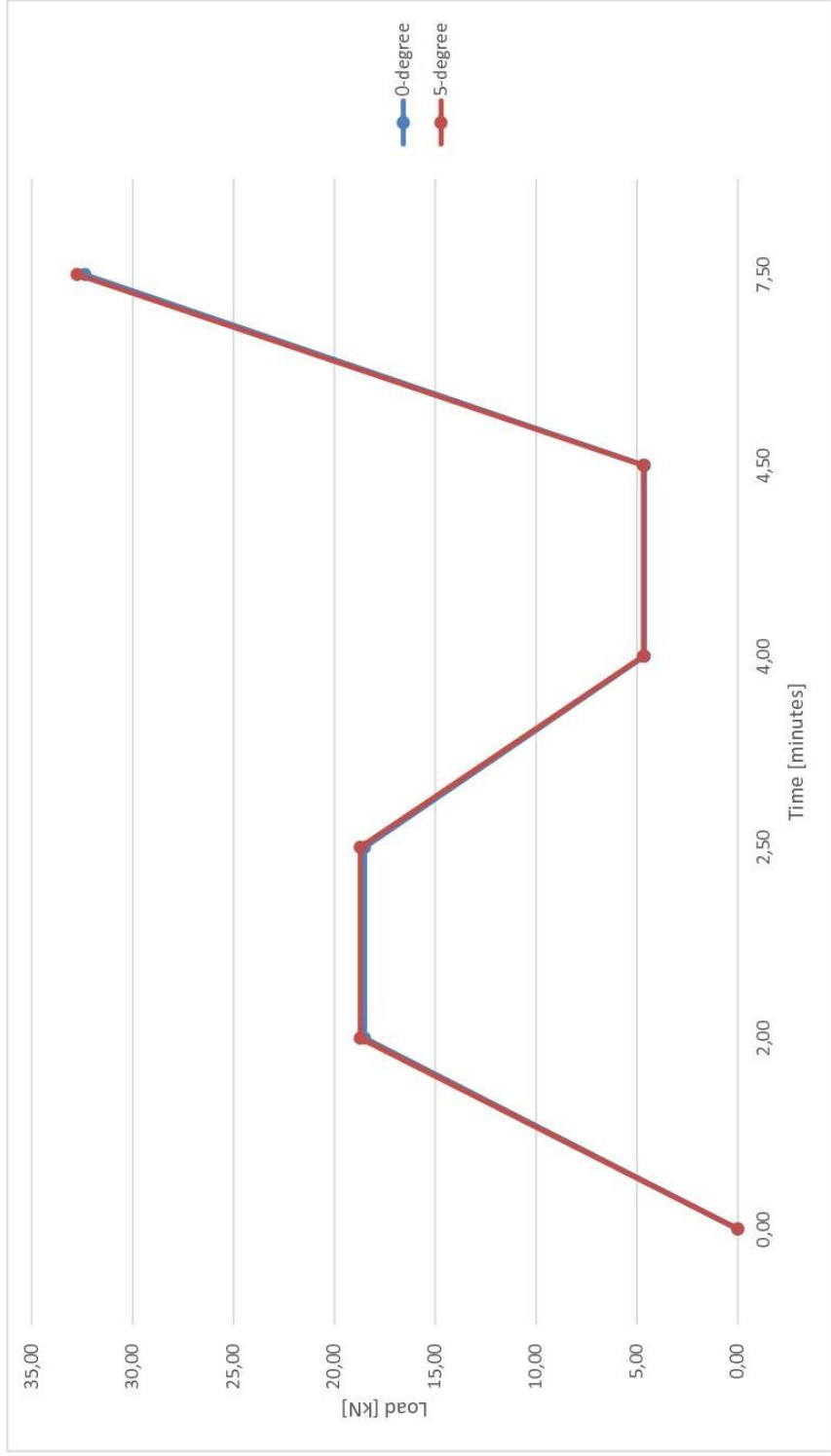
Appendix F

Load parameter	0-degree	5-degree
R	0,1	0,1
fmax	0,75	0,75
Fref	39,01	41,11
Fmax	29,2575	30,8325
Fmin	2,92575	3,08325
Fmean	16,091625	16,957875
Famplitude	13,165875	13,874625

Sinusoidal wave and necessary load parameters
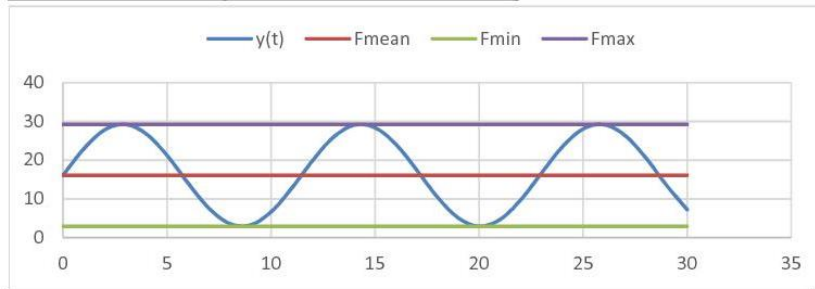
t	Fmean	Fmin	Fmax	y(t)
0	16,091625	2,92575	29,2575	16,091625
1	16,091625	2,92575	29,2575	22,9542962
2	16,091625	2,92575	29,2575	27,8049137
3	16,091625	2,92575	29,2575	29,2213341
4	16,091625	2,92575	29,2575	26,7882797
5	16,091625	2,92575	29,2575	21,2190933
6	16,091625	2,92575	29,2575	14,146594
7	16,091625	2,92575	29,2575	7,64435473
8	16,091625	2,92575	29,2575	3,61875477
9	16,091625	2,92575	29,2575	3,2500522
10	16,091625	2,92575	29,2575	6,64634625
11	16,091625	2,92575	29,2575	12,8118838
12	16,091625	2,92575	29,2575	19,9390026
13	16,091625	2,92575	29,2575	25,9381159
14	16,091625	2,92575	29,2575	29,0503551
15	16,091625	2,92575	29,2575	28,3632485
16	16,091625	2,92575	29,2575	24,0782477
17	16,091625	2,92575	29,2575	17,451664
18	16,091625	2,92575	29,2575	10,426333
19	16,091625	2,92575	29,2575	5,06199831
20	16,091625	2,92575	29,2575	2,93141919
21	16,091625	2,92575	29,2575	4,6592561
22	16,091625	2,92575	29,2575	9,73892777
23	16,091625	2,92575	29,2575	16,6811348
24	16,091625	2,92575	29,2575	23,4505046
25	16,091625	2,92575	29,2575	28,0623383
26	16,091625	2,92575	29,2575	29,164501
27	16,091625	2,92575	29,2575	26,4338518
28	16,091625	2,92575	29,2575	20,6709845
29	16,091625	2,92575	29,2575	13,5655034
30	16,091625	2,92575	29,2575	7,20065117

Appendix G – Documentation of inspection.

Name	S5-L7-45678	Type	Static
Degrees	5	Failure mode	Mode 1
Picture			
Notes	Clear shear zone, no cracks, no knots		
*For more information on specimen, see excel file.			

Name	S5-L6-45678	Type	Static
Degrees	5	Failure mode	Mode 1

Picture	
Picture	
Notes	Clean shear zone, clean pullout, no knots, no cracks
*For more information on specimen, see excel file.	

Name	S5-L2-5678	Type	Static
Degrees	5	Failure mode	Mode 1
Picture			
Picture			
Notes	Clean shear with crack and knot, no visible disturbance or affect of knot on rod.		
*For more information on specimen, see excel file.			

Name	S5-L2-2345	Type	Static

Degrees	5	Failure mode	Mode 1
Picture 1			
Notes	Clean tear out shear		
*For more information on specimen, see excel file.			

Name	S5-L3-45678	Type	Static
Degrees	5	Failure mode	Mode 1
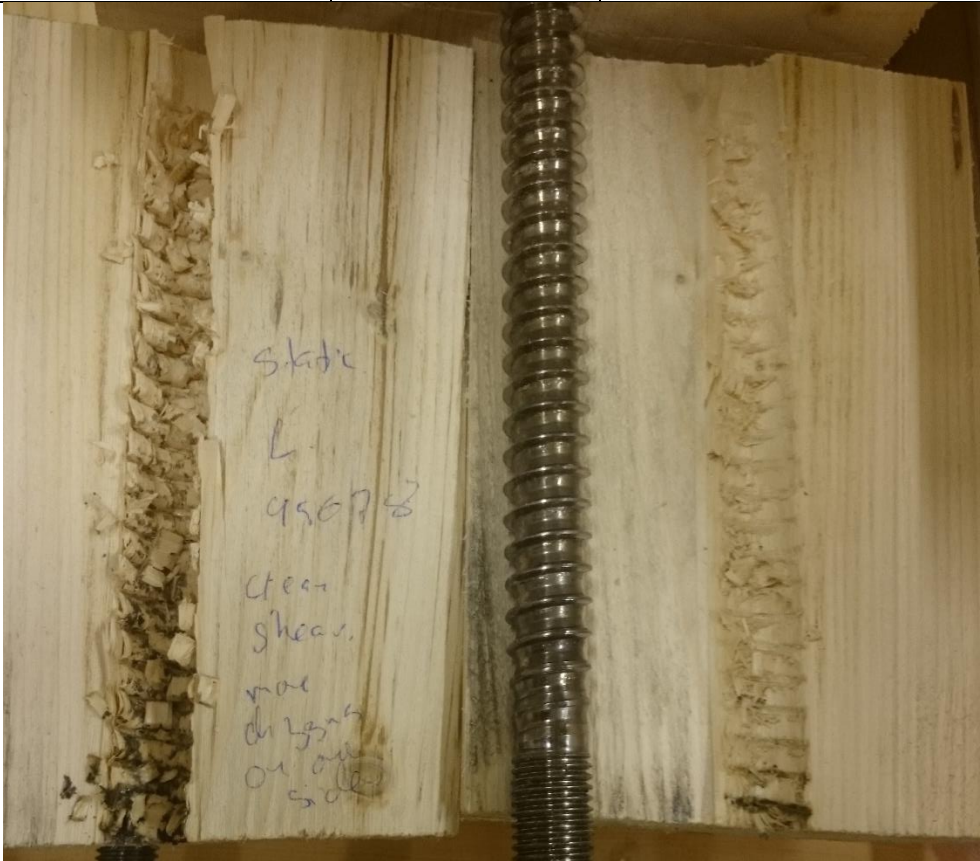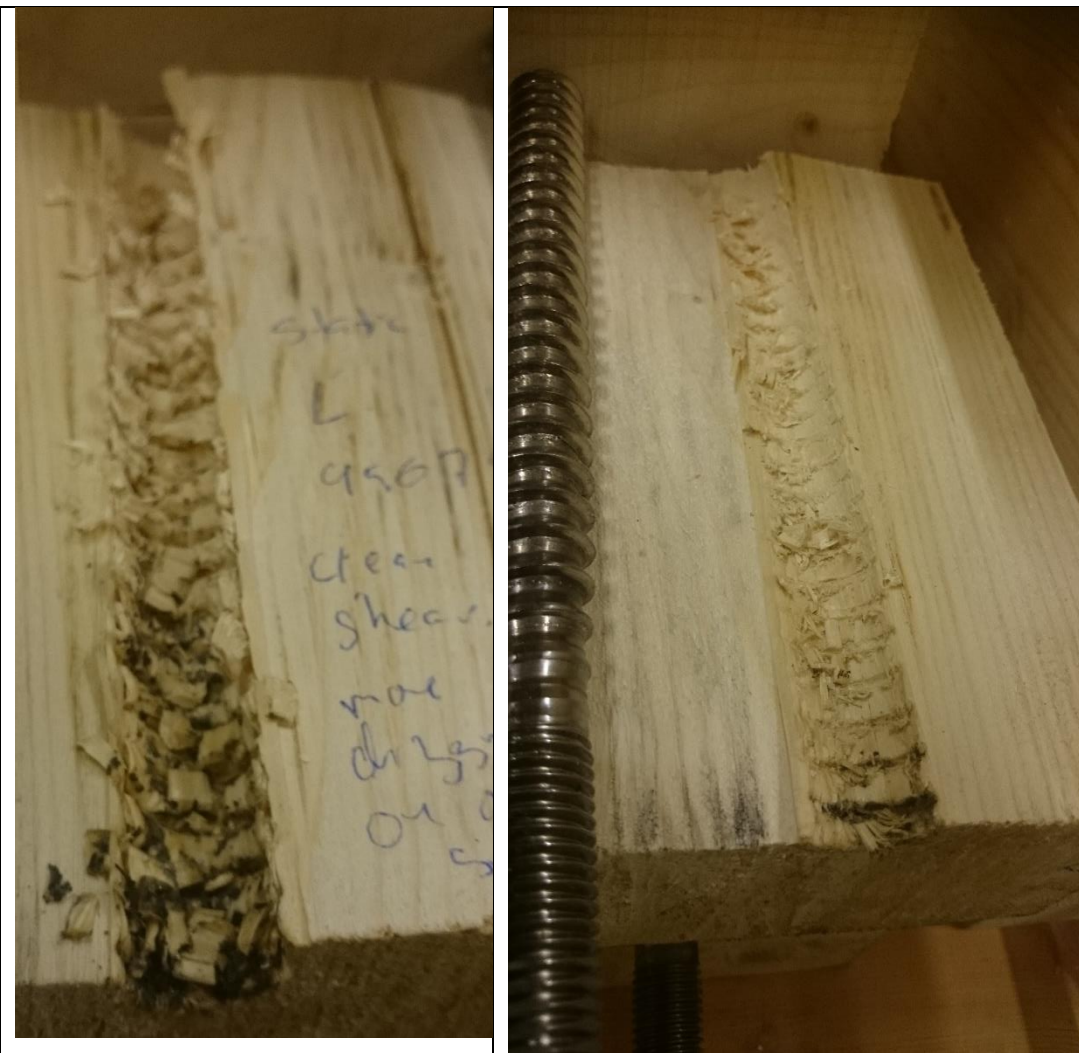
Picture 1	
Picture 2	
Notes	Clean tear out, with crack

13

*For more information on specimen, see excel file.

Name	F5-L4-45678	Type	fatigue
Degrees	5	Failure mode	Mode 1
Picture			

Picture	
Notes	Clean shear, but more digging into wood on one side, less on the other side, seems to be because of a knot, higher density forcing the rod into the other side of the specimen.

*For more information on specimen, see excel file.

Name	F5-L7-12345	Type	fatigue
Degrees	5	Failure mode	No damage, ended at 2,5 million cycles
Picture			
Picture of splitting	Was not split due to no failure, was saved for later continuation of testing.		
Notes			

*For more information on specimen, see excel file.

Name	F5-L1-567	Type	fatigue
Degrees	5	Failure mode	No damage, ended at 2,5 million cycles
Picture			

Picture of splitting	Was not split due to no failure, was saved for later continuation of testing.		
Notes			

*For more information on specimen, see excel file.

Name	F0-D1-345	Type	fatigue
Degrees	0	Failure mode	No damage, ended at 2,78 million cycles

Picture 1 and 2	

Picture of splitting	Was not split due to no failure, was saved for later continuation of testing.		
Notes			

*For more information on specimen, see excel file.

Name	F0-E7-345	Type	Fatigue
Degrees	0	Failure mode	Mode 1

Picture 1 and 2	
Notes	Clean pullout, no deviations
*For more information on specimen, see excel file.	

Name	F0-E7-678	Type	Fatigue
Degrees	0	Failure mode	Mode 1
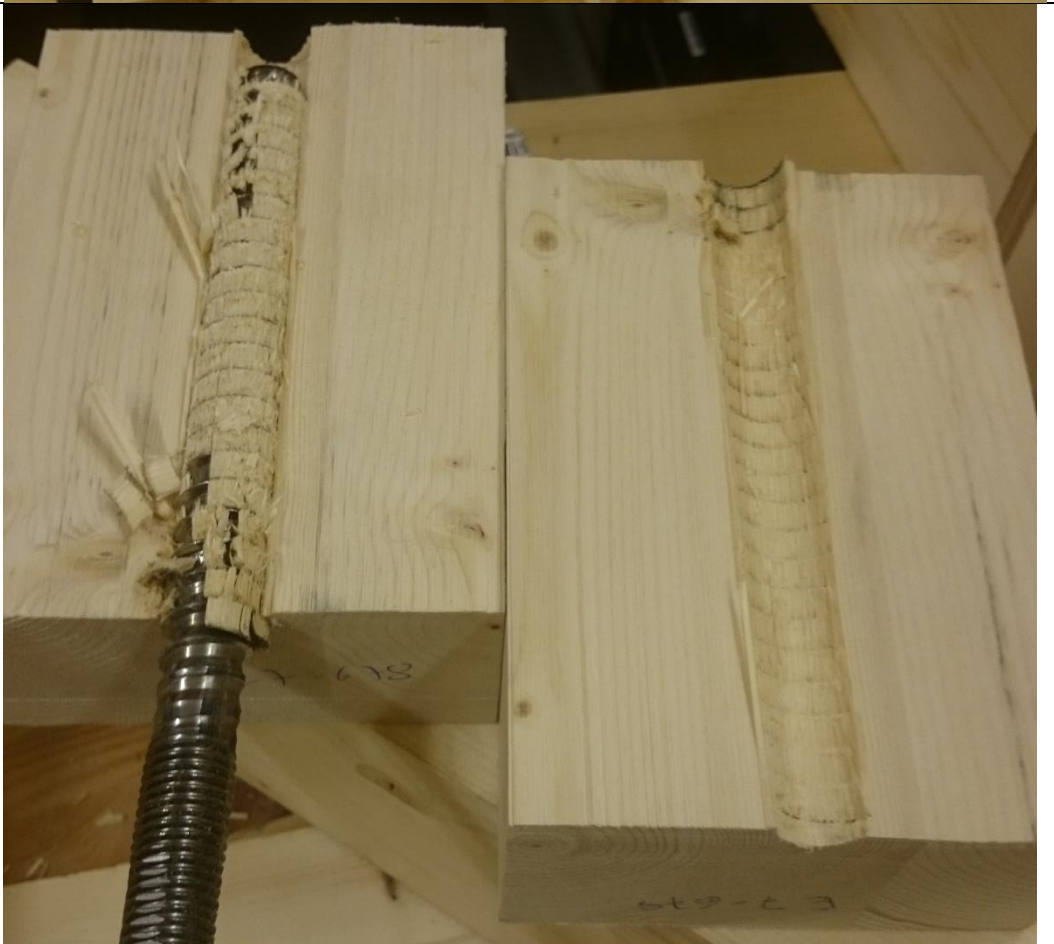
| Picture 1 | |
| Picture 2 | |

Notes	Clean shear pullout
*For more information on specimen, see excel file.	

Name	F0-D7-678	Type	fatigue
Degrees	0	Failure mode	Mode 3
Picture 1			
Picture 2			
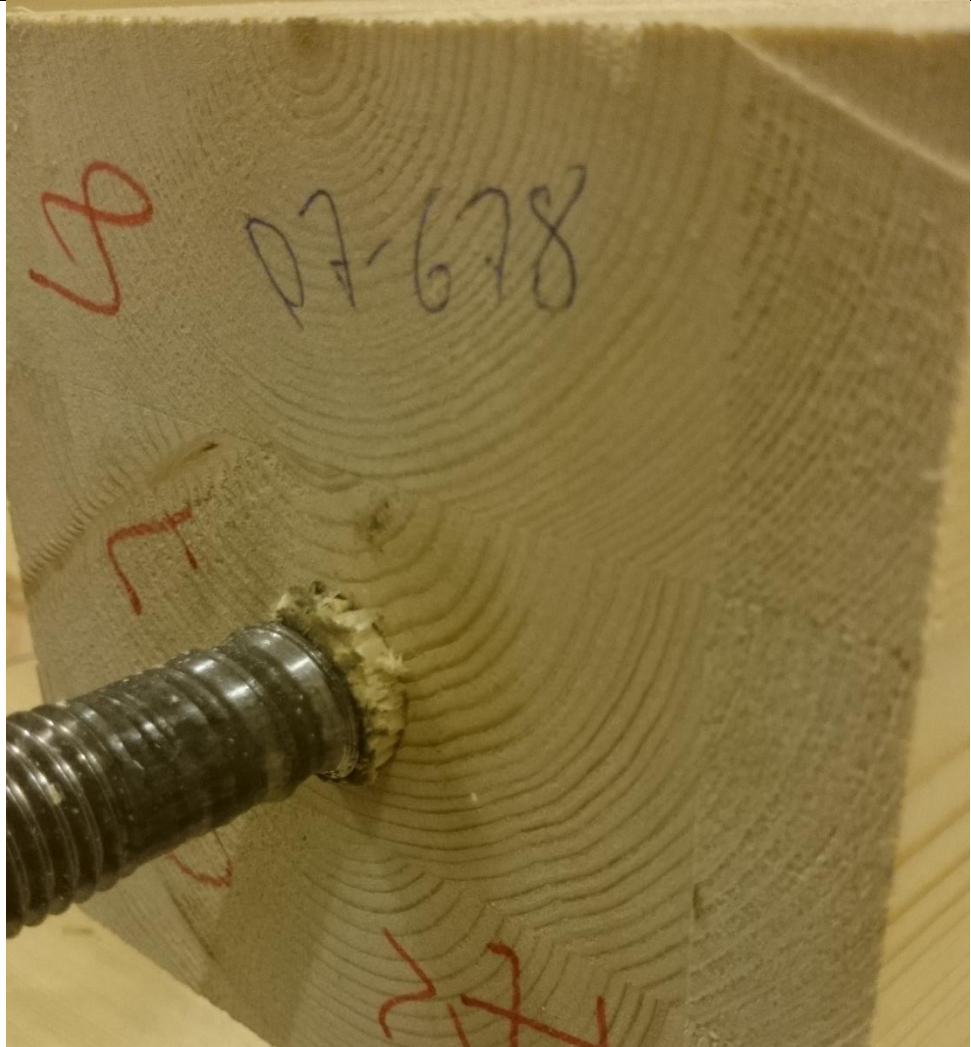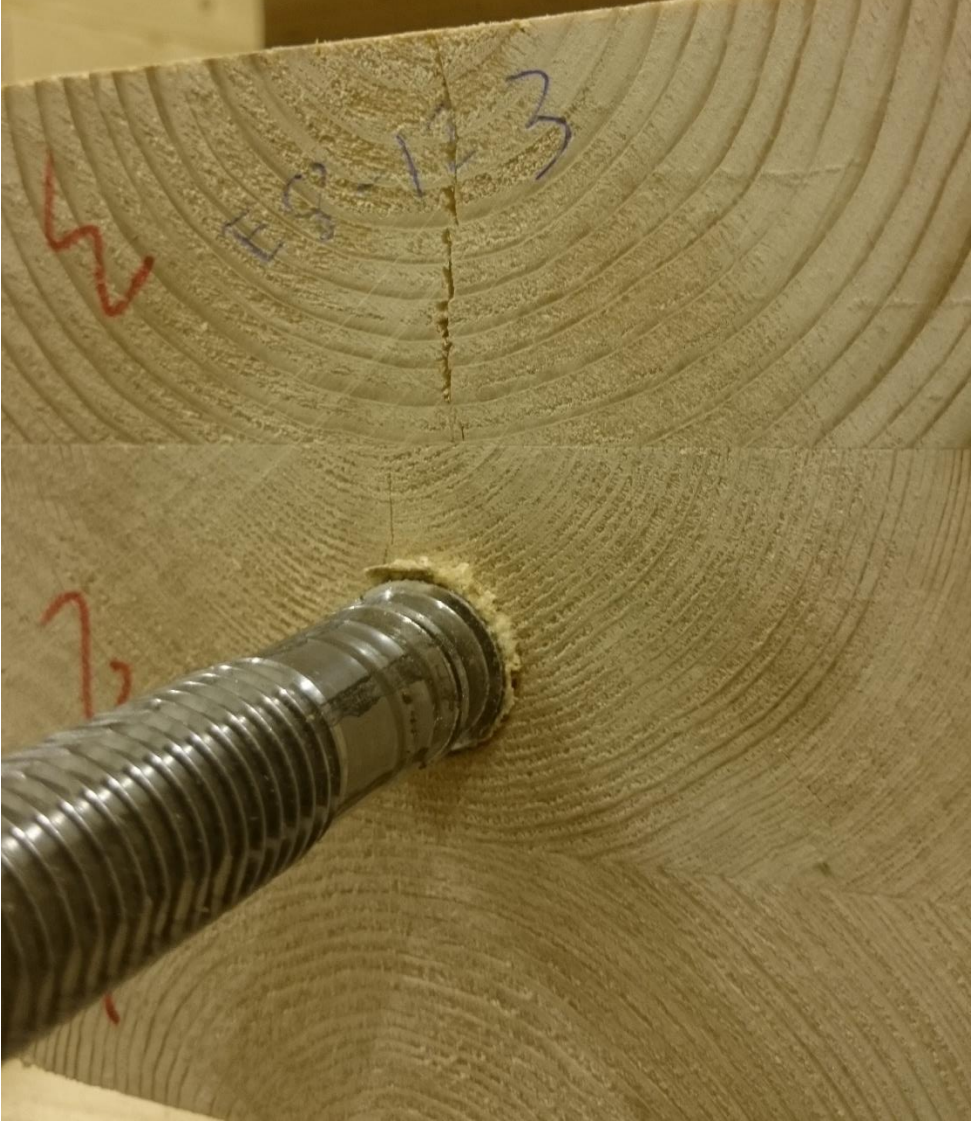
Notes	Combination mode, can be regarded as mode 1, but some fibers are torn along with the shear zone.
*For more information on specimen, see excel file.	

Name	F0-E8-123	Type	fatigue
Degrees	0	Failure mode	Mode 3
Picture 1			
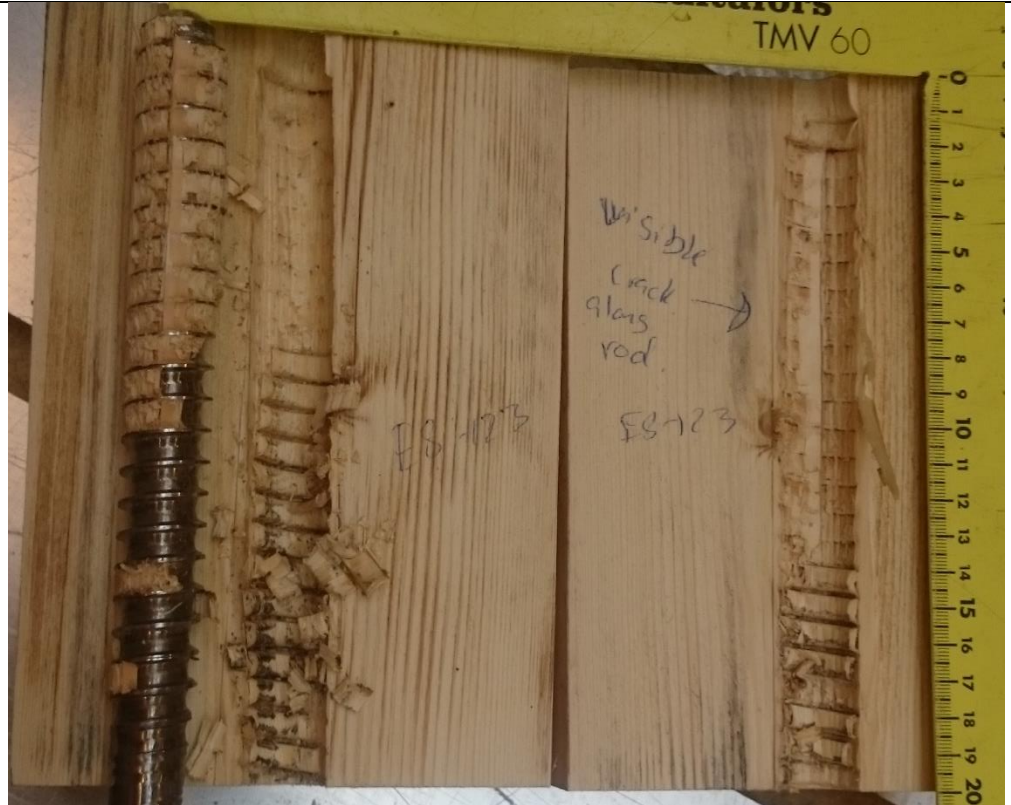
Picture 2	
Notes	Clean shear pullout, but crack cause partly block tear-out, visible crack along rod, also knot but no deviation in rod path, probable reason is that the knot is far into the specimen.
*For more information on specimen, see excel file.	
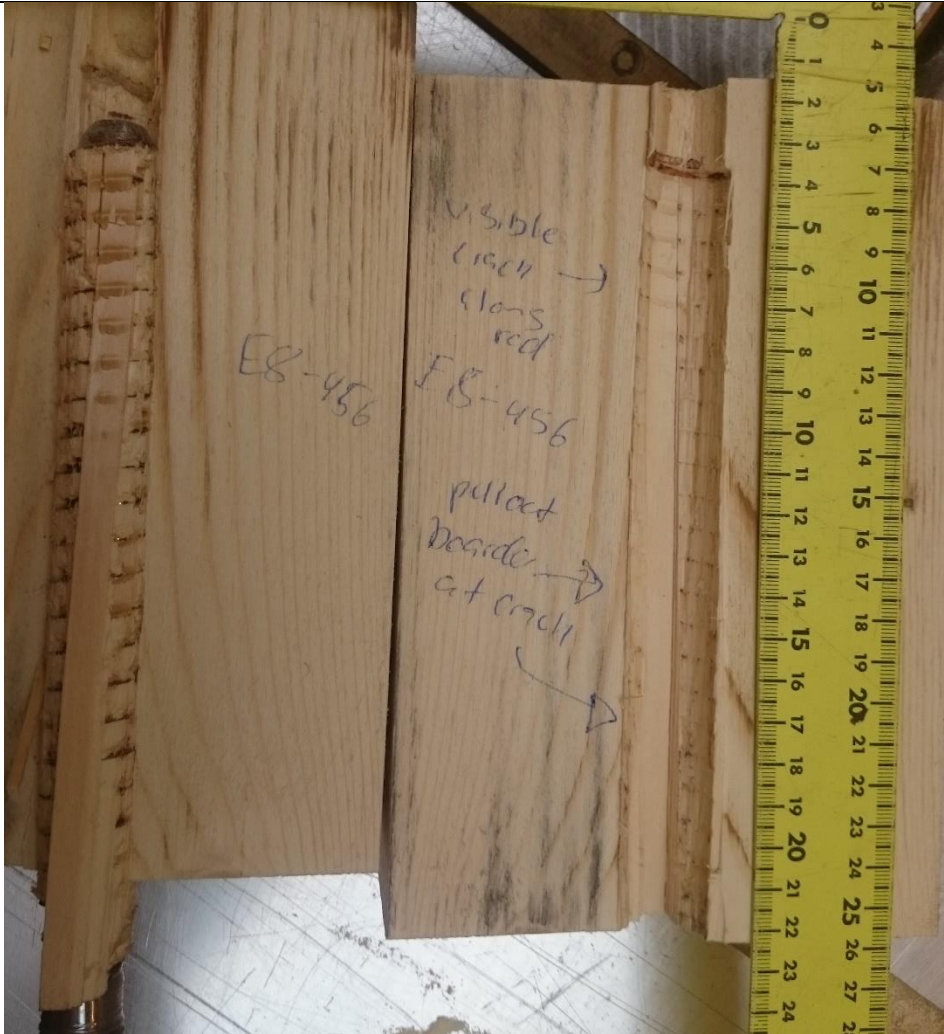
Name	F0-E2-123	Type	fatigue
Degrees	0	Failure mode	

Picture	
Notes	Not tested

*For more information on specimen, see excel file.

Name	F0-E8-456	Type	fatigue
Degrees	0	Failure mode	Mode 3

| Picture | |

23

Picture	
pictures	
Notes	Pullout of shear zone and fibers. The fibers that are pull out propagates from a large crack. This crack can be seen as a straight line on the picture.

*For more information on specimen, see excel file.

Appendix H – Fatigue testing of rods

0-degrees; Loading procedure

0-degrees; displacment during loading procedure
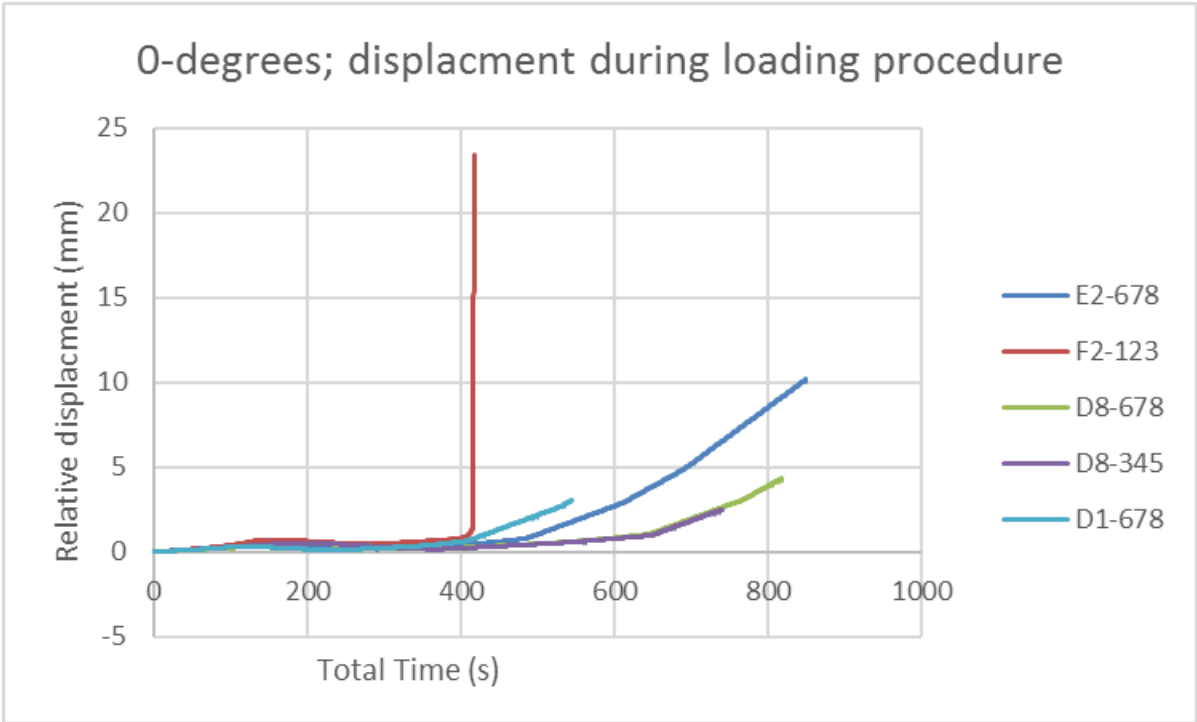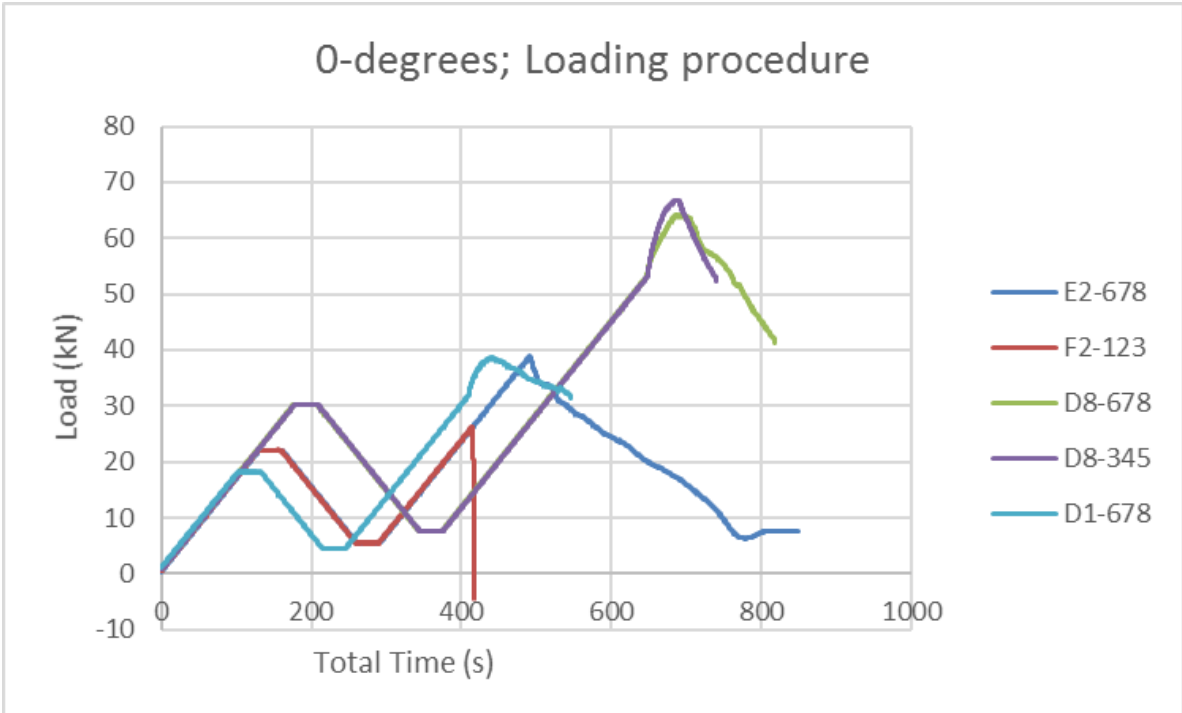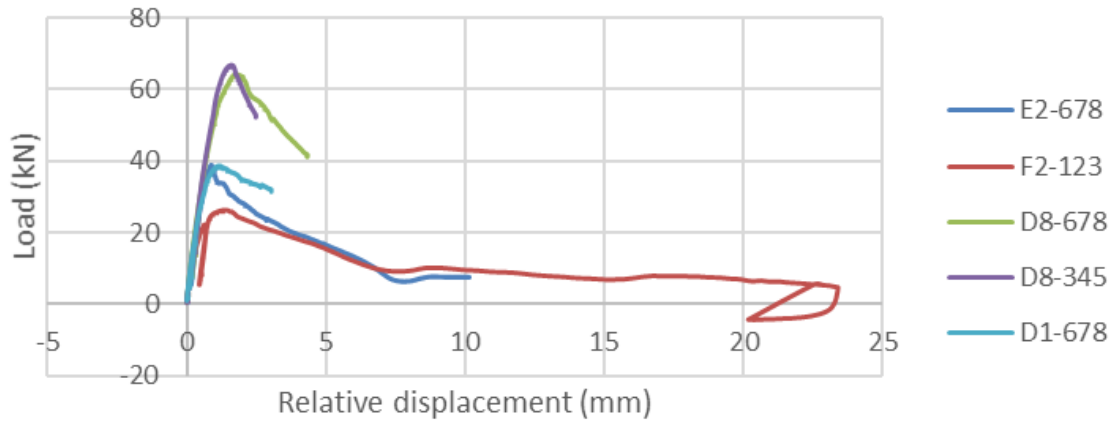
0-degrees: Relative displacement to force, stiffness

5-degrees; relative displacement to force, stiffness

26
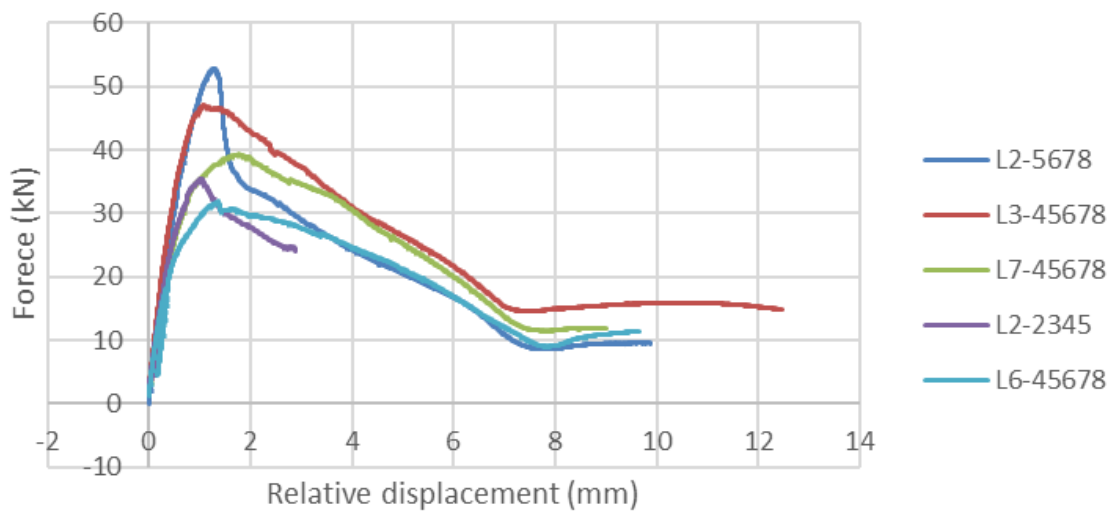
5-degree; Load development, static testing
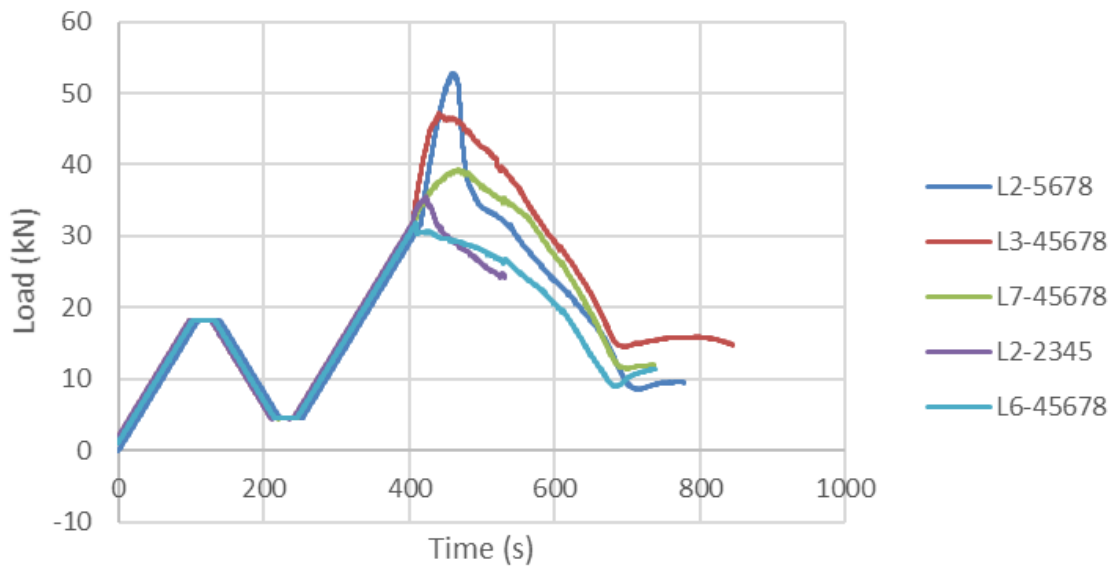
5-degrees; Relative displacement, static testing

27
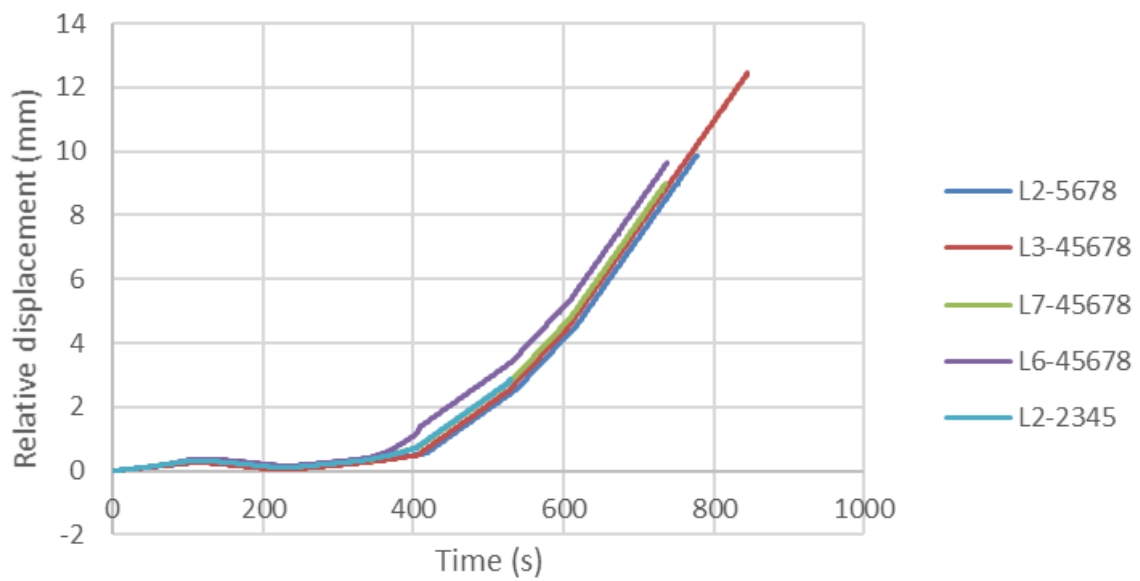
Appendix I- Results from shear testing

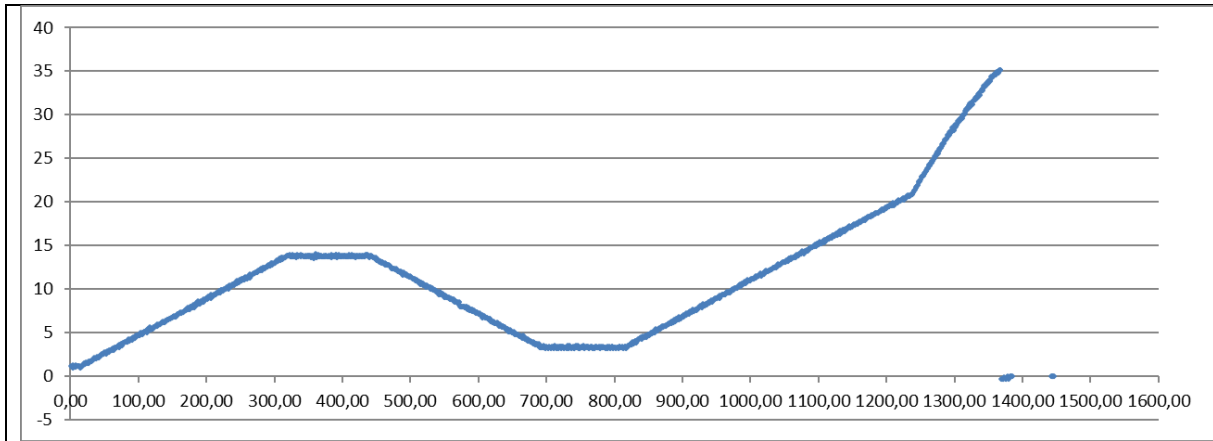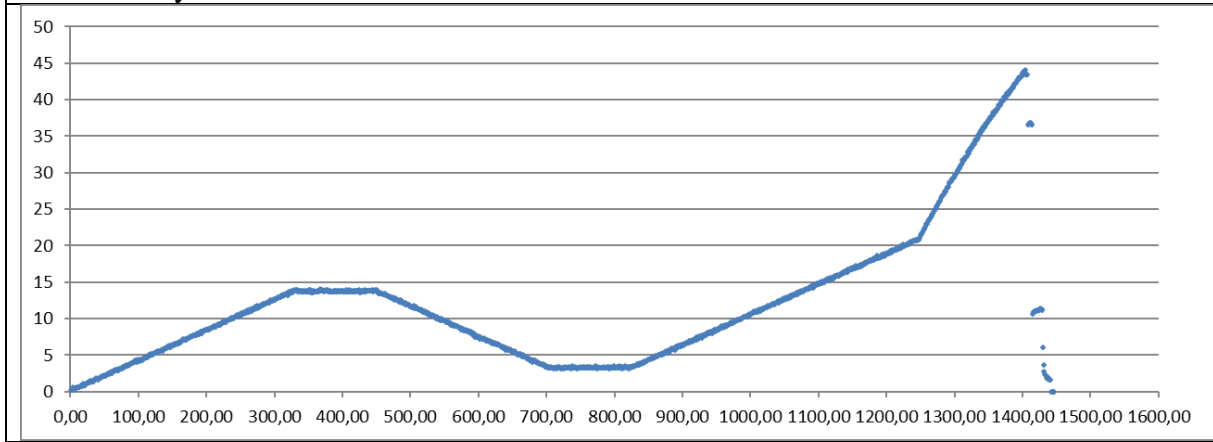| Specimen: S90-TL-A1-567	G-modulus: 1427,9

Stress-strain curve:

Force-Relative displacement:

Loading history
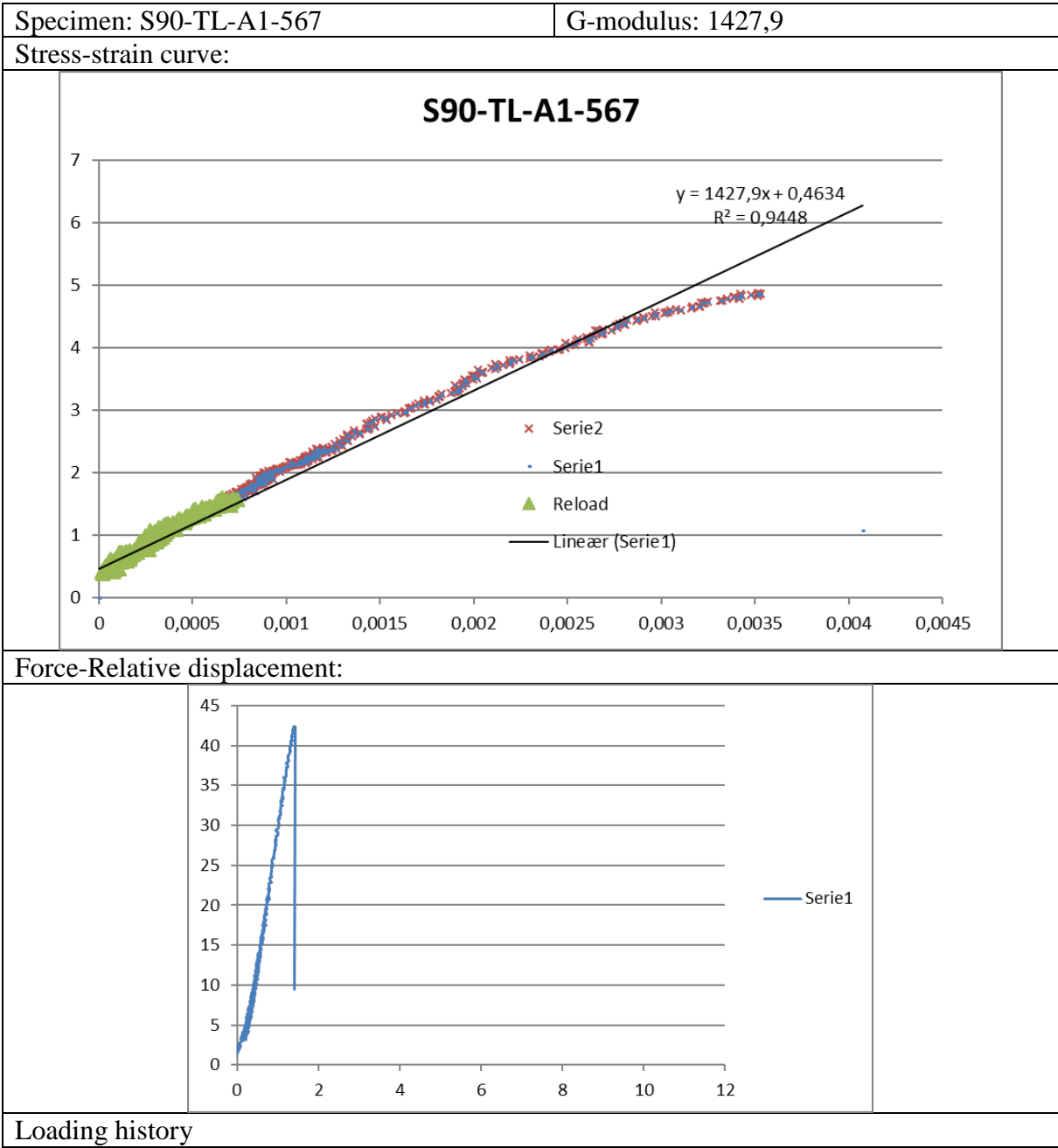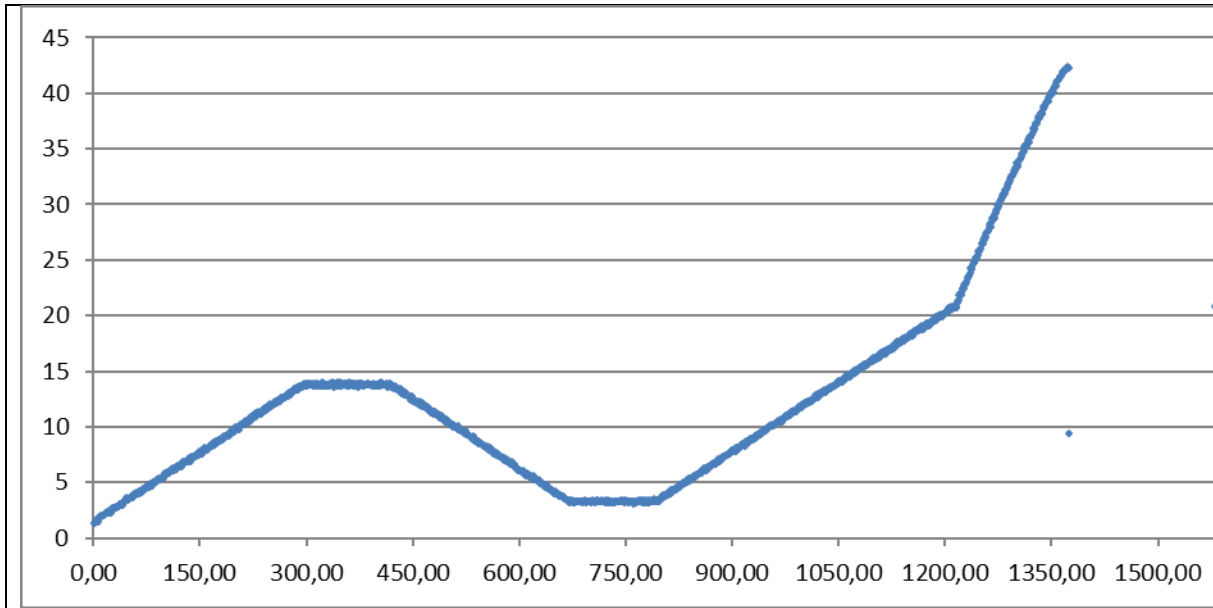
Specimen: S90-TL-C2-456	G-modulus:
Stress-strain curve:	

τ(εxy) data for specimen S90-TL-C2-456

y = 1496,3x + 1,1327
R² = 0,9872

Shear stress RL [MPa]

Shear strain
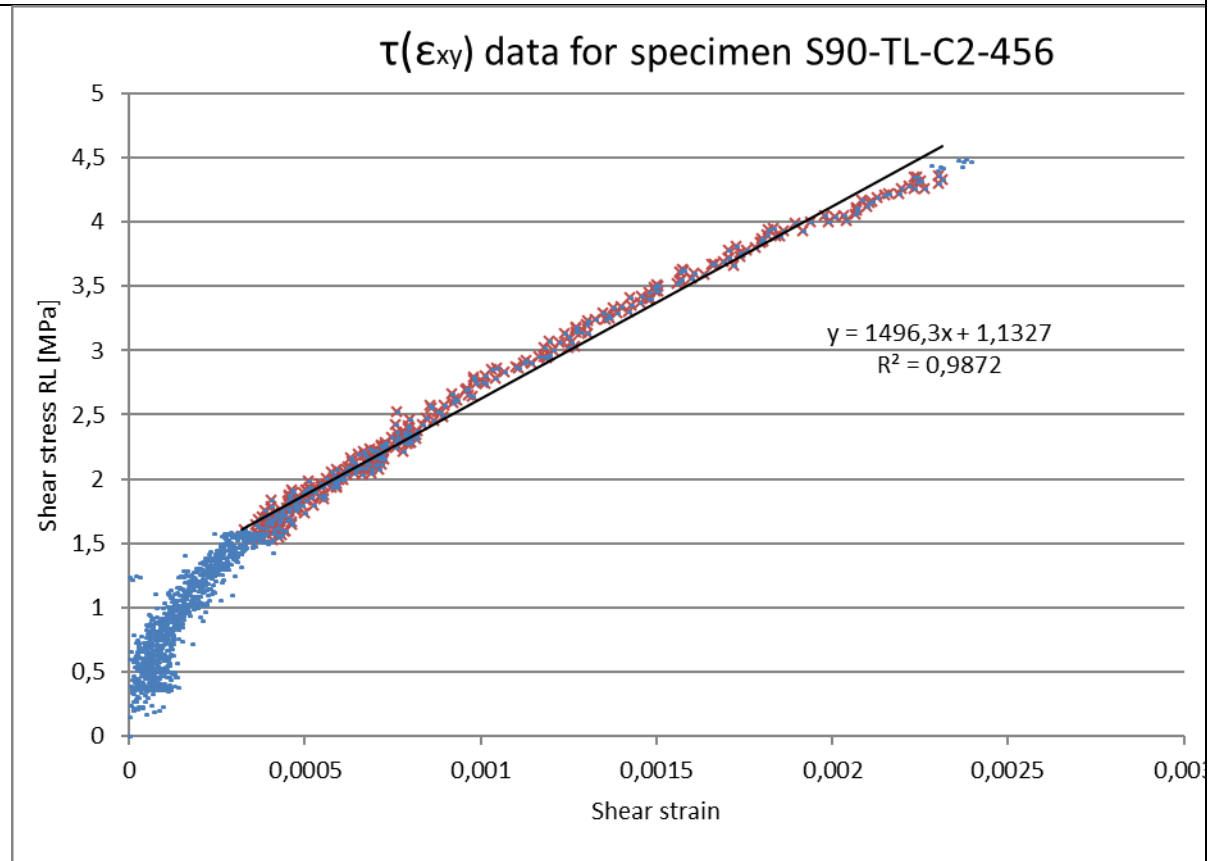
Force-Relative displacement
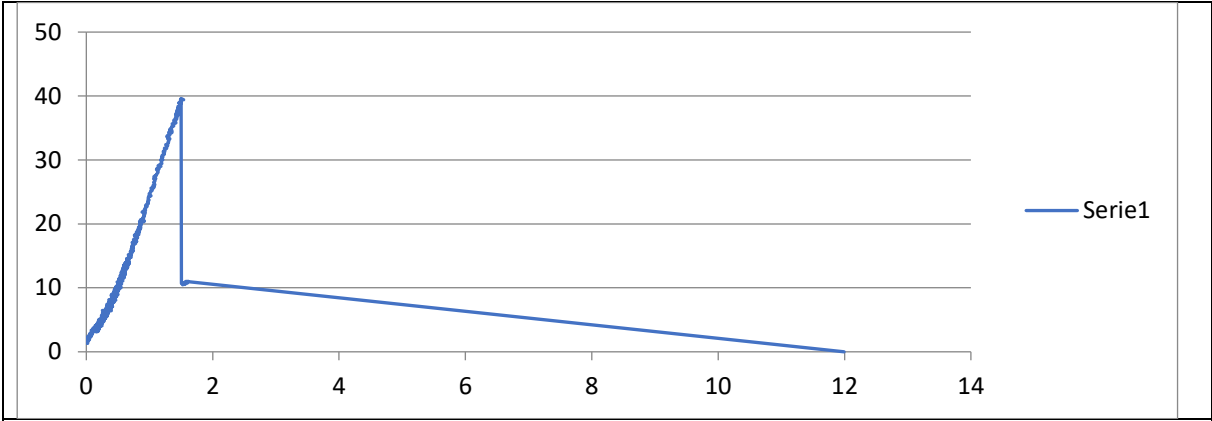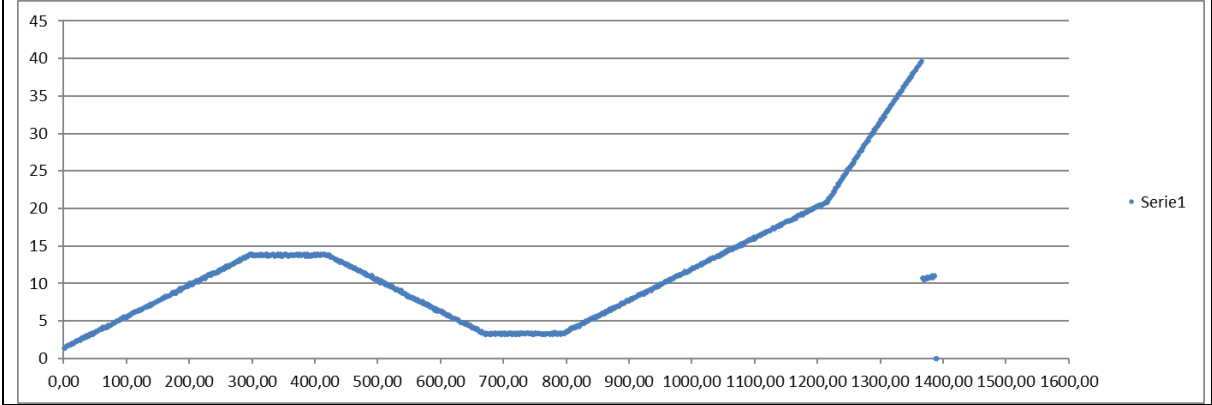
Load History

Specimen: S90-TL-A4-123	G-modulus:

Stress-strain curve:

y = 995,18x + 1,2552
R² = 0,9947

y = 1036,1x + 1,139
R² = 0,9918

y = 1331,4x + 0,9365
R² = 0,9221
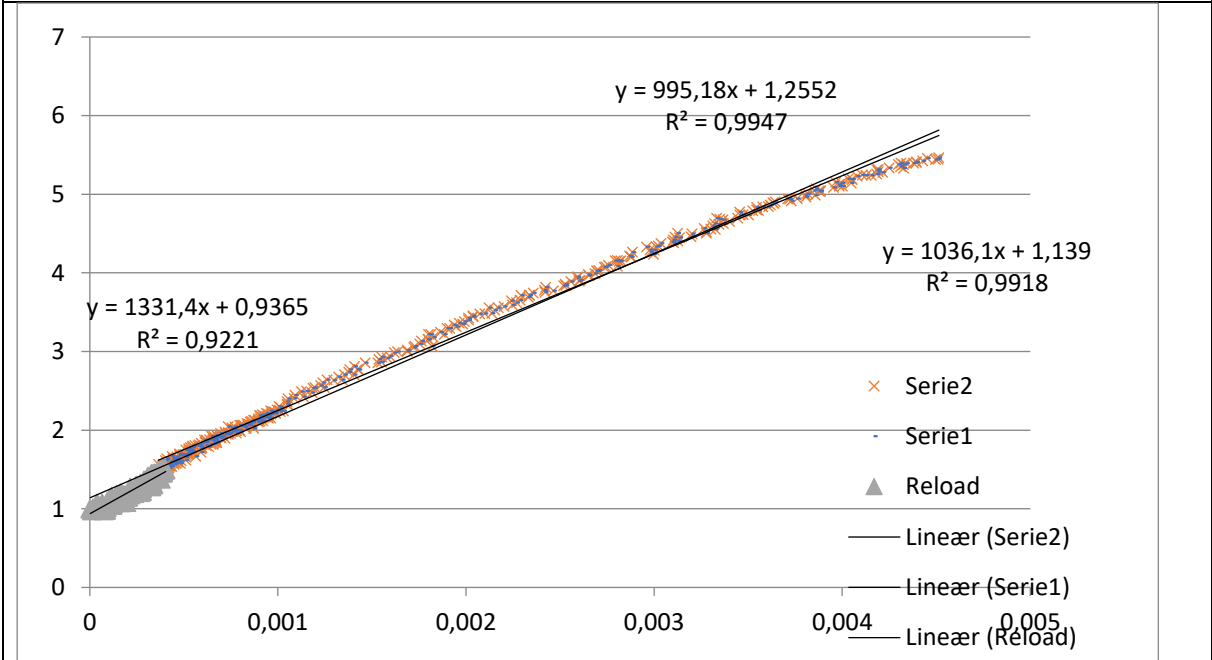
Force-Relative displacement
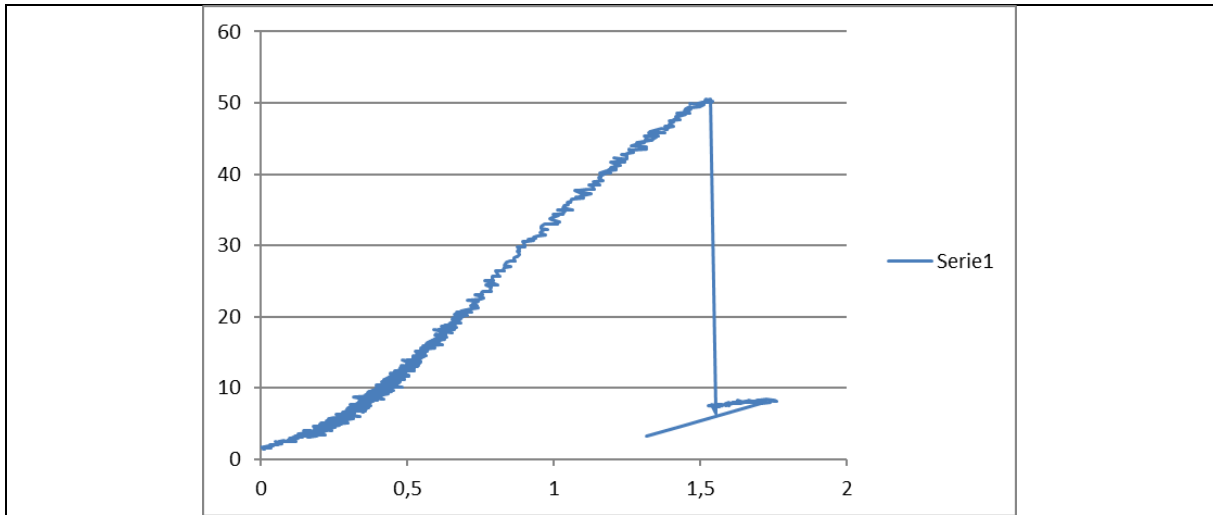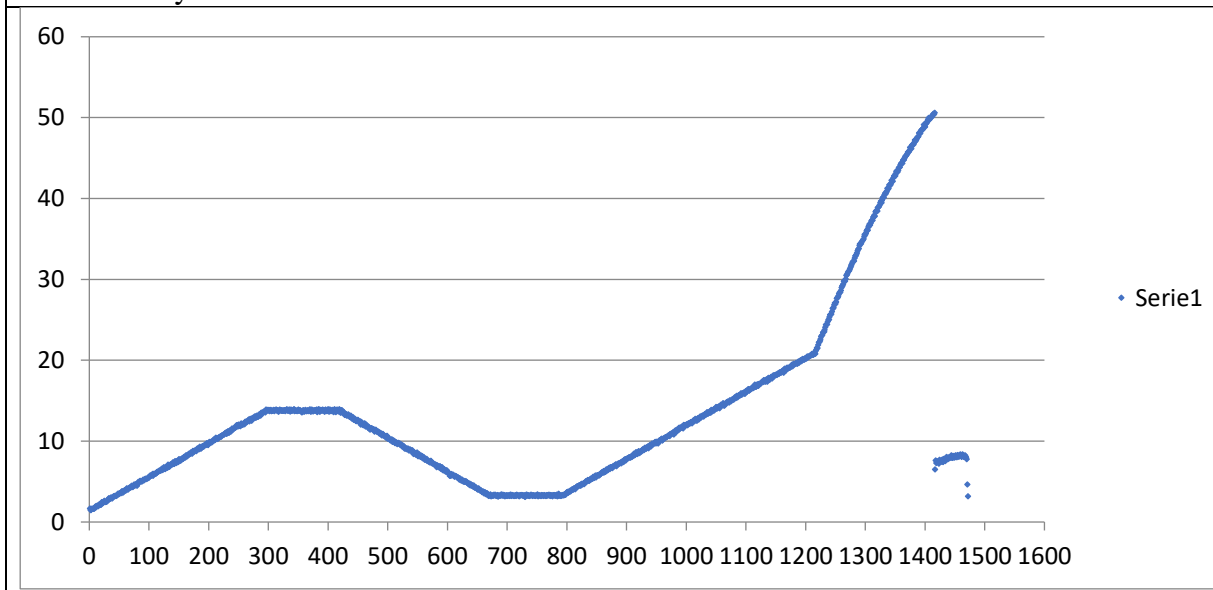
Load History

Specimen: S90-TL-B2-123	G-modulus:
Stress-strain curve:	

Force-Relative displacement

Load History

Loading procedure for static compression test
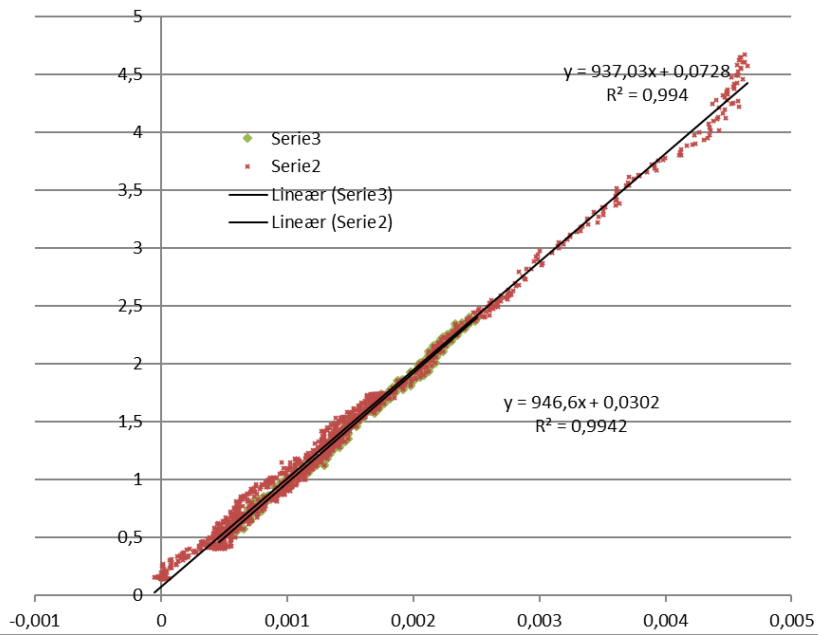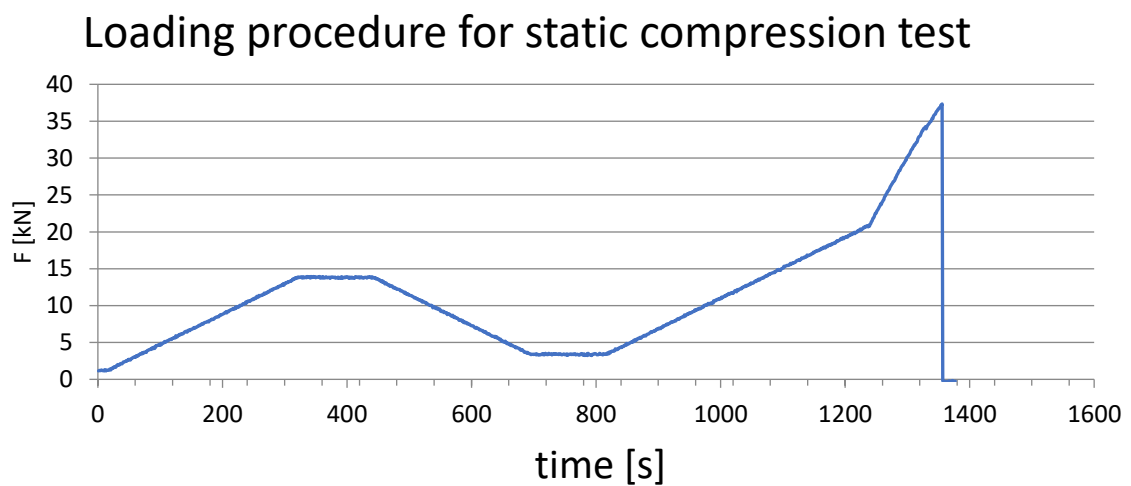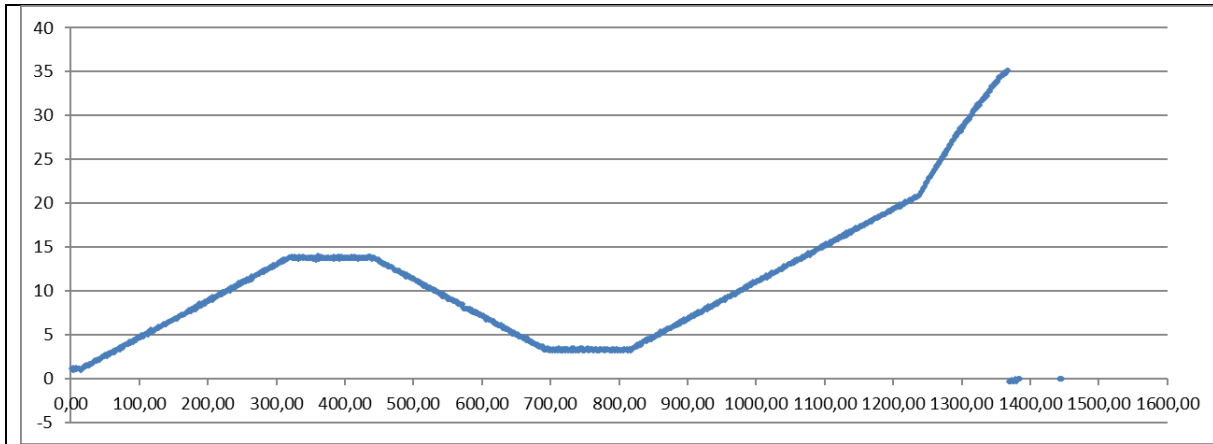
Specimen: S90-RL-B7-234	G-modulus:
Stress-strain curve:	
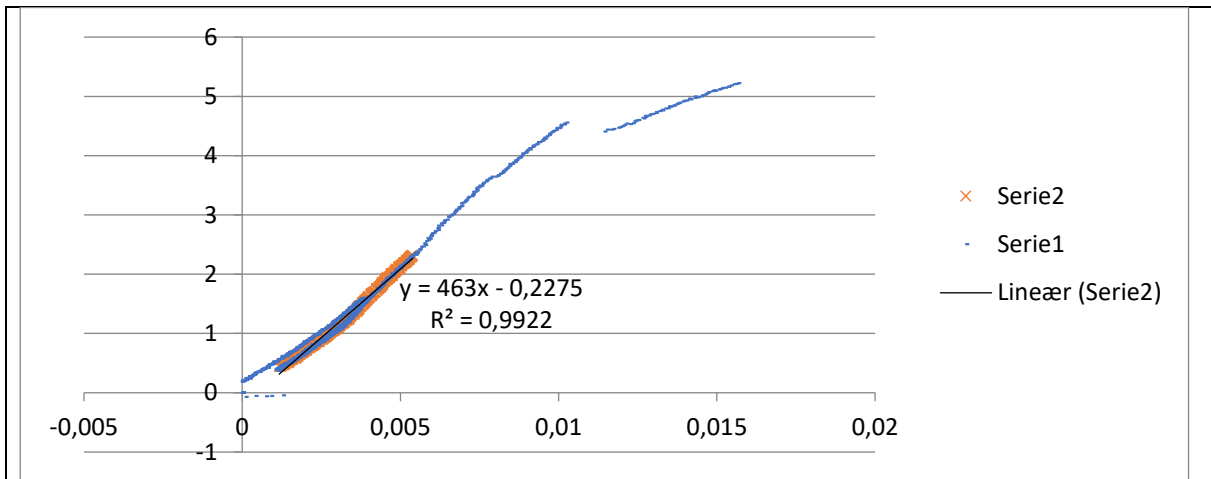
Force-Relative displacement
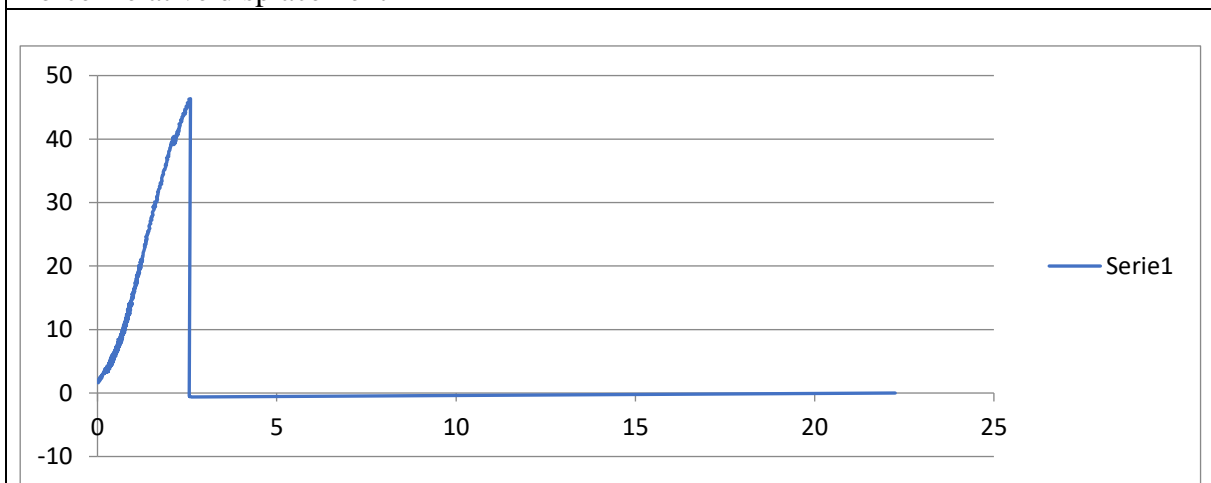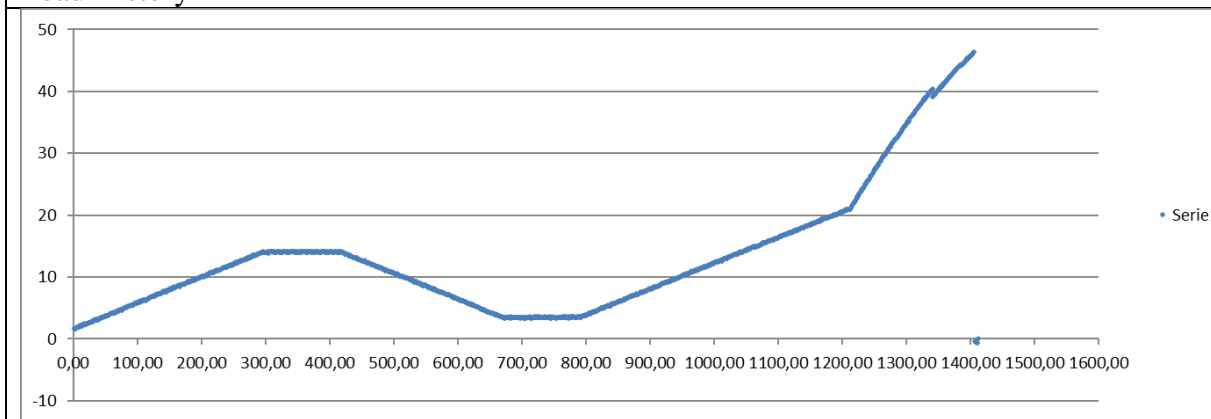
Load History

Specimen: S90-RL-B3-123	G-modulus:
Stress-strain curve:	

33
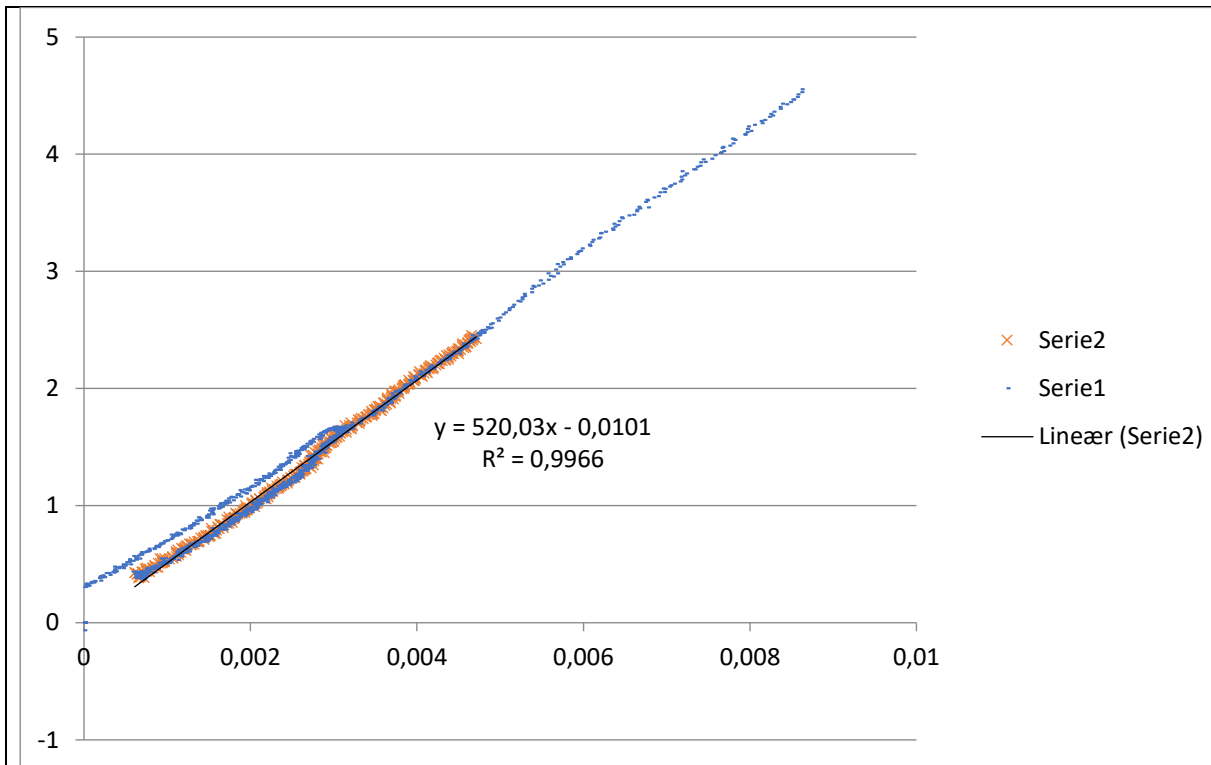
Force-Relative displacement
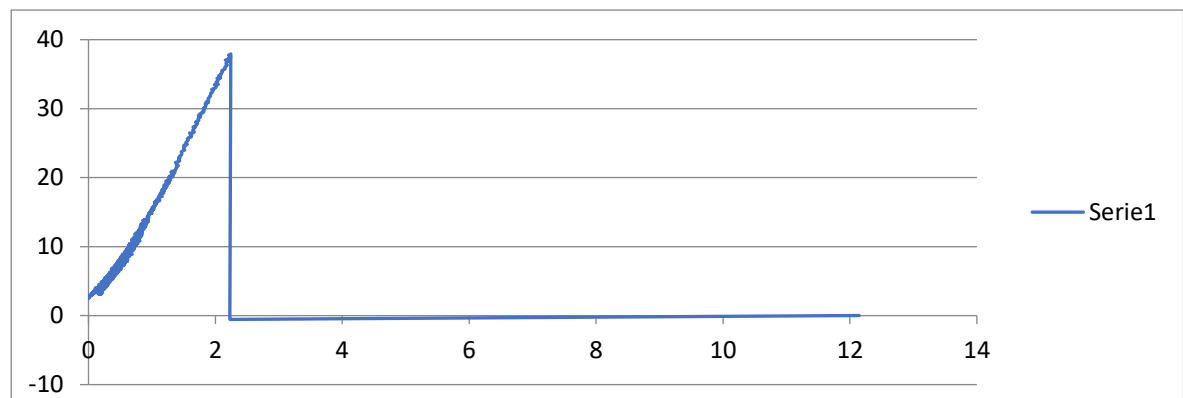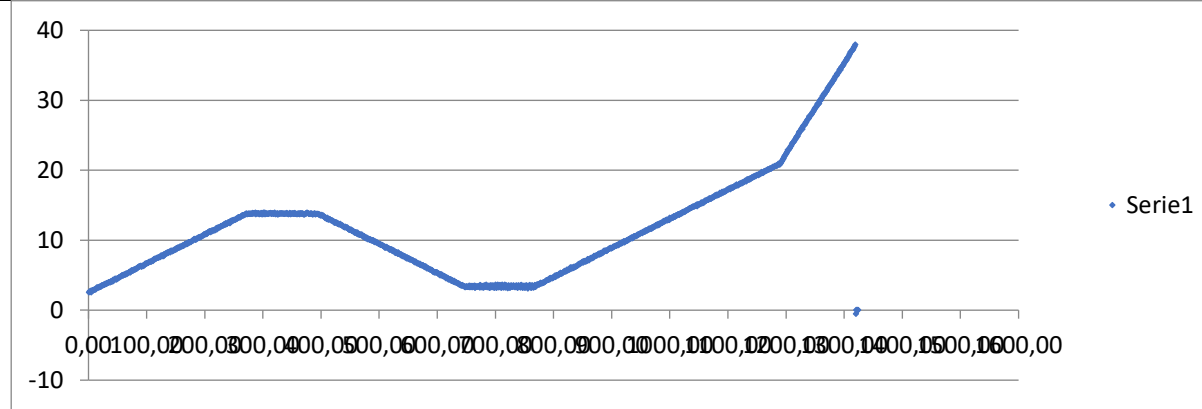
Load History

Specimen: S90-RL-B4-321	G-modulus:
Stress-strain curve:	

The chart in the top panel includes the equation:

$$y = 520{,}03x - 0{,}0101$$
$$R^2 = 0{,}9966$$

Legend (top chart):
- Serie2
- Serie1
- Lineær (Serie2)
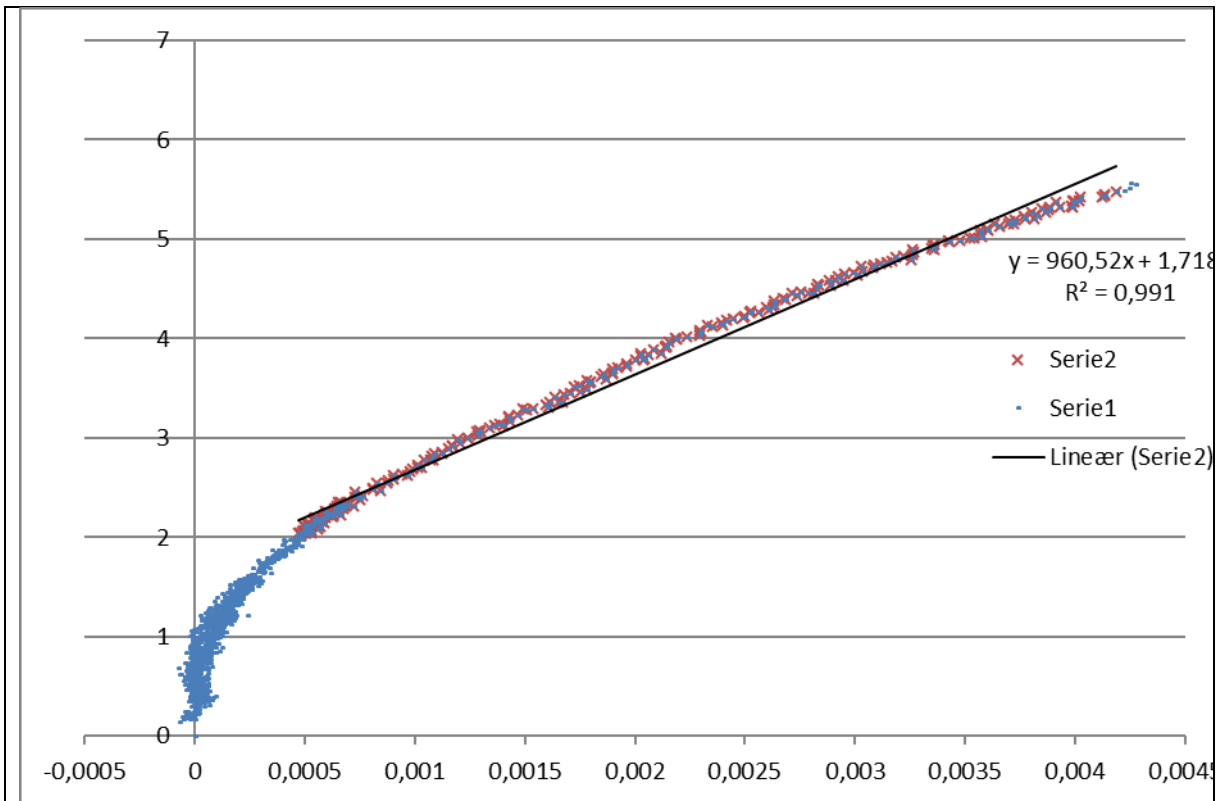
Force-Relative displacement
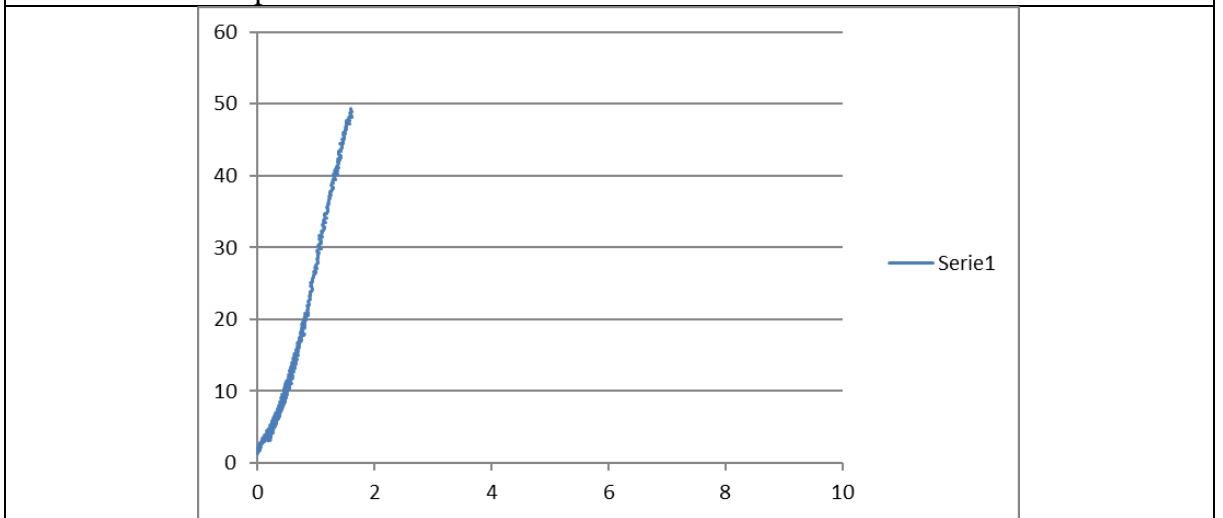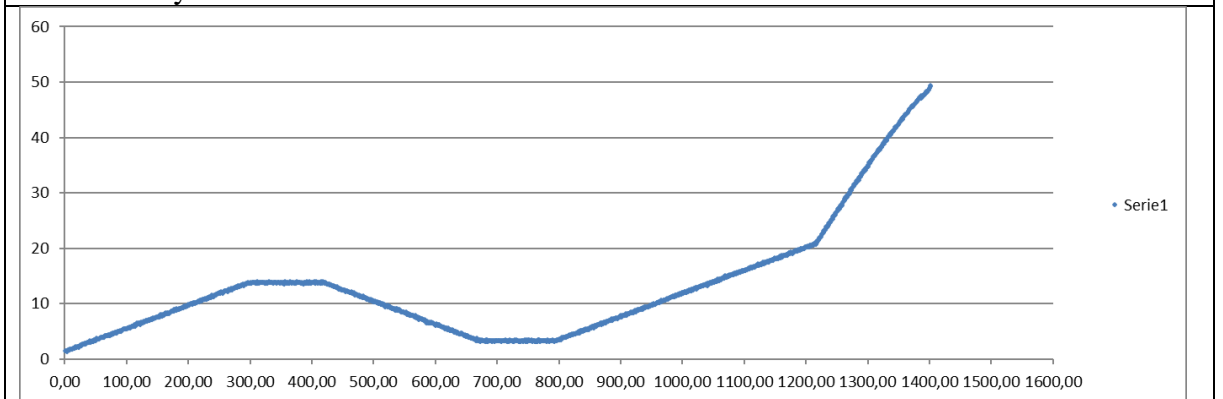
Load History

Specimen: Straigth-RL-C6-123	G-modulus:

Stress-strain curve:

τ(εxy) data for specimen C1-456

y = 1049,5x + 1,4058
R² = 0,9584

Shear stress RL [MPa] (vertical axis)
Shear strain (horizontal axis)

Force-Relative displacement

Serie1
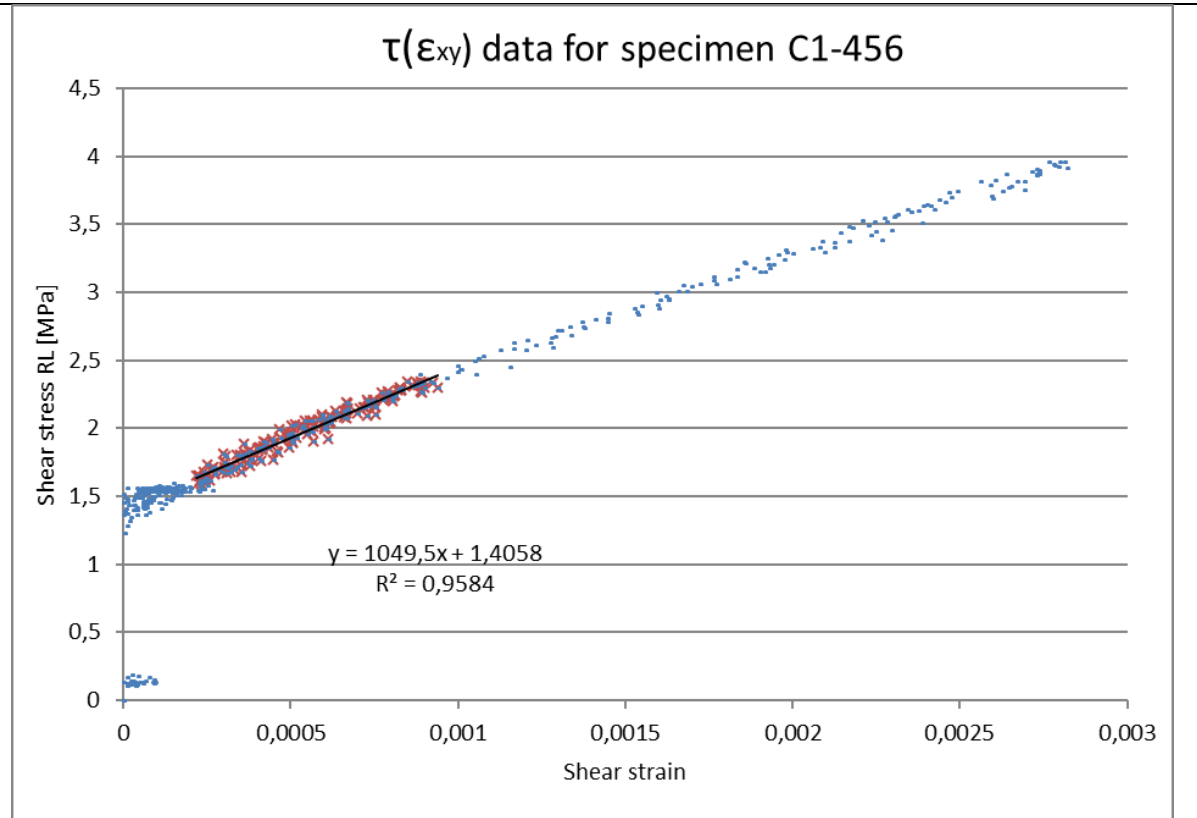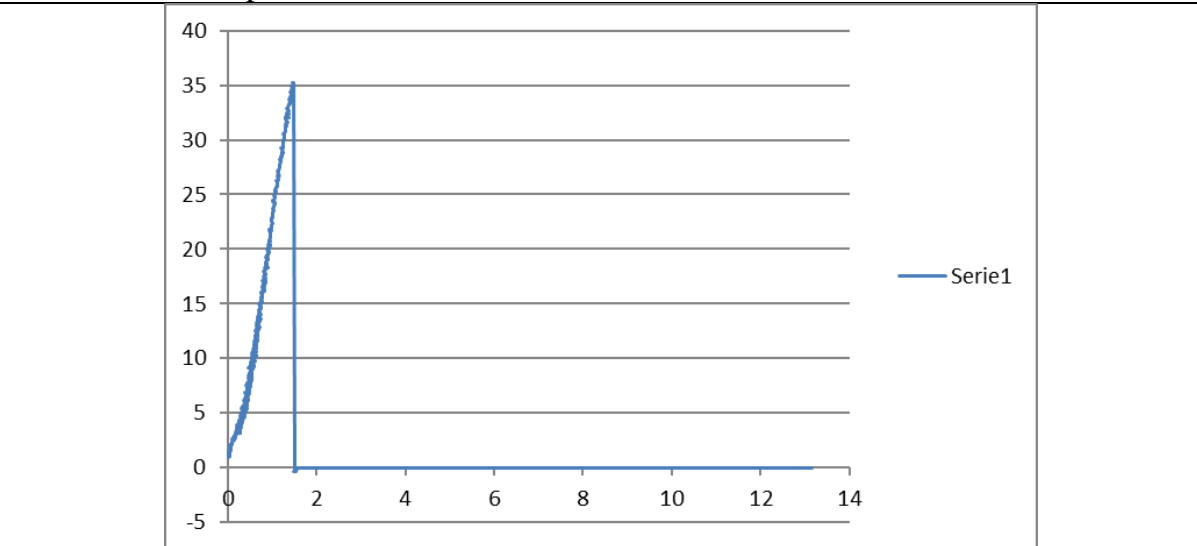
Load History

Specimen: S90-TL-C2-123	G-modulus:
Stress-strain curve:	

τ(εxy) data for specimen C2-123

Shear stress RL [MPa]

Shear strain

y = 1006,8x + 0,9085
R² = 0,9752
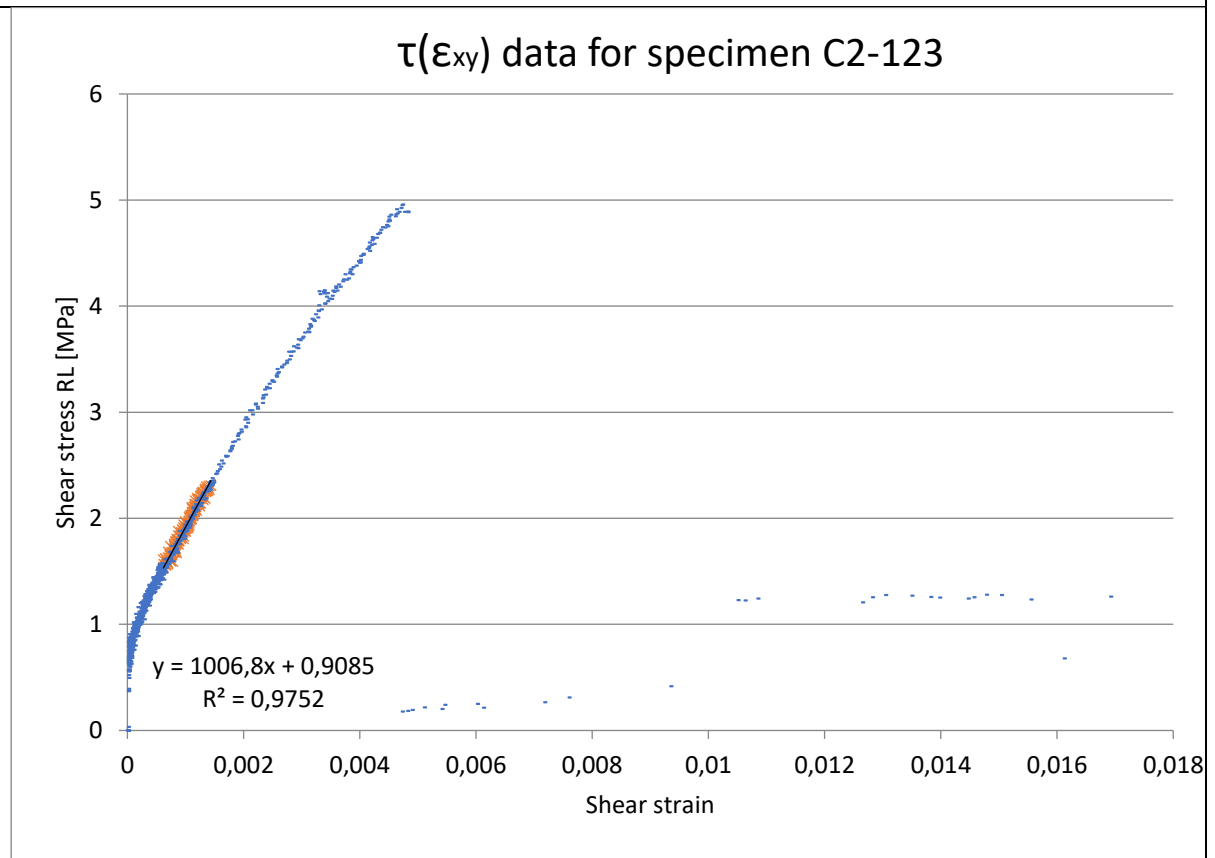
Force-Relative displacement
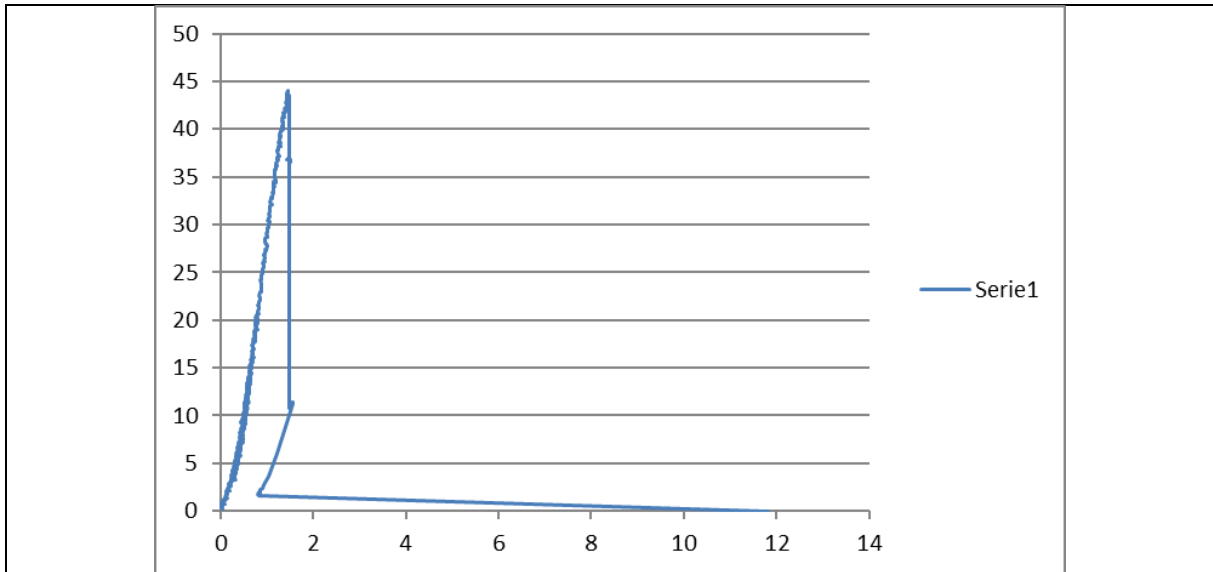
Load History

Specimen: S90-TL-C1-456	G-modulus:
Stress-strain curve:	

τ(εxy) data for specimen C1-456

y = 1049,5x + 1,4058
R² = 0,9584

Force-Relative displacement

Load History

39
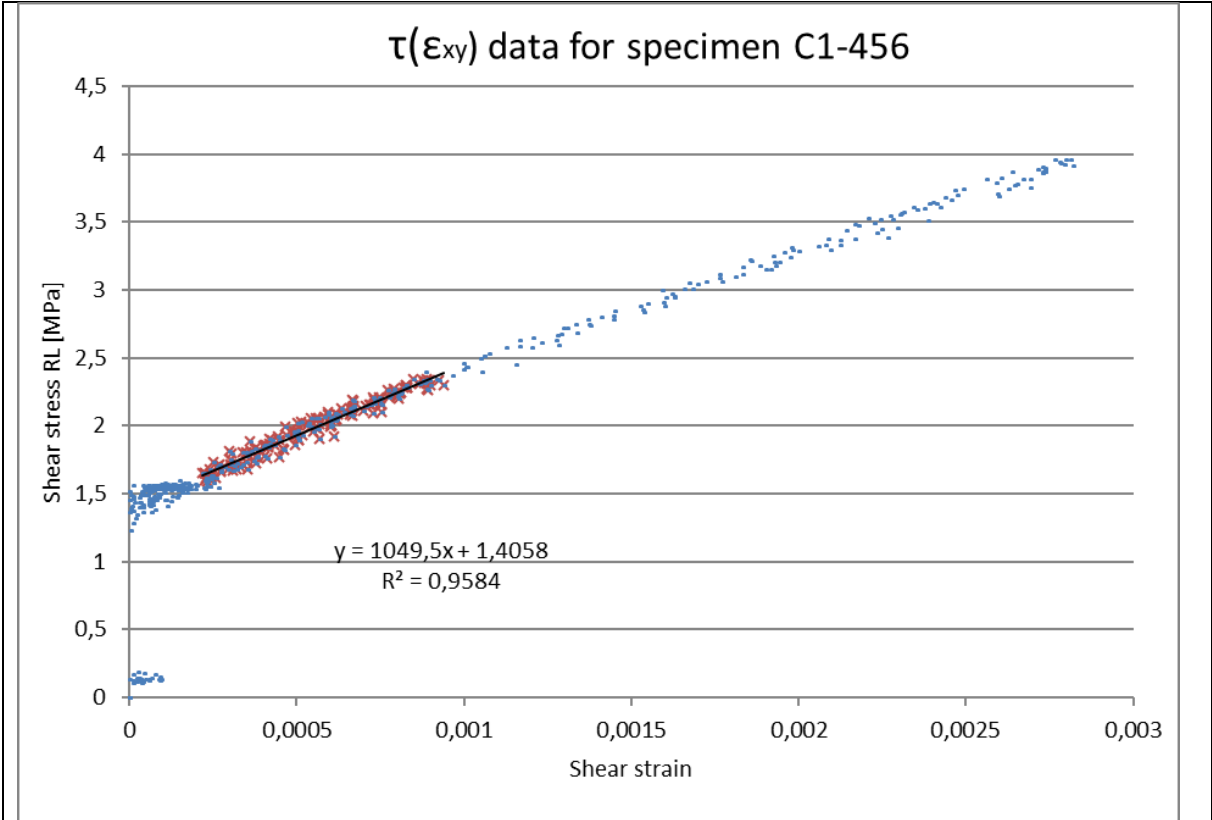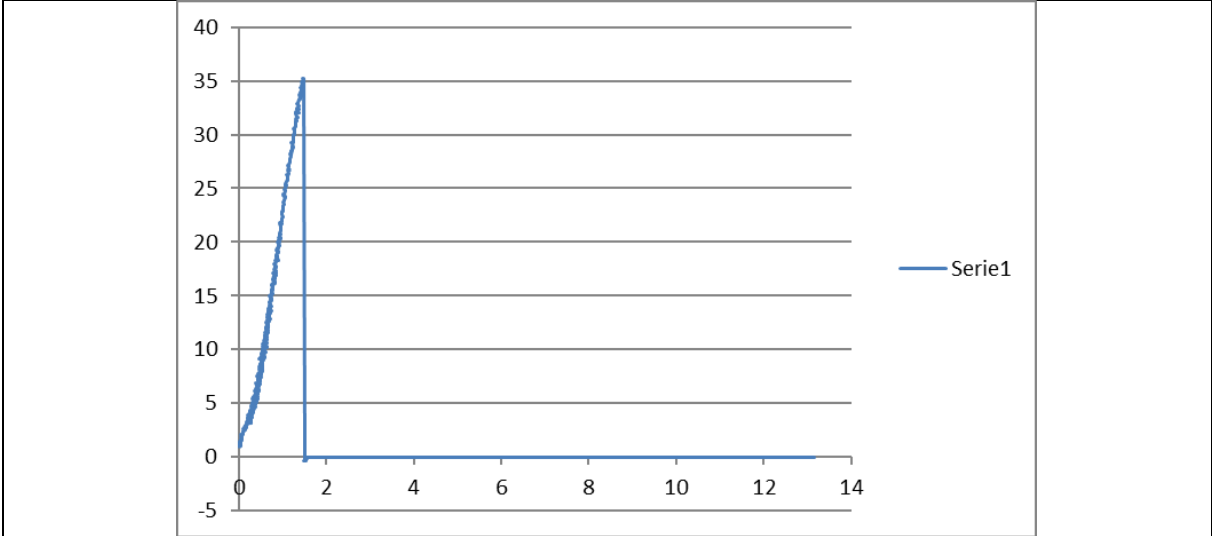
Specimen: S90-TL-A6-678	G-modulus:
Stress-strain curve:	

τ(ε$_{xy}$) data for specimen A6-678

$y = 666,42x + 0,9247$
$R^2 = 0,9963$

$y = 775,3x + 0,7632$
$R^2 = 0,9774$

Shear stress RL [MPa]

Shear strain
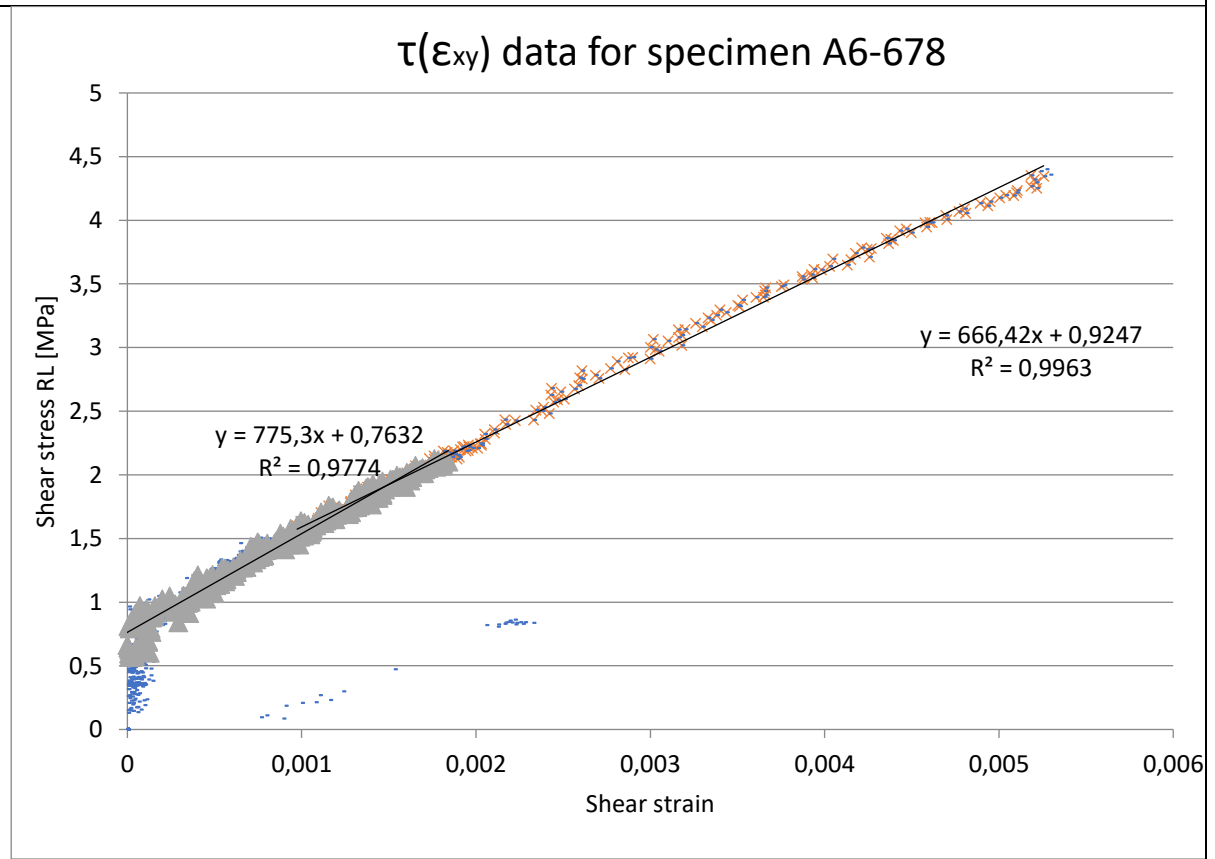
Force-Relative displacement
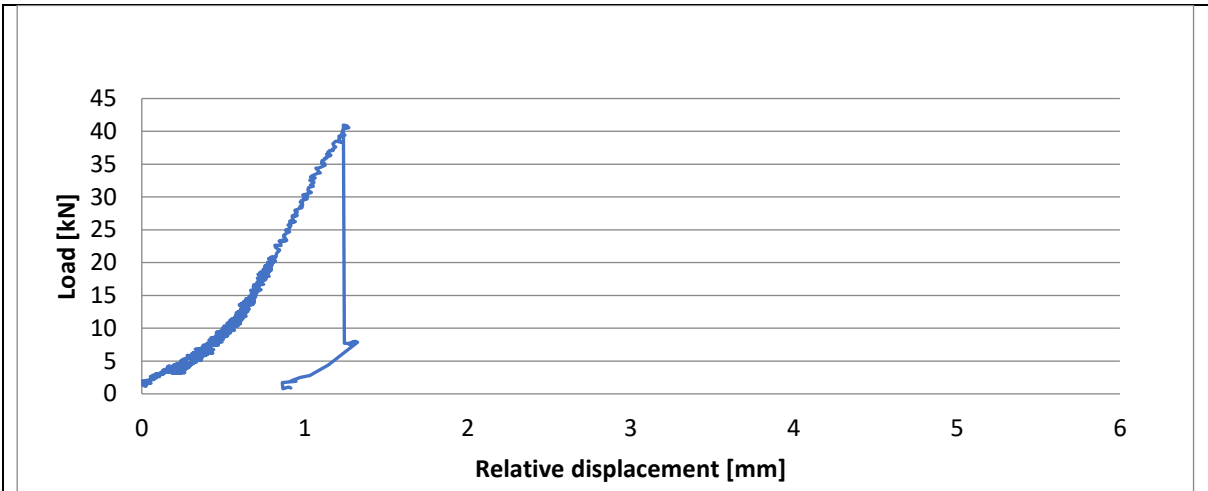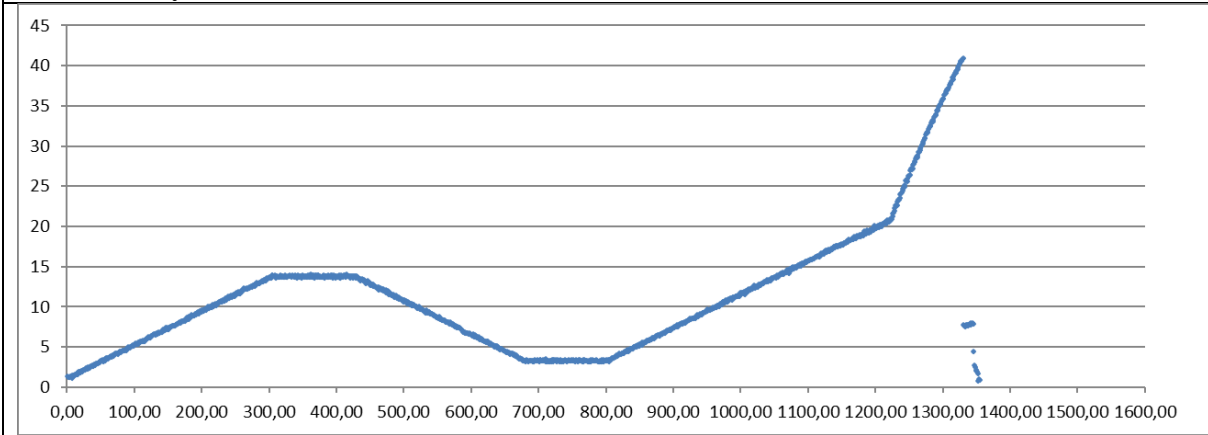
Load History

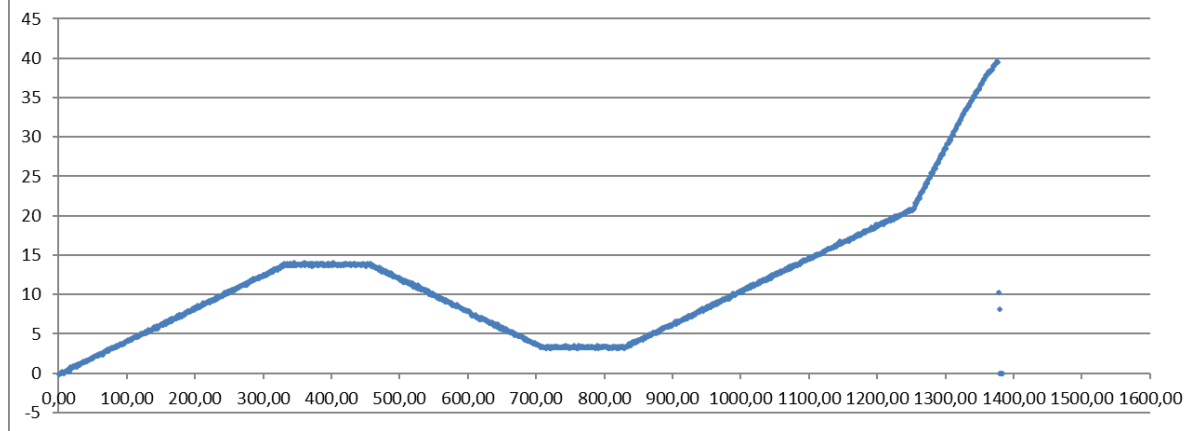| Specimen: S90-TL-A6-345	G-modulus:
Stress-strain curve:	

τ(εxy) data for specimen A6-345

y = 1020,8x + 2,0405
R² = 0,9908
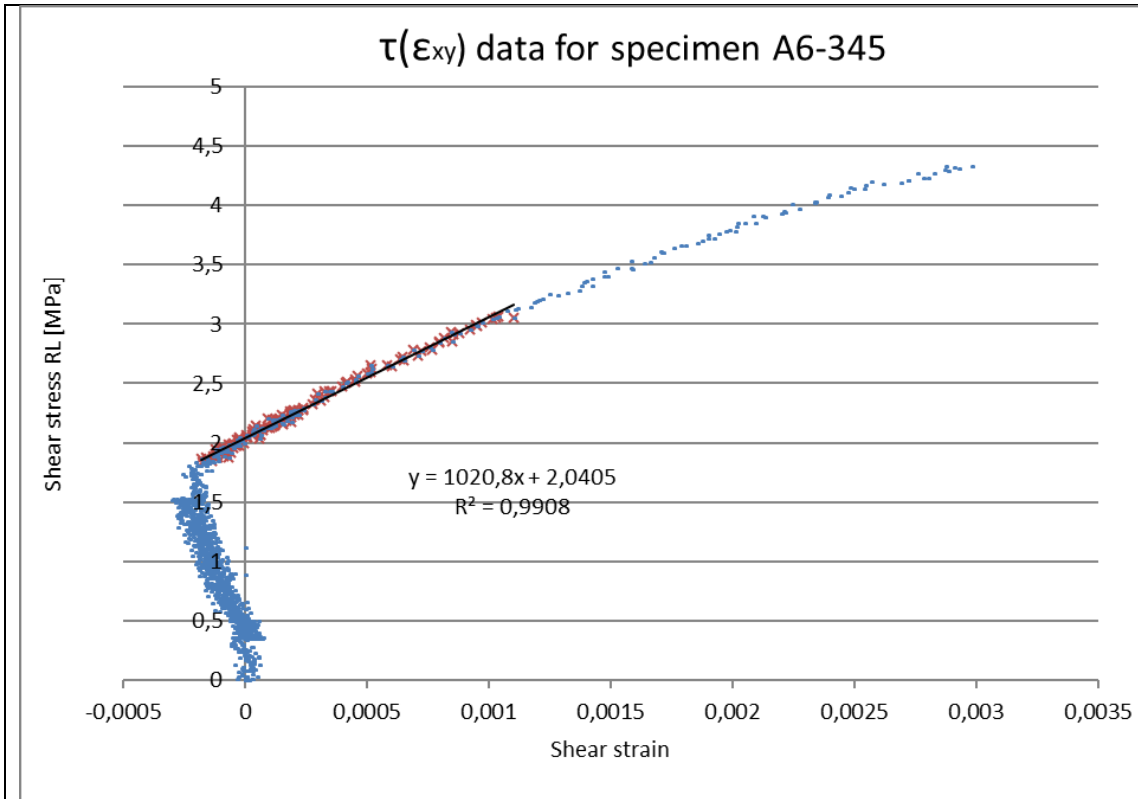
Force-Relative displacement
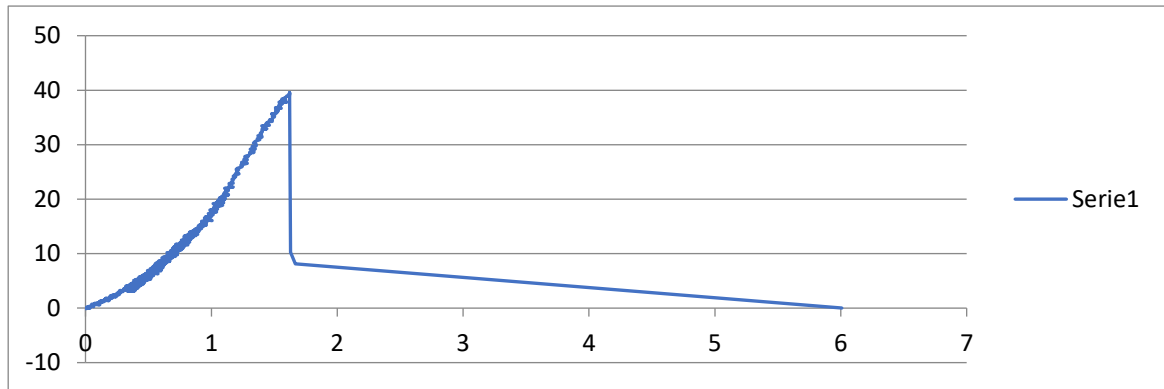
Load History

Specimen: SRound-A5-345	G-modulus:
Stress-strain curve:	

τ(εxy) data for specimen A5-345

Re-oloding path
Experimental points
Lineær (Re-oloding path)

$y = 615{,}19x - 0{,}4768$
$R^2 = 0{,}9905$

Shear stres τxy [MPA]
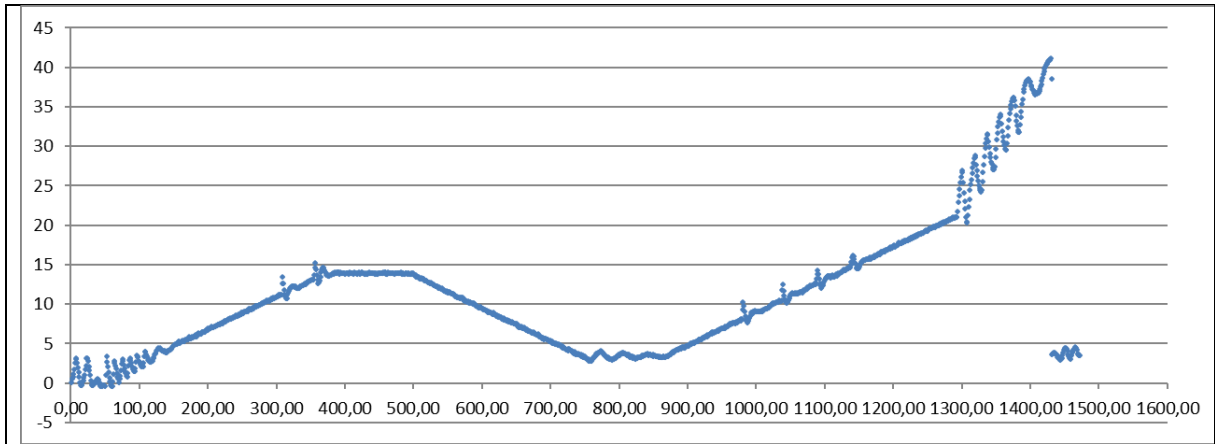
Shear strain εxy

Force-Relative displacement
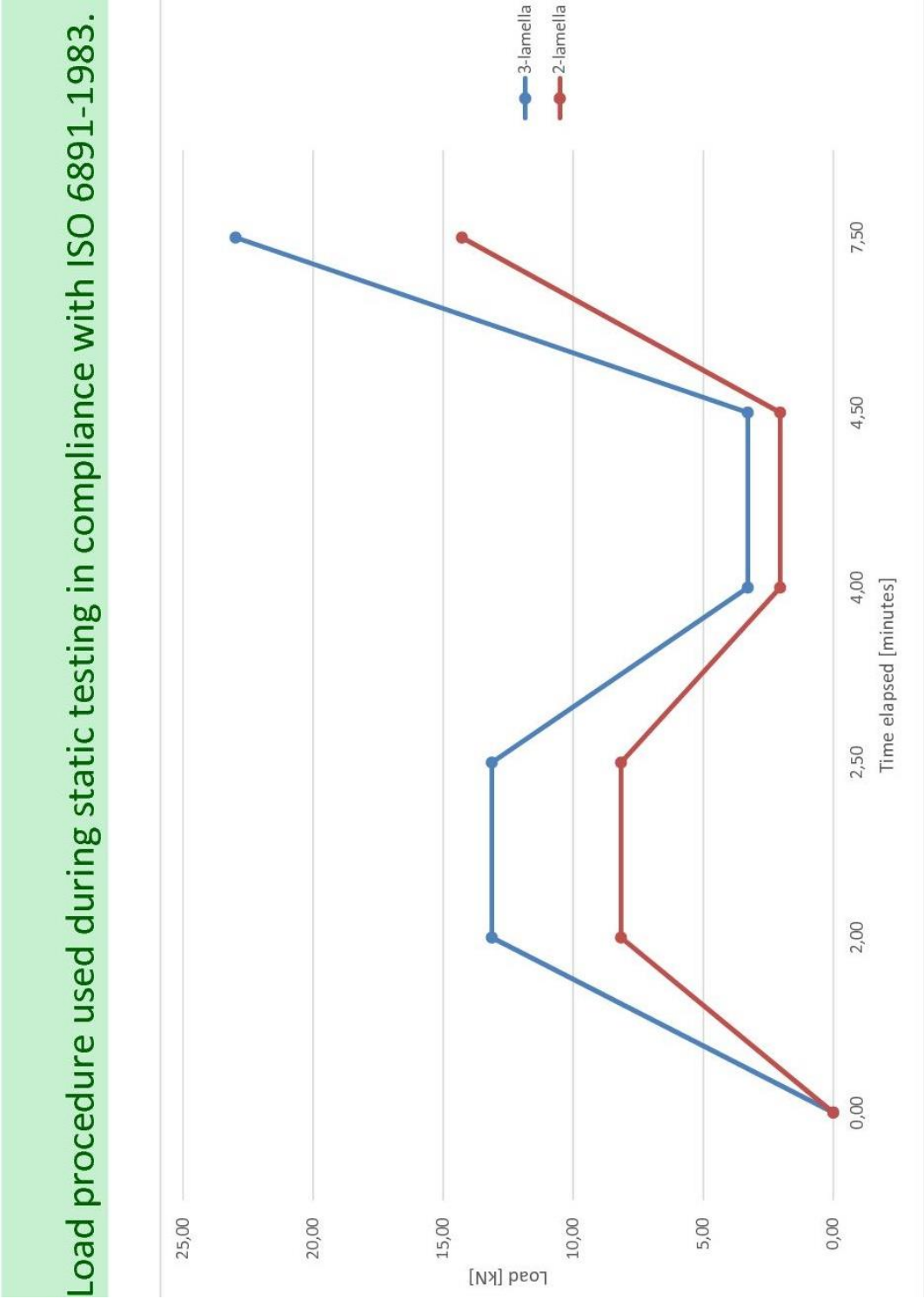

Serie1

Load History

43
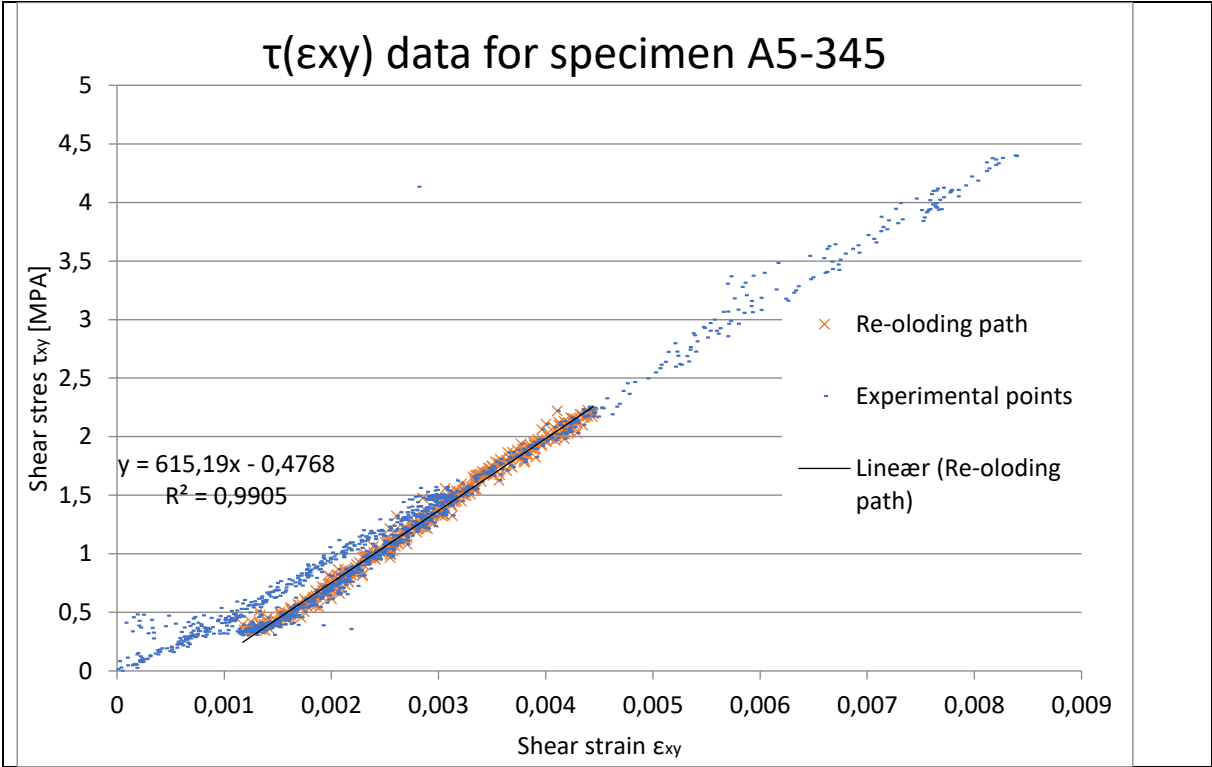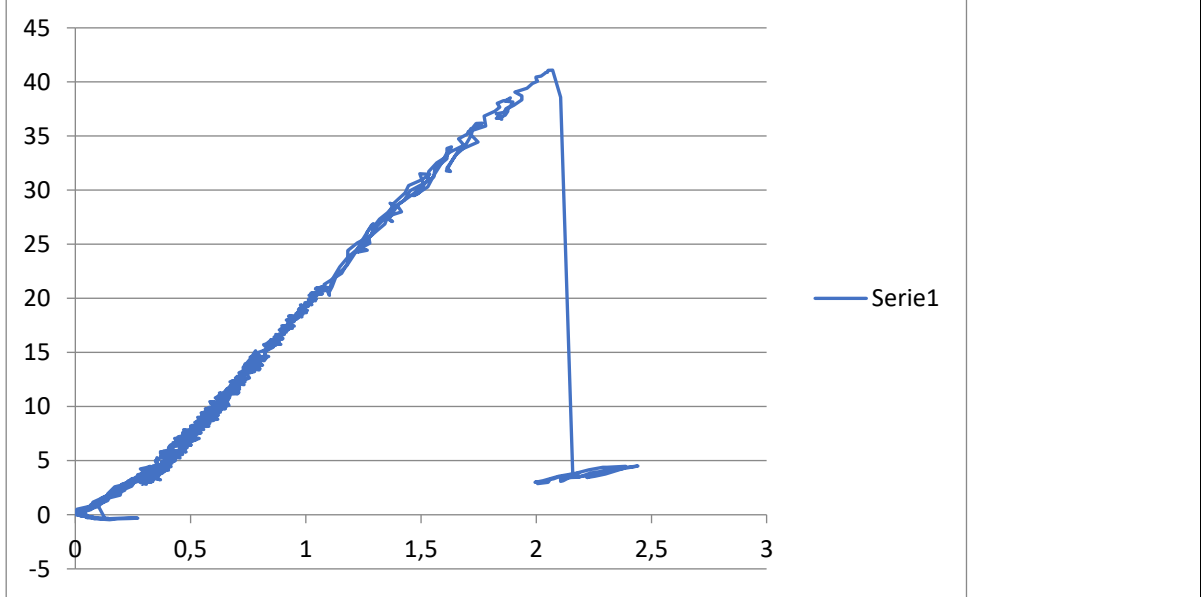
Appendix J- fracture documentation of shear specimen

# Appendix K – Static load procedure for shear tests

Load procedure used during static testing in compliance with ISO 6891-1983.

47

Load procedure used during static testing in compliance with ISO 6891-1983.

3-lamella

Parameters			Control	Load Stage	load [kN]	load rate	interval [min]	time elapsed[mm]
f$_{char}$	3,5	N/mm2		0	0,00		0	0,00
h	67	mm		0,4*F$_{est}$	13,13		2	2,00
d	140	mm	Load controled	hold for 30s	13,13	6,566	0,5	2,50
F$_{est}$	32,83	kN		0,1*F$_{est}$	3,28		1,5	4,00
				hold for 30s	3,28		0,5	4,50
				0,7*F$_{est}$	22,98		3	7,50
			displacement controled	constant rate of slip for 3-5 min			4,00	11,50
				1,0*F$_{est}$	32,83			11,50
				rate of load last stage:				#DIV/0!

2-lamella

Parameters			Control	Load Stage	load [kN]	load rate	interval [min]	time elapsed[mm]
f$_{char}$	3,5	N/mm2		0	0,00		0	0,00
h	67	mm		0,4*F$_{est}$	8,16		2	2,00
d	87	mm	Load controled	hold for 30s	8,16	4,080	0,5	2,50
F$_{est}$	20,4015	kN		0,1*F$_{est}$	2,04		1,5	4,00
				hold for 30s	2,04		0,5	4,50
				0,7*F$_{est}$	14,28		3	7,50
			displacement controled	constant rate of slip for 3-5 min			4,00	11,50
				1,0*F$_{est}$	20,4015		4	11,50
				rate of load last stage:				1,53

Appendix L – Drawings

(not in scale due to printer settings)

49

140

181

17

17

205

600

17

17

181

140

181
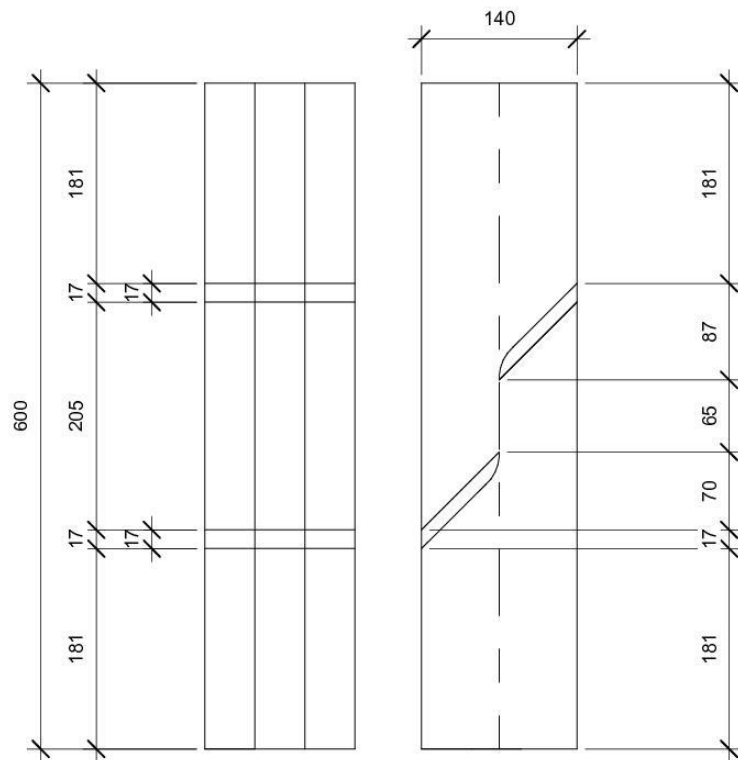
17

70

ø 12

66

69

17

181
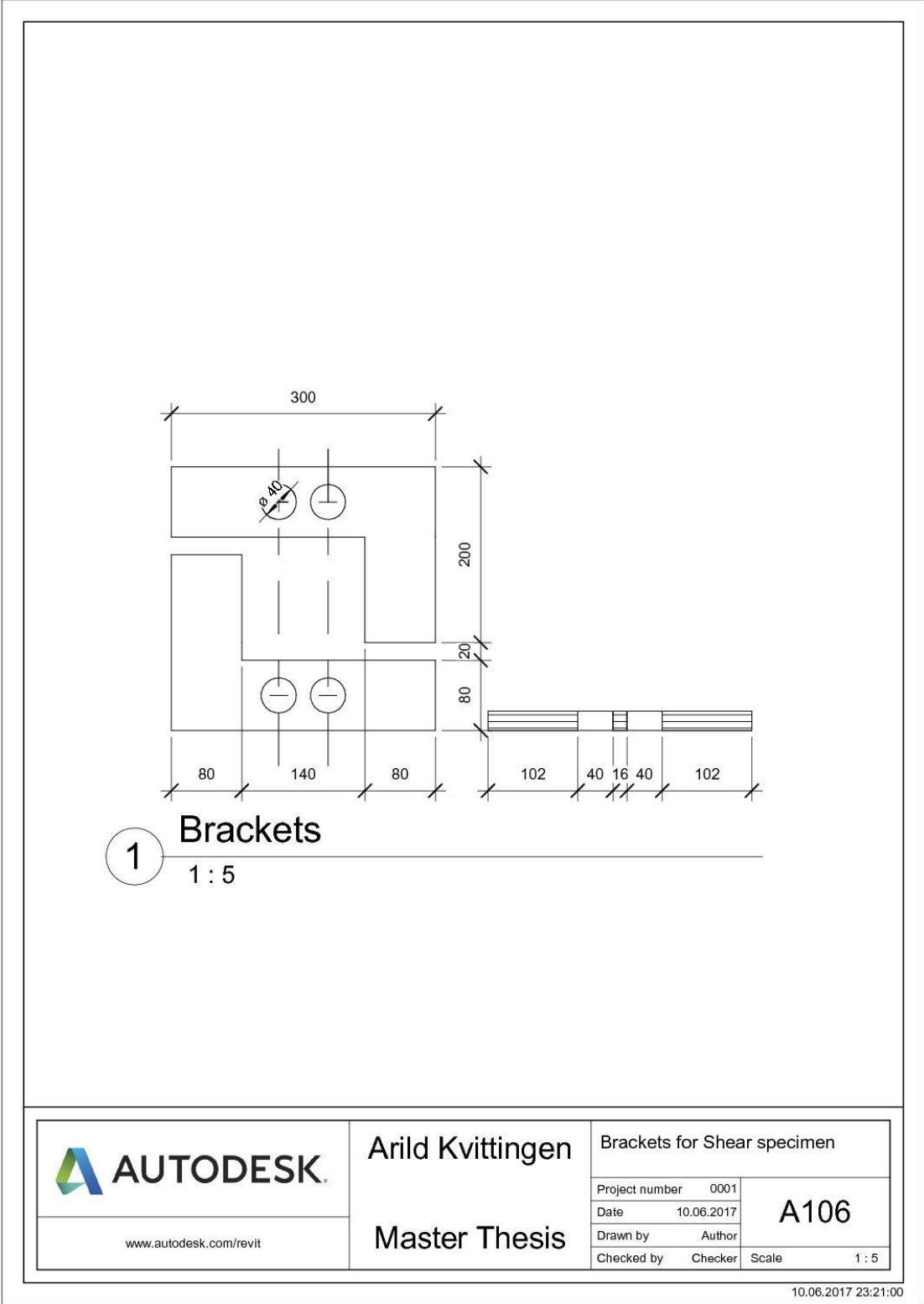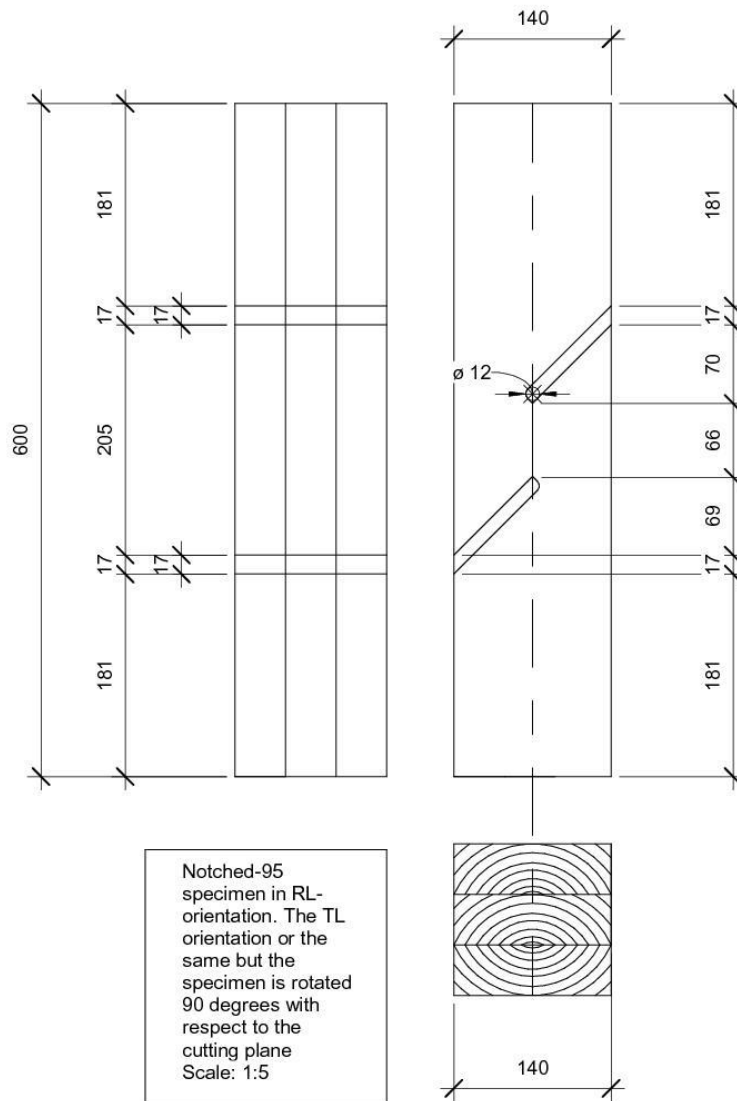
Notched-95 specimen in RL-orientation. The TL orientation or the same but the specimen is rotated 90 degrees with respect to the cutting plane
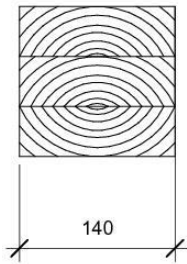Scale: 1:5

140

N90-RL

1 : 5

①

Arild Kvittingen

Master Thesis

Notched-90 RL-Oriented

Project number	0001	
Date	10.06.2017	**A103**
Drawn by	Author	
Checked by	Checker	Scale 1 : 5

10.06.2017 23:20:46

Notched-45 specimen in RL-orientation. The TL orientation or the same but the specimen is rotated 90 degrees with respect to the cutting plane
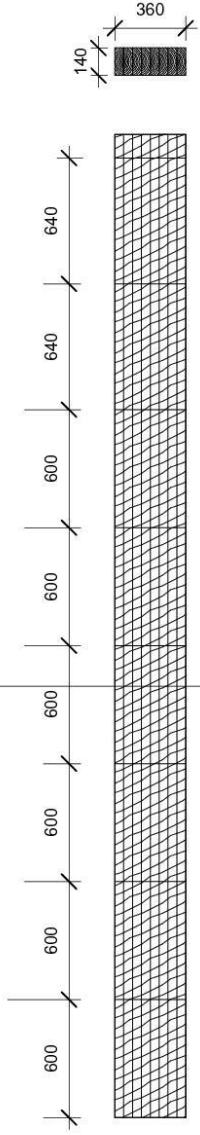Scale: 1:5

140

181
17
17
600
205
17
17
181

140
181
17
70
65
87
181

N45-RL
1 : 5

Arild Kvittingen

Master Thesis

Notched-45 RL-Oriented

Project number	0001	A102
Date	10.06.2017	
Drawn by	Arild F.K	
Checked by	Checker	Scale	1 : 5

AUTODESK.

www.autodesk.com/revit

10.06.2017 23:20:39

360

140

Beam 0

(1) 1 : 25

640

640

600

600

600

600

600

600

Arild Kvittingen	Beam 0-degree cut		
	Project number	0001	**A104**
	Date	10.06.2017	
Master Thesis	Drawn by	Author	
	Checked by	Checker	Scale 1 : 25

10.06.2017 23:20:50

360

140

45

5000

Beam 5

1 : 25

640

5.00°

640
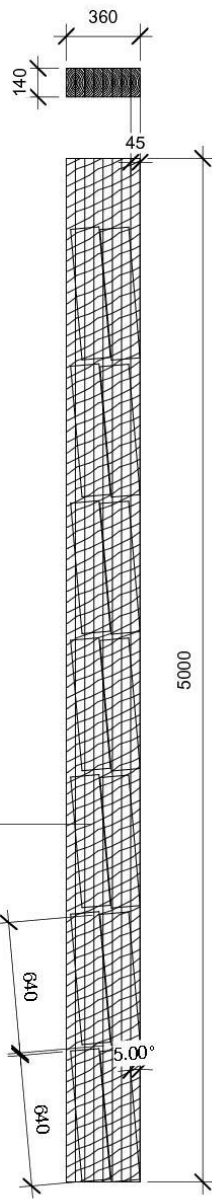
Arild Kvittingen

Master Thesis

Beam 5-degree cut

Project number	0001	A105
Date	10.06.2017	
Drawn by	Author	
Checked by	Checker	Scale	1 : 25

10.06.2017 23:20:55

53